Resource

Developmental Cell

Molecular profiling of adult *C. elegans* glia across sexes by single-nuclear RNA-seq

Graphical abstract

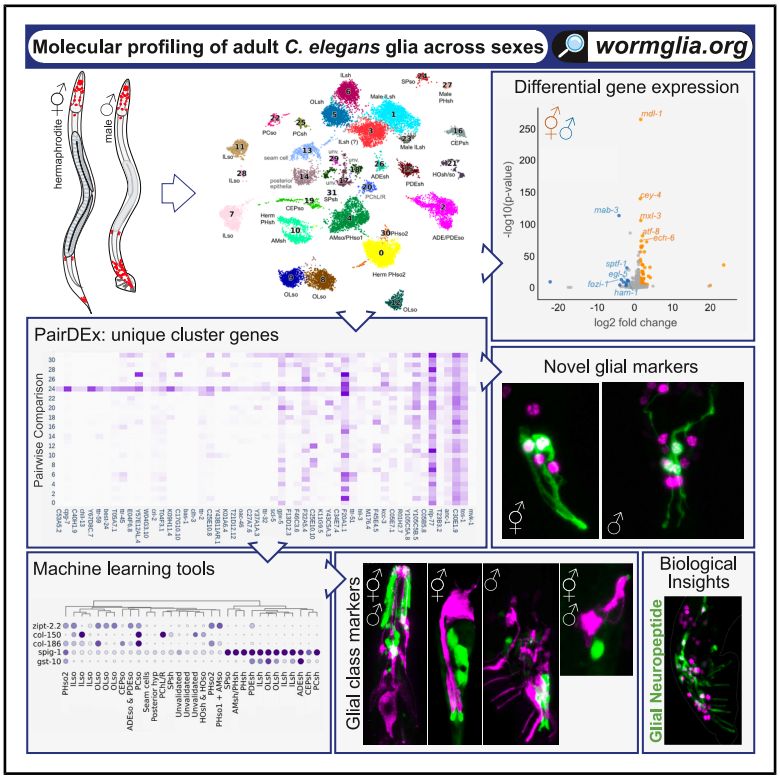

Highlights

- Gene expression profiles of all neuroectoderm-derived glia across adult *C. elegans* sexes
- Molecular markers identified glial classes and pan-glial signatures
- Glial sex dimorphism varies across cell types and regions
- Glial cells process and release neuropeptides via distinct mechanisms

Authors

Maria D. Purice, Elgene J.A. Quitevis, R. Sean Manning, ..., Michael Zager, Manu Setty, Aakanksha Singhvi

Correspondence

msetty@fredhutch.org (M.S.), asinghvi@fredhutch.org (A.S.)

In brief

Purice et al. present single-nuclear RNA-seq profiling of adult *C. elegans* glia by sex (wormglia.org) with custom computational analytics, and identify glial heterogeneity, molecular markers, and sex dimorphism. Complementing existing connectome and neuron profiling datasets, this work now provides insight into the molecular topology of the complete nervous system of a metazoan.

Purice et al., 2025, Developmental Cell *60*, 1–20
December 15, 2025
https://doi.org/10.1016/j.devcel.2025.05.013

CellPress

Developmental Cell

CellPress
OPEN ACCESS

Resource

Molecular profiling of adult *C. elegans* glia across sexes by single-nuclear RNA-seq

Maria D. Purice,[1] Elgene J.A. Quitevis,[1,2] R. Sean Manning,[1] Liza J. Severs,[1] Nina-Tuyen Tran,[1] Violet Sorrentino,[1,3] Connor Finkbeiner,[1,2,4] Feinan Wu,[5] Michael Zager,[6] Manu Setty,[1,2,7,9,*] and Aakanksha Singhvi[1,8,9,10,*]

[1]Division of Basic Sciences, Fred Hutchinson Cancer Center, Seattle, WA 98109, USA
[2]Herbold Computational Biology Program, Public Health Sciences Division, Fred Hutchinson Cancer Center, Seattle, WA 98109, USA
[3]Molecular and Cell Biology Graduate Program, Fred Hutchinson Cancer Center and University of Washington, Seattle, WA 98109, USA
[4]Department of Genome Sciences, University of Washington, Seattle, WA 98109, USA
[5]Genomics and Bioinformatics Shared Resource, Fred Hutchinson Cancer Center, Seattle, WA 98109, USA
[6]Data Visualization Core, Fred Hutchinson Cancer Center, Seattle, WA 98109, USA
[7]Translational Data Science IRC, Fred Hutchinson Cancer Center, Seattle, WA 98109, USA
[8]Department of Neurobiology and Biophysics, University of Washington School of Medicine, Seattle, WA 98195, USA
[9]These authors contributed equally
[10]Lead contact
*Correspondence: msetty@fredhutch.org (M.S.), asinghvi@fredhutch.org (A.S.)
https://doi.org/10.1016/j.devcel.2025.05.013

SUMMARY

A comprehensive understanding of nervous system function requires molecular insight into the diversity and sex dimorphism of both its component cell types, glia and neurons. Here, we present a single-nuclear RNA sequencing (RNA-seq) census of all neuroectoderm-derived glia in the adult *C. elegans* nervous system, across sexes. By iteratively coupling computational modeling and custom analytics with *in vivo* validations, we uncovered molecular markers for all glia, as well as class-specific and pan-glial molecular signatures. These identified that each glia is functionally heterogeneous across the nervous system and variably sex dimorphic between sexes. Thus, this glial transcriptome (wormglia.org) offers deep mechanistic insights into glial biology brain wide. Complementing the existing *C. elegans* neuronal transcriptome and mapped connectome, it also enables single-cell and molecular resolution insight into the entire nervous system of an adult metazoan.

INTRODUCTION

The nervous system consists of two major cell types—neurons and glia, with glia comprising about half the cells and volume of the human brain.[1,2] Glia modulate neuronal properties, influencing animal behaviors such as sensory perception,[3–9] learning and memory,[10–13] sleep,[14–16] and motor control.[16–18] Defects in glial functions thus correlate with many neurodevelopment and neurodegenerative disorders.[19–24]

In both the central nervous system (CNS) and peripheral nervous system (PNS), glia have been historically classified by anatomy.[25–27] Recent advances in single-cell and single-nuclear RNA sequencing (scRNA-seq and snRNA-seq) suggest that this classification may be too simplistic and show that even anatomically identical glia can be molecularly heterogeneous. For instance, astrocytes, oligodendrocytes, and microglia all exhibit diverse transcriptional profiles across brain regions.[28–35] Similarly, PNS enteric glia are molecularly heterogeneous across the gastrointestinal tract,[36] and even peripheral sense organ and satellite glia are heterogeneous.[37–40] Despite these insights, lack of validated markers for different glial cells limits our understanding of how molecular heterogeneity informs their identity or function.[2,27,41–46]

There is also conflicting evidence on whether analogous glia are dimorphic between sexes.[47–50] In corollary, despite evidence for sexual dimorphism in brain regions like the hypothalamus,[51,52] the molecular bases for this across the CNS/PNS are barely explored.[53–55] Given that most neurological diseases have sex-biased etiology, this is a major knowledge gap in dissecting glial roles in neural functions or disease.[56,57]

C. elegans is a powerful model to mechanistically evaluate glial heterogeneity and sex dimorphism organism wide. Its nervous system consists of 302 neurons and 56 glia in hermaphrodites (somatically female) and 389 neurons and 82 glia in males.[58] Each neuron and glia is born of an invariant developmental lineage[59,60] and integrates into a cellularly invariant and mapped sex-dimorphic connectome.[58,61,62] Although the individual neurons in this system are well-characterized molecularly and functionally,[58,63–68] molecular heterogeneity or sexual dimorphism of glia has been largely unexplored.[69,70] Thus, *C. elegans* presents an ideal experimental platform where a glial transcriptome will rapidly shed light on how glia across the nervous system influence neural functions and animal behavior.[69,71–73]

Please cite this article in press as: Purice et al., Molecular profiling of adult *C. elegans* glia across sexes by single-nuclear RNA-seq, Developmental Cell (2025), https://doi.org/10.1016/j.devcel.2025.05.013

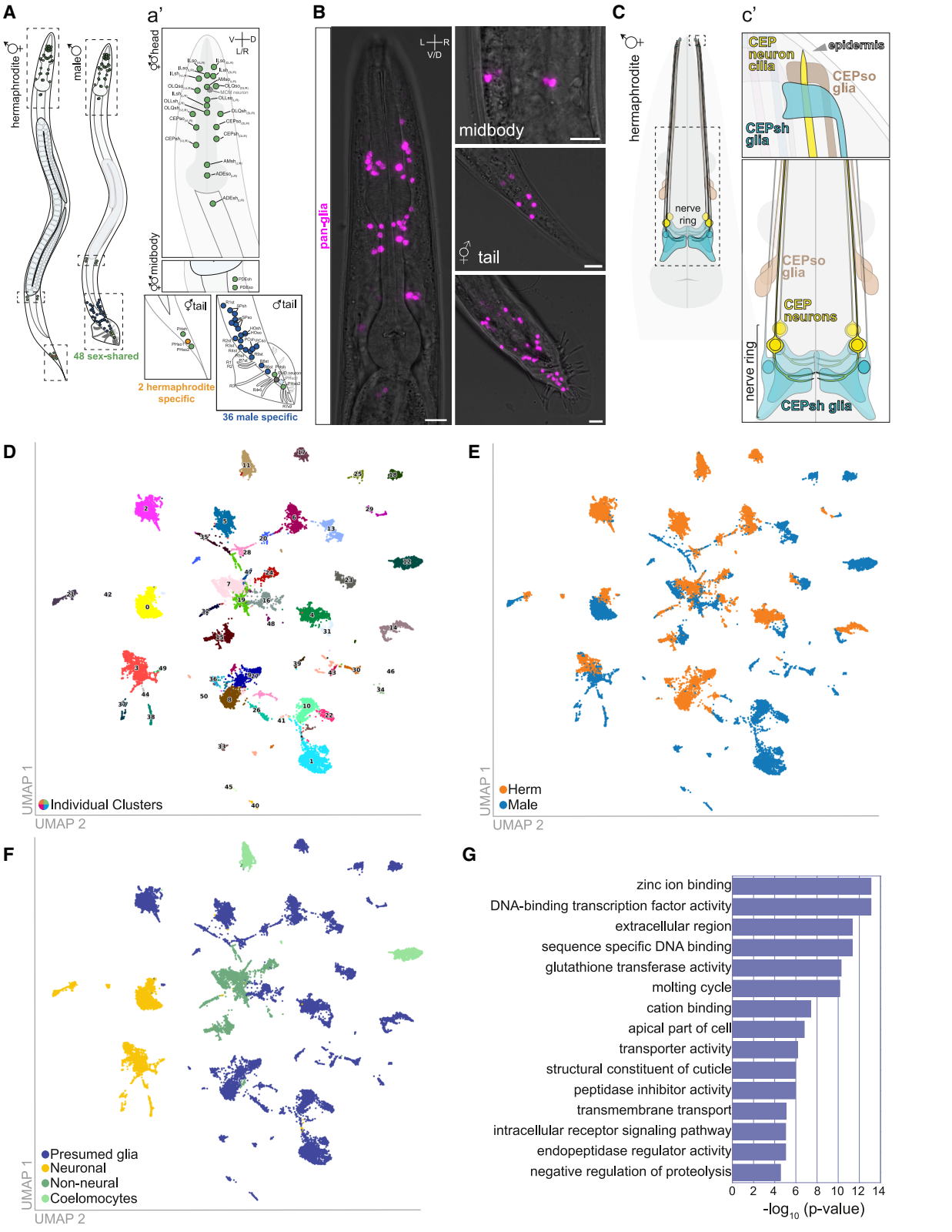

(legend on next page)

Please cite this article in press as: Purice et al., Molecular profiling of adult *C. elegans* glia across sexes by single-nuclear RNA-seq, Developmental Cell (2025), https://doi.org/10.1016/j.devcel.2025.05.013

Six *C. elegans* glia are of mesodermal lineage (glial-like cells of the nerve ring, GLR) in both sexes and not discussed further here.[58,74] The remaining glial cells (50 in hermaphrodite, 76 in male) derive from the neuroectoderm,[75,76] localize primarily in the animal head and tail (Figures 1A and 1B), and reside within sense organs (Figure 1C). In each sense organ, glia are anatomically subcategorized into sheath (sh) and socket (so) glial classes, such that each sense organ has 1–2 glial cells of each class contacting cognate neuron(s) (Figure 1C; Table S1). Within the sense organ, sh and so glia contact each other, as well as the cognate sensory neuronal dendrite endings (Figure 1C). Sheath-glia-secreted factors bathe dendrite endings, while so glia also attach to the overlying epidermis (Figure 1C′).

Males have an additional 28 sex-specific glial cells (36 nuclei) in the male mating apparatus (Figures 1A and S1A; Table S1). Besides sh and so, these include the 18 ray structural cells (R*n*st) with presumed dual sh (secrete factors) and so (attach to epidermis) functions.[77] In addition, four sex-shared glia are known to exhibit sexually dimorphic features: male amphid so (AMso) divide to generate CEM neurons,[78] male cephalic sh and so glia (CEPsh and CEPso) then interact with these CEM neurons,[55,79] and male phasmid so 1 (PHso1) transdifferentiate to neurons[80] (Figures 1A, 1B, and S1A) (Table S1). The molecular mechanisms underlying these glial sex-dimorphic features are unknown. Similarly, how the other anatomically shared glia compare between sexes or contribute to observed sexually dimorphic animal behaviors[81,82] is also unknown.

Here, we present the single-nuclear molecular transcriptome of all neuroectoderm-derived glia of the adult *C. elegans* nervous system across sexes (wormglia.org). By combining bespoke computational analytic and machine learning tools to compare these related cell types, with *in vivo* transcriptional reporter validation analyses, we identified glial-specific/class molecular signatures. This validated molecular census has identified several mechanistic insights into glial molecular properties. Glia have striking molecular heterogeneity, with each anatomically distinct glial cell defining one or more clusters and each cluster defining 1–2 anatomically distinct glia. Individual glia cluster by class identity (sh or so) and not sense organ, anatomy, or developmental lineage. Molecular and anatomical sexual dimorphism appear to be independent glial attributes. Lastly, although glia express neuropeptides,[83,84] they deploy distinct machinery to process and release these compared with neurons. Thus, this integrated profiling of glia, combining single-cell transcriptomics, modeling, and *in vivo* validations, has yielded deep single-cell and single-gene insights into glia across the entire nervous system of a metazoan. This comprehensive study of glial molecular heterogeneity and sex dimorphism brain wide also offers a powerful foundation and molecular tools for directed mechanistic studies of glial roles in neural functions across sexes.

RESULTS

Isolation and sequencing of adult *C. elegans* glia by sex

C. elegans was the first animal to be profiled by single-cell sequencing, but all molecular atlases reported thus far have focused on either whole animals or neurons, with glial cells under-represented and largely unannotated.[45,63,65,70,85–88] Therefore, we built a single-cell transcriptomic atlas enriched for glia. Like glia of other species, *C. elegans* glial processes intricately contact neurons. Thus, we opted for snRNA-seq to reduce confounding contamination from physically contacting neuronal cell material. Day 1 adult glia were profiled, as animal behaviors are most robust at this stage.[89]

Glial nuclei were isolated using a transcriptional reporter consisting of a nuclear localization signal fused to a red fluorescent protein (NLS:RFP) under the pan-glial *mir-228* promoter[90,91] (Figure 1B). This reporter labeled both glial and non-glial cells and, by cell counts, captured most, if not all, neuroectoderm-lineage glia (Figures S1B and S1C). $P_{mir\text{-}228}$:NLS:RFP was not expressed in early embryos, germ line, or mesoderm lineage GLR glia (Figures S1D and S1E), meaning that embryonic glial precursors would not confound our adult dataset. Males (0.1% of the population) were enriched by a combinatorial strategy (see STAR Methods).[92]

We recovered 31,410 RFP+ nuclei (16,887 hermaphrodite nuclei; 14,723 male nuclei) and confirmed glial gene enrichment in these (Figures S1F and S1G). After quality control and preprocessing (Figures S1H and S1I) (see STAR Methods), the non-batch-corrected data categorized into 51 clusters, of which 17 were manually annotated as "non-glia" by marker gene expression[45,86,90] (Figures 1D–1F and S1J; Table S1). Differential expression and Gene Ontology (GO) analysis on the remaining clusters uncovered enrichment of transporters and structural proteins (Figure 1G), as expected for putative glial clusters. These clusters comprised 20,810 nuclei, implying ~200× coverage of each glia (Figures 1A–1A′ and 1F; Table S1).

Computational and experimental annotation of glial cell types

Batch correction and re-clustering of the putative glia yielded 32 glial clusters: 1 hermaphrodite specific, 9 male specific, and 22 sex shared (Figures 2A, 2B, and S2A). This already suggested a previously unappreciated molecular heterogeneity for the 14 anatomically sex-shared glia (Figure 2B; Table S1).

Figure 1. Anatomical and molecular characterization of adult *C. elegans* neuroectoderm glia

(A and a′) Schematic of both sexes, showing shared, hermaphrodite-specific, and male-specific neurectoderm glial nuclei. (a′) Close up of the glia within the head, midbody, and tails.

(B) Pan-glial nuclear localized RFP. Scale bars, 10 μM.

(C) Schematic of *C. elegans* cephalic sense organ as example, consisting of sensory neuron(s) (yellow) contacting one so (light brown) and one sh (cyan) glia.

(c′) Close up of CEP's dendritic (top box) and axonal (lower box) glial interactions.

(D) UMAP colored by 51 non-batch-corrected clusters.

(E) UMAP showing sex contribution to each cluster (male: blue; hermaphrodite: orange).

(F) UMAP showing contribution of non-glial tissues (glia: blue; neuron: yellow; non-neural cells: green; coelomocytes: light green).

(G) GO term analysis of putative glial clusters compared with neuronal clusters.

Please cite this article in press as: Purice et al., Molecular profiling of adult *C. elegans* glia across sexes by single-nuclear RNA-seq, Developmental Cell (2025), https://doi.org/10.1016/j.devcel.2025.05.013

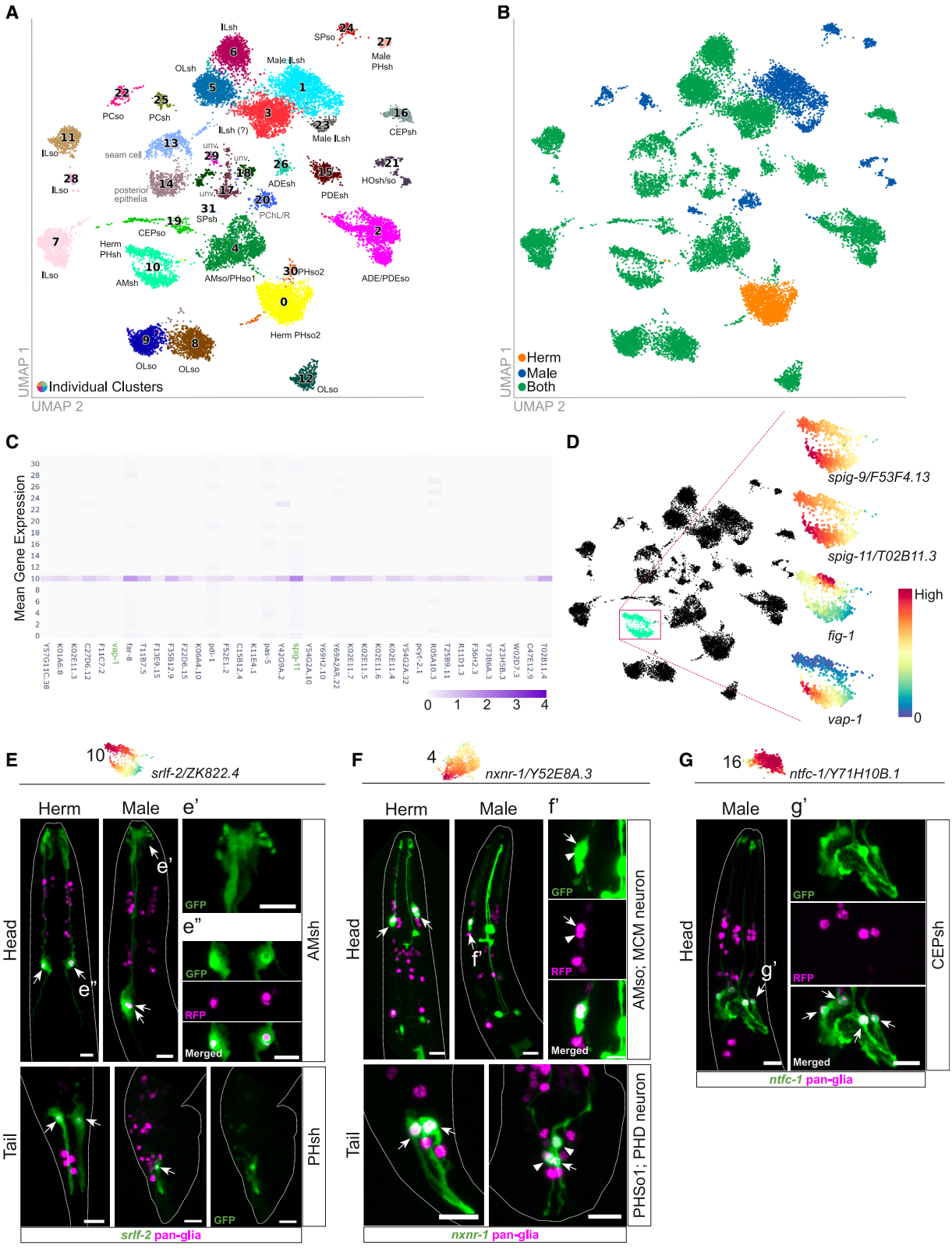

Figure 2. Computational and experimental annotation of glial cell types

(A) Uniform manifold approximation projection (UMAP) colored by 32 batch-corrected putative glial clusters and their identities.

(B) UMAP depicting sex specificity (orange: hermaphrodite; blue: male; green: sex shared).

(legend continued on next page)

Please cite this article in press as: Purice et al., Molecular profiling of adult *C. elegans* glia across sexes by single-nuclear RNA-seq, Developmental Cell (2025), https://doi.org/10.1016/j.devcel.2025.05.013

Although *him-5* is broadly used to study sex dimorphism in *C. elegans*,[61,66] it has not been evaluated for glial biology. We thus compared hermaphrodite snRNA-seq data between wild-type N2 hermaphrodites (11,115 nuclei) and *him-5* hermaphrodites (8,078 nuclei). Given equivalence between putative glial clusters in the two datasets, we inferred that the *him-5* mutation does not globally alter glial identity (Figure S2B). Thus, all subsequent analyses were performed on wild-type hermaphrodite and *him-5* male batch-corrected data, unless noted.

Because most *C. elegans* glia are molecularly enigmatic, we undertook a data-driven approach to annotate each cluster. Existing gene expression analysis tools identify genes expressed in multiple clusters of these homotypic glial cells. To enrich for genes that uniquely express in individual clusters, we developed a pairwise differential expression analysis (PairDEx) to uncover cluster-enriched genes (CEGs) that were specific to individual clusters (Table S2). Briefly, we performed differential gene expression analysis between cells of one cluster separately against cells of every other cluster and enumerated the number of times a gene is identified to be statistically different (see STAR Methods; wormglia.org). We then generated double-labeled transgenic animals expressing a transcriptional GFP reporter for a curated CEG with the pan-glial $P_{mir\text{-}228}$:NLS:RFP. Each cluster was tested with 1–4 independent CEGs (Tables S2 and S4). As proof of concept for this pipeline, we turned to the best-studied glia in the animal, the related amphid and phasmid sh (AMsh and PHsh),[91,93,94] which express *spig-9*, *spig-11*, *fig-1*, and *vap-1*[90,91,93] (Figures 2C, 2D, and S2D; Mendeley data). PairDEx-derived cluster 10 CEGs included all these genes, suggesting that cluster 10 corresponds to AMsh/PHsh glia (Figure 2C and 2D; Mendeley data). We selected a CEG not previously reported in AMsh/PHsh glia, *srlf-2*, for *in vivo* validation and found that its transcriptional reporter expressed specifically in AMsh/PHsh glia (Figures 2E and S2E, wormglia.org). Deeper analyses of cluster 10 showed it as a super-cluster of two subclusters (Figure S2C), with only one expressing *vap-1*, a gene expressed in AMsh but not PHsh glia[95] (Figures 2D and S2C). These findings confirmed that PairDEx can effectively annotate glial cell profiles and uncover cluster-specific gene signatures.

The limited literature was less reliable for glia with fewer validated genes in our clusters, with minimal overlap with PairDEx-derived CEGs for any one cluster[90] (Table S1). This included 4/10 known genes for AMso and PHso, 0/4 known genes for CEPsh, and 2/5 known genes for inner labial so (ILso) glia[90] (Figures S2F, S2H, and S2I). *In vivo* validation of PairDEx-derived CEGs by transcriptional reporters identified cluster 4 as AMso/PHso1, 16 as CEPsh, and 7/11/28 as ILso glia (Figures 2F, 2G, S2G, and S2J), respectively. We found that the reporter for the AMso/PHso1 cluster 4 CEG *nxnr-1* also expressed in male-specific MCM and PHD neurons derived from these glia (Figure 2F). Further, although it was initially surprising that known CEPsh genes were barely expressed in our dataset, RT-qPCR of *ptr-10* confirmed low mRNA abundance, despite its transcriptional reporter expressing in adult glia[96] (Figures S1G and S2H). This implied a mismatch between RNA levels and transcriptional reporters rather than snRNA-seq data quality.

To annotate the remaining clusters ab initio, we validated CEGs specific to each cluster (Table S2). For some clusters, we additionally co-labeled with known markers and/or markers for the cognate sense organ neuron.[60,90,97] For example, reporters for the CEGs *spig-14* and *ttr-59* validated the male-specific cluster 24 as *mir-228*$^+$ spicule so (SPso) glia (Figures 3A–3C and S3A) of both wild-type and *him-5* males (Figures 3B, S3B, and S3C). These genes were not expressed in hermaphrodite glia (Figures 3B and S3C, left). Further, $P_{spig\text{-}14}$:GFP colocalized with the known SPso marker, CAT-2/tyrosine hydroxylase[98,99] (Figure 3C). A reporter for a third cluster 24 CEG, *spig-8*, also expressed in male-specific cluster 27 (Figures 3A, 3D, and S3D), which we identified as male PHsh glia.

PairDEx analyses did not uncover CEGs that uniquely differentiated between five of the clusters (clusters 1, 3, 5, 6, and 23), indicating that these clusters are closely related. Hierarchical clustering of the mean expression profiles confirmed their high similarity (Figures S3E and S3F), and we tentatively annotated these as inner labial (IL) and outer labial (OL) sh glia by elimination (Figure 2A). We re-ran PairDEx within this subset, and reporter expression analyses of the resulting CEGs identified clusters 1, 3, 6, and 23 as ILsh glia—with clusters 1 and 23 being male specific—and cluster 5 as OLsh (Figures 2A, 3E–3G, and S3H–S3P). Thus, these findings also identified previously unappreciated molecular heterogeneity and sex dimorphism for the six anatomically equivalent ILsh glia. Overall, our pipeline successfully validated glial identities to 29/32 clusters (Figure 2A) to yield a census of *C. elegans* neuroectoderm glia across sexes.

Although PairDEx-derived CEGs readily identify individual glia, they can also be expressed in non-glial tissues (Table S2). For example, a transcriptional reporter for the CEPsh glia CEG *ntfc-1* (Figure 2G) also expressed in cells around the pharynx (Figure S3Q); SPso glia CEG *ttr-59* also had low expression in epithelia (Figure S3R) and ILsh glia CEG *spi-2* also expressed in non-*mir-228*$^+$ (likely arcade) cells[100] (Figure 3E). We reasoned this was because PairDEx analyses ranked genes based on differential expression between glial clusters, but did not penalize for expression in non-glial cells, and also that *mir-228* expression is not glia-exclusive. In line with this, CEGs for clusters 13, 14, and 20 showed these as epithelial cells missed by our literature-based annotations (Figure 1F), expressing epithelial genes like collagen (Mendeley data). Validations identified these as

(C) Zoomed-in PairDEx results for cluster 10 (see Mendeley data) showing mean expression of genes (*x* axis) per cluster (*y* axis). Previously characterized genes, green font.
(D) UMAP showing imputed expression of known AMsh/PHsh genes in cluster 10.
(E–E″) (E) CEG *srlf-2/ZK822.4* GFP reporter expression in AMsh/PHsh glia (arrows) in heads (top) and tails (bottom). Zoom-in of AMsh tip (e′) and cell body (e″).
(F and F′) CEG *nxnr-1/Y52E8A.3* GFP reporter expression in AMso (arrows) and PHso1 of both sexes (arrows). Males show additional expression in AMso-derived MCM neuron (f′) (arrowhead) and PHso1-derived PHD neuron (arrowhead) in tail.
(G) CEG *ntfc-1/Y71H10B.1* GFP transcriptional reporter expression in CEPsh. Zoom-in of the four CEPsh cell bodies (arrows, g′).
(D–G) Markov affinity-based graph imputation of cells (MAGIC)[148] imputed expression for all genes. Dotted line, animal outline. Scale bars, 10 μM.

Please cite this article in press as: Purice et al., Molecular profiling of adult *C. elegans* glia across sexes by single-nuclear RNA-seq, Developmental Cell (2025), https://doi.org/10.1016/j.devcel.2025.05.013

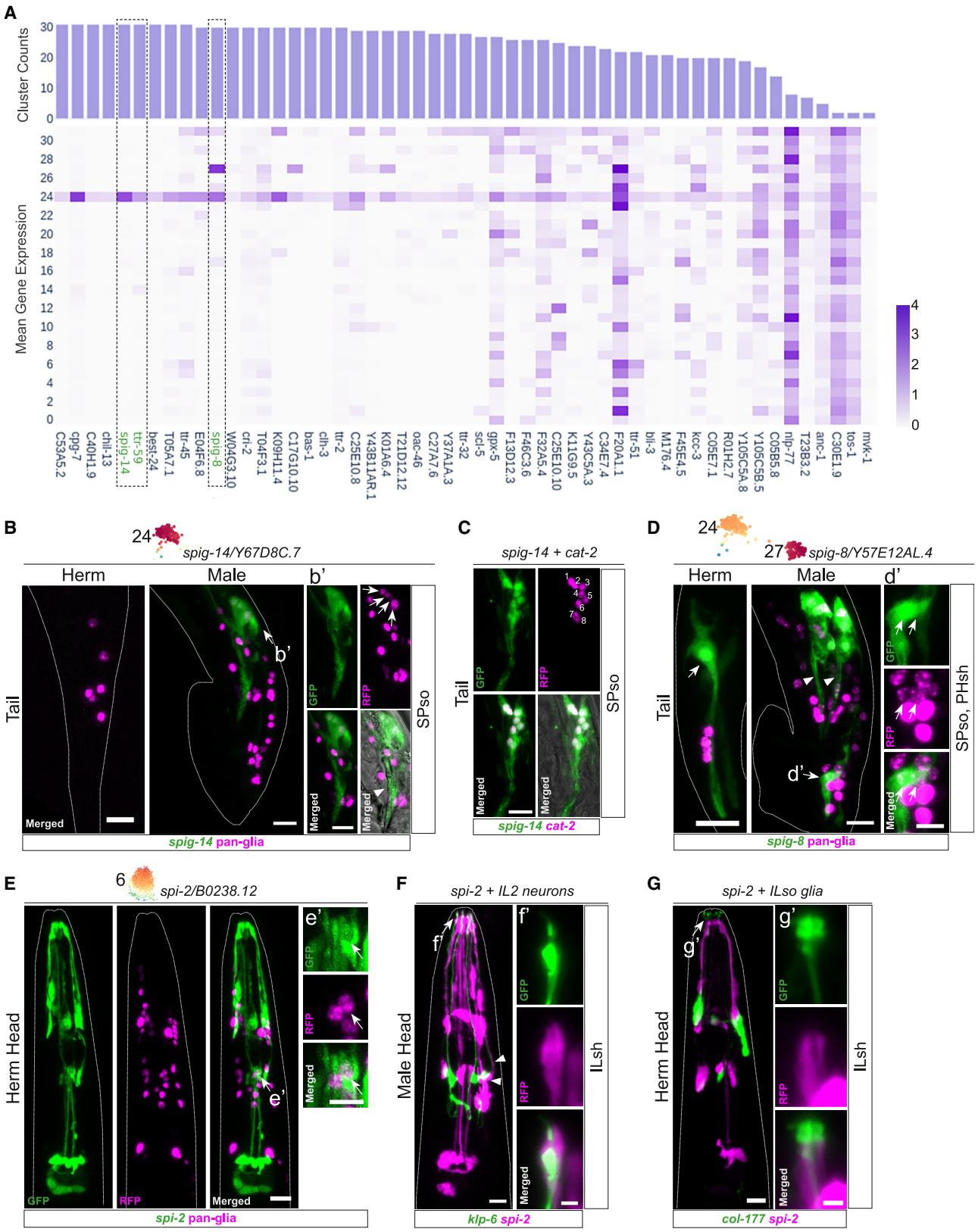

Figure 3. Identification of molecular markers for glial cell types

(A) PairDEx for male-specific cluster 24. Heatmap shows mean expression of genes (*x* axis) per cluster (*y* axis). Top histogram: number of times the gene was significantly different. Dotted outline and green font: genes validated *in vivo*. CEG *spig-8/Y57E12AL.4* for clusters 24 and 27.

(legend continued on next page)

Please cite this article in press as: Purice et al., Molecular profiling of adult *C. elegans* glia across sexes by single-nuclear RNA-seq, Developmental Cell (2025), https://doi.org/10.1016/j.devcel.2025.05.013

seam cells/cluster 13 (CEG *grd-10*),[101] posterior epithelial cells/cluster 14 (CEG *spig-15*), and male sense organ post-cloacal hypodermal cell (PCh)/cluster 20 (CEG *spi-3*) (Figures S3S–S3U)—all tissues that are known to express *mir-228*[90,102] (Figures S1B and S1C).

Pan-glial molecular signatures

Next, to define a pan-glial-specific molecular signature, we trained a machine learning model to classify glial/non-glial cells using imputed gene expression (Figure S4A) using a logistic regression model with sparsity constraints to identify a minimal set of genes that best distinguish glia versus non-glia. To ensure generalization, we trained our model on hermaphrodite data and tested it on male data, which achieved near-perfect accuracy (Figures S4A and S4B). This suggests that glial transcriptional identity is sex independent.

We next devised an iterative gene-ranking procedure to select a subset of genes that are predictive across the different glial cell types (see STAR Methods). The top 10 genes from this approach (Figure S4E) achieved near-perfect accuracy (>99% confidence) across all clusters, including those that are male specific (Figures S4B bottom and S4C). Importantly, no one gene expressed in all glia or was glial exclusive (Figure S4E), implying that no gene is pan-glial *and* glial exclusive.

We thus defined a "pan-glial signature"—a minimal gene set that distinguishes glial from non-glial cells. We tested all combinations of the top 10 genes identified above and found that a core set of 6 genes (Figure 4A; *col-34*, *gst-28*, *spig-16*, *glam-1*, *cnc-10*, and *glb-1*) classified all glial cells with >95% confidence (Figure S4D outline). We tested the robustness of this signature using independent datasets. When applied to an aging transcriptome atlas of *C. elegans*[86] (hereafter, "Roux dataset"), our pan-glial signature was able to successfully identify all 13 presumptively annotated glial cell types (Figure S4F; Mendeley Data). We integrated both datasets and re-ran the analysis, comparing our glia with non-glial cells from the Roux dataset because our non-glia fraction was limited. Analysis showed that 4 out of 6 genes of the pan-glial signature were retained as top genes in the classifier (Figures S4G and S4H). This objective, data-driven validation underscored the robustness of our dataset in reliably extracting glial properties and for annotating glia across datasets.

Glial TFs, channels, and transporters

We also examined expression of all predicted transcription factors (TFs) (wTF 3.0; 941 TFs, Table S1).[103] In *Drosophila*, the TF *repo* labels all glia. In *C. elegans*, all non-neuronal neuroectodermal cells, including glia, express LIN-26/C2H2 zinc finger TF during development,[104,105] but this was absent from our dataset. We also did not identify any other pan-glial TF. Rather, each TF is variably expressed across clusters (Figure 4B), suggesting that TFs may work in combination to maintain different adult glial functional modules.

Deeper analyses of the dataset yielded further insights into glial TF biology. The MAB-9/T-Box TF, which regulates the fate of the spicule progenitor B blast cell,[106] labeled the B cell-derived male-specific cluster 31/SPsh *in silico* (Figure 4B, outlined), and expressed in four adult *mir-228*$^+$ glia *in vivo* (Figure S4I), consistent with the binucleated syncytial SPsh glia. Thus, MAB-9 may play roles in SPsh glial function in the adult male. Further, although CEH-27/NK2 Hox and LIM-7/LIM Hox TFs labeled all 3 ILso and 3 OLso clusters (Figure 4B, dotted outlines), their expression levels varied reciprocally between these in both our (Figure S4J) and annotated Roux datasets (Figure S4K). This suggested that the ratio of expression between TFs may be one mechanism underlying glial heterogeneity.

A critical glial function is maintaining ion homeostasis and cell volume,[6,71,72,107–110] and different subsets of channels and transporters were variably expressed across individual glia (Figure 4C; Table S1). As expected, the K^+/Cl^- cotransporter *kcc-3* was expressed in multiple glia, including the AMsh[6] (Figure 4C, yellow box). The glutamate transporter *glt-1* expressed in CEPsh glia, which is associated with brain neuropil synapses[18] (Figure 1C) and also other sh glia that do not (Figure 4C, yellow box). Further, many sh glia expressed vacuolar H ATPases (*vha* genes) (Figure 4C, black asterisks), indicative of lysosomal degradation burden in these cells. Finally, mammalian astrocytes express aquaporin channels that transport water and small solutes.[111] We found that aquaporins expressed differentially across glia (Figure 4C, red asterisks). Mammalian astrocytic aquaporin-4 (AQP4) acts with the inward rectifier potassium channel Kir4.1 to regulate K^+ and water.[111,112] Of the three predicted inward rectifier potassium channels in the *C. elegans* genome,[113] *irk-3* enriched in a subset of glia (CEPsh, AMsh, PHsh, and PDEsh) both *in silico* and *in vivo* by a transcriptional reporter (Figures 4C, 4D, and S4L). Together, these findings suggested that each glial cell in *C. elegans* is a distinct cell type defined by a unique combination of TFs, channels, and proteins.

We next expanded our analyses to investigate how *C. elegans* glial profiles compared across human glial types.[41,114] We used web-based cell-type-specific enrichment analysis of genes (WebCSEA)[115] to uncover cell-type signatures using orthologous genes.[116] Globally, we observed broad enrichment of multiple

(B–G′) MAGIC[148] imputed expression illustrated for genes noted. Images are transcriptional GFP reporters *in vivo*. Dotted line, animal outline. (B) CEG *spig-14/Y67D8C.7* reporter expression. Close up of SPso in male tail depicts multinucleated GFP expression (b′, arrows) extending into the spicule (b′, arrowhead). Scale bars, 10 and 5 μM in (b′).

(C) *spig-14/Y67D8C.7* GFP and *cat-2* nuclear RFP reporters show colocalization in 8 nuclei. Scale bar, 5 μM.

(D) CEG *spig-8/Y57E12AL.4* reporter expression PHsh (arrows) across sexes, and male SPso (arrowheads). Zoom-in depicts $P_{mir\text{-}228}$:NLS:RFP co-expression with the GFP$^+$ male PHsh (d′, arrows). Scale bar, 10 and 5 μM in (d′).

(E) CEG *spi-2/B0238.12* reporter expression in putative arcade cells (bright) and RFP$^+$ cells (dim) (e′, arrow). Scale bar, 10 and 5 μM in (e′).

(F) *spi-2/B0238.12* mScarlet$^+$ and inner labial (IL2) neuron GFP$^+$ reporters. Close interactions between the two cell types observed (arrowheads). Zoom-in (F′) shows single GFP$^+$ IL2 dendritic tip apposing mScarlet$^+$ ILsh glia. Scale bar, 10 and 1 μM in (F′).

(G) *spi-2/B0238.12* mScarlet$^+$ and *col-177* reporters. Zoom-in (g′) shows single GFP$^+$ ILso glial projection apposing mScarlet$^+$ ILsh glia. Scale bar, 10 and 1 μM in (G′).

Please cite this article in press as: Purice et al., Molecular profiling of adult *C. elegans* glia across sexes by single-nuclear RNA-seq, Developmental Cell (2025), https://doi.org/10.1016/j.devcel.2025.05.013

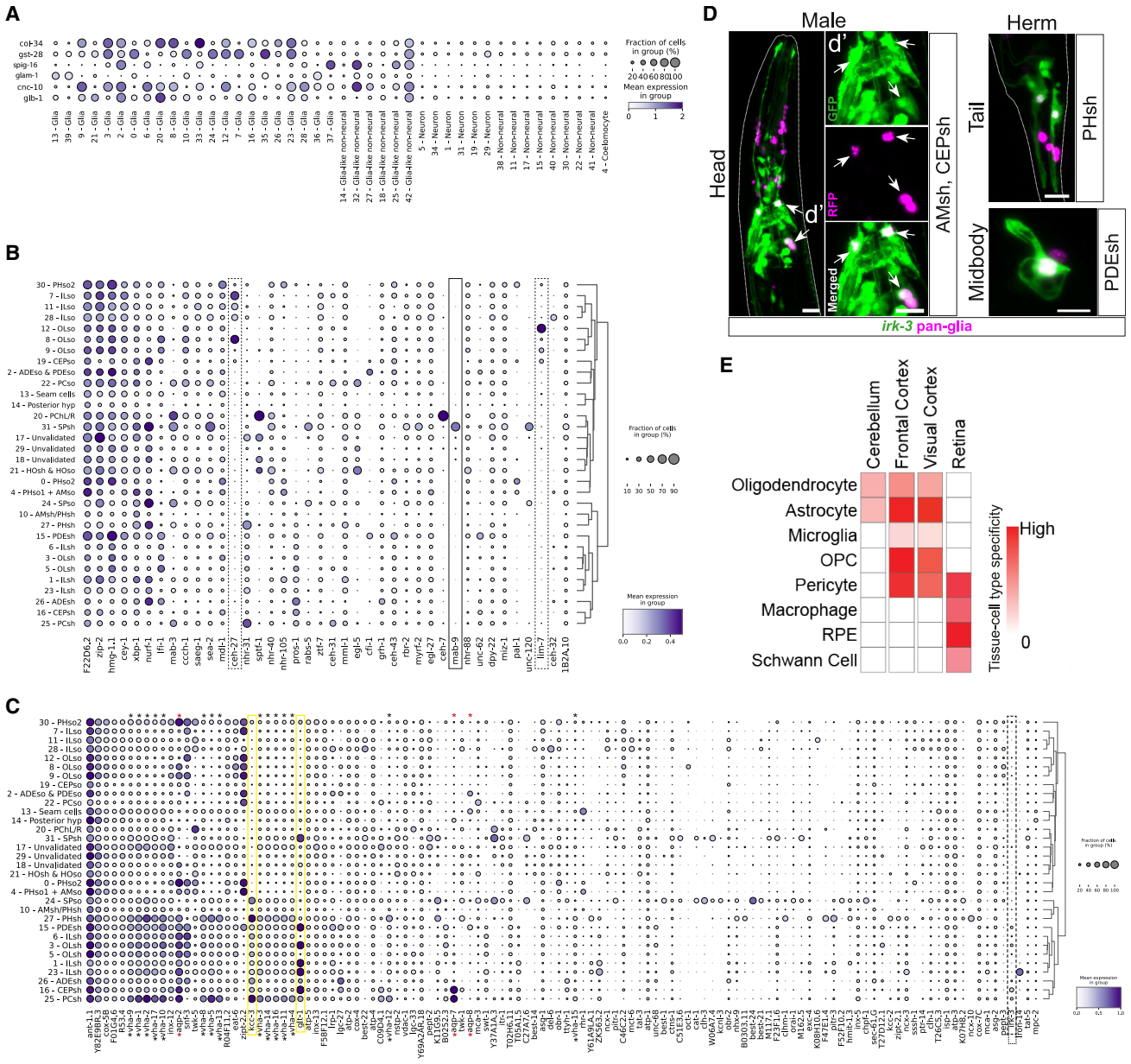

Figure 4. Molecular characteristics of *C. elegans* glia

(A–C) Dot plots showing expression of the (A) six-gene pan-glial signature, (B) predicted TF expression, and (C) predicted ion channels and transporters. Color intensity indicates mean expression in the cluster, dot size indicates fraction of cells expressing the gene. (B) Black box: *mab-9*; dashed box: *ceh-27* and *lim-7*. (C) Yellow box: *kcc-3* and *glt-1*; black asterisks: *vha* genes; red asterisks: aquaporins; dashed black line: *irk-3*.

(D and D′) *irk-3* transcriptional reporter expression, including CEPsh (d′, top arrows), AMsh (d′, bottom arrow), PHsh, and PDEsh. Scale bars, 10 μM, except PDEsh panel scale bar, 2 μM.

(E) Enrichment of *C. elegans* glial genes in different human glia/glia-like cells. Uncorrected *p* value < 0.05. Heatmap color is proportional to the tissue-cell-type specificity of inquiry gene list.

glia/glia-like cell types (Figure 4E; Table S3). At the individual glial level, CEPsh glia, which transcriptionally resemble mouse astrocytes,[18] also showed a similar transcriptional profile to human astrocytes (Figure S4M). In addition, CEPsh also displayed an analogy to oligodendrocytes, consistent with their posterior processes enwrapping axons (Figure 1C) and expressing HLH-17, an ortholog of the oligodendrocyte differentiation gene Olig2.[69,96,117] Similarly, we uncovered relatedness between AMsh glia and astrocytes (Figure S4N; Table S3), which tracks that both glial cell types express genes like thrombospondin and KCC-3 and engulf neuronal fragments.[5,6,93,118–120] These feature analogies are likely non-random, as, for example, ADEsh glia did not exhibit similar relatedness to any glial class but were broadly related to all neuroectoderm glia (Figure S4O; Table S3). In summary, these results indicate that each *C. elegans* glia has a combinatorial functional relatedness with subsets of human glia.

Please cite this article in press as: Purice et al., Molecular profiling of adult *C. elegans* glia across sexes by single-nuclear RNA-seq, Developmental Cell (2025), https://doi.org/10.1016/j.devcel.2025.05.013

CellPress
OPEN ACCESS

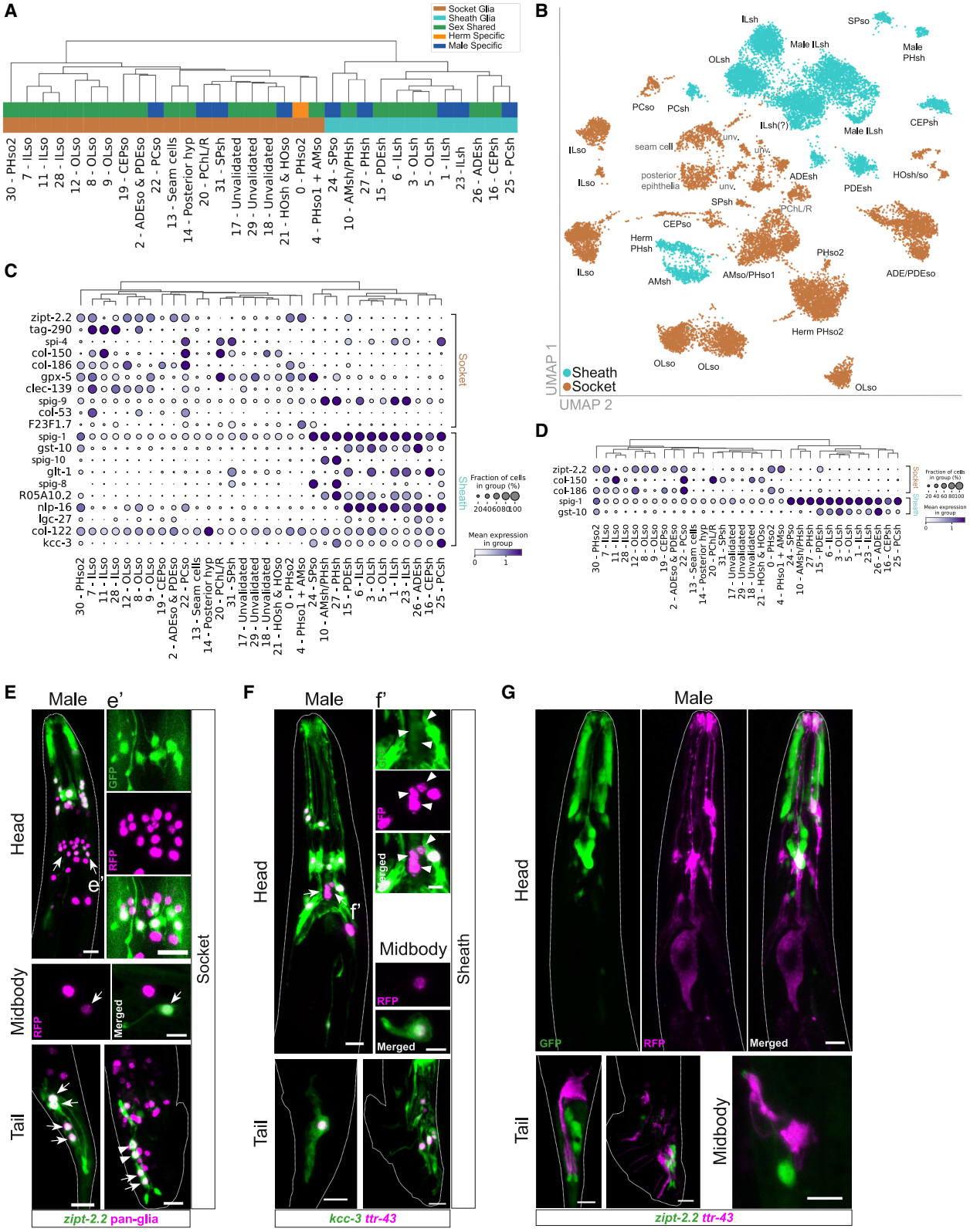

Figure 5. Identification of glial class signatures

(A) Hierarchical clustering of glial clusters.

(B) UMAP colored by glial class.

(legend continued on next page)

Please cite this article in press as: Purice et al., Molecular profiling of adult *C. elegans* glia across sexes by single-nuclear RNA-seq, Developmental Cell (2025), https://doi.org/10.1016/j.devcel.2025.05.013

Glial class signatures

We next leveraged our glial transcriptome dataset to probe molecular phylogeny between different glia. We performed hierarchical clustering of all glial clusters and found that they segregated into two distinct groups: sh and so (Figures 5A and 5B). Thus, glia cluster by functional relatedness and not proximity within a sense organ (sh and so of each organ), regional proximity in the body plan, or developmental lineage.[79] Two male-specific glia were the only outliers to this molecular phylogeny. One, the spicule sh (SPsh) and SPso glia clustered with the opposite groups (Figures 5A and 5B). Two, hook sh/so (HOsh/so), glia which co-clustered together (cluster 21), grouped with so glia (Figure 5A). The HOsh/so are the only glia to cluster together by sense organ, and this is the only glia-containing organ to not be laterally symmetric.[77] Lastly, like the epithelial clusters (clusters 13, 14, and 20), the three unvalidated clusters (clusters 17, 18, and 29) also segregated with the so glia, hinting at shared so glial-epithelial functions.

Do sh and so glia across sense organs share molecular signatures that define them as distinct cell classes? We adapted the pan-glial signature binary classification model to distinguish between sh and so clusters (Figure S5A). This model achieved near-perfect accuracy in distinguishing between sh and so cells across sexes, suggesting that sh versus so identity is sex agnostic (Figure S5B). Seven genes in each glial group were sufficient to predict each sh and so type with >99% accuracy (Figures 5C and S5C). A combination of three genes (*zipt-2.2*, *col-150*, and *col-186*) could achieve >99% accuracy in annotating so clusters (Figures 5D, S5C, and S5D). For sh glia, *spig-1* predicted most sh clusters and inclusion of *gst-10* achieved >99% accuracy (Figures 5D, S5C, and S5D). To obtain additional genes that mimic the expression of the minimal set that was derived using sparsity constraints, we retrained our classification model with non-sparsity-inducing regularization (see STAR Methods). This identified multiple genes broadly expressed in either so or sh clusters (Figure S5F). Genes like *col-34* and *col-186* resembled expression patterns of *zipt-2.2*. Of the genes resembling pan-sh expression like *spig-1* (Figure S5F), *kcc-3*, *spig-9*, and *glt-1* had previously been reported as glia enriched.[6,18,121]

To validate these findings *in vivo*, we selected *zipt-2.2* as proof of concept (Figure S5C). Its transcriptional reporter expressed in the easily detectable AMso, PHso1/2, and PDEso, as well as labeling 22–24 cells in hermaphrodite heads, 20 of which are glia (Figures 5E and S5E). We concluded that *zipt-2.2* labeled all 26 hermaphrodite so glia. Expression was also observed in epithelia and excretory duct cells *in vivo* (Figure S5I). In males, expression was also seen in PCso and HOso glia and so glia-derived neurons (Figures 5F and S5I).

For sh glia, we curated *spig-1*, *ttr-43*, and *kcc-3* for validation by transcriptional reporters. Extrachromosomal transgenic arrays for these were unstable but expressed consistently in AMsh, CEPsh, PHsh glia, glia around the anterior pharyngeal bulb, and male R*n*st and other tail glia (Figure S5J). No expression was seen in PHso1/2 or AMso cells (Figure S5J, arrowheads). Both *kcc-3* and *ttr-43* colocalized broadly across sh glia, with *kcc-3* lacking expression in few glia anterior to CEPsh (Figure 5F). Cell counting of P_{ttr-43}:mScarlet$^+$ cells that were also $P_{mir-228}$:GFP$^+$ in hermaphrodites identified 24 cells, as expected for a pan-sh glia marker (Figure S5E). These validations confirmed that *ttr-43* is a pan-sh-glia marker. Further, we generated stably integrated double-transgenic animals with so glia labeled by $P_{zipt-2.2}$:GFP and sh glia with P_{ttr-43}:mScarlet. These reporters did not overlap in expression (Figure 5G).

Three further observations independently corroborated sh and so glia as distinct cell types. One, GO analyses[122,123] of sh-glia-enriched terms included transporter activity, transmembrane transport, and ion homeostasis (Figure S5G), whereas so terms enriched for cuticle, regulation of proteolysis, and guidance of neuronal projections (Figure S5H). Two, hierarchical clustering showed that so glia are molecularly more related to neuronal and epithelial cell clusters than sh glia are (Figure S5K). Lastly, WebCSEA[115] analysis of differentially expressed genes in sh or so glia indicated that sh glia related to astrocytes and OPCs in the cortex and RPE in the retina, whereas so glial signatures were broadly enriched across multiple glial types (Figure S5L). Thus, both *in silico* and *in vivo* reporter studies showed that sh and so glia are distinct cell types, with different functions and molecular attributes.

C. elegans glia are variably sex dimorphic

Having both sexes in our annotated transcriptome enabled analysis of sex-specific differences in glial cells with single-cell and single-gene precision. Because sex is transcriptionally encoded in *C. elegans*,[124] we investigated whether any TFs were expressed in a sex-specific manner. Differential gene expression analysis uncovered that TFs like MDL-1/MAD and CEY-4/Y-box were upregulated in hermaphrodite glia (Figures 6A and S6A). In corollary, MAB-3/Doublesex, expressed in male intestines and neurons,[125] also expressed in male glia (Figures 6A and S6B). Further, of the sex-determination TFs, only the feminizing TRA-2 TF expressed in one of the three OLso (sex-shared) glial clusters (cluster 9), with higher expression in male cells (Figures 6B, 6C, and S6C), indicating potential "feminization" of a subset of male OLso glia. Thus, anatomically sex-shared glia have differing and molecularly dimorphic TF expression profiles.

These analyses also identified molecular sex dimorphism in the sex-shared PHsh and OLsh glia not previously predicted by

(C) Dot plot of the top 14 genes distinguishing sh/so clusters.
(D) Minimal gene set that predicts sh and so types with >99% accuracy.
(C and D) Dot plot color and size as per Figures 4A–4C.
(E–G) Transcriptional GFP reporters *in vivo*. (E) *zipt-2.2* reporter expression in several so cells. High expression in ILso and AMso, anterior RFP$^+$ cells. Increased GFP intensity in dimly expressing glia (arrows, e′), most likely CEPso and OLso. Expression in the midbody PDEso, hermaphrodite PHso1/PHso2, male PHso2 (arrows), and PHD neurons (arrowheads). Scale bars, 10 μM except for midbody, where scale bar, 5 μM. (F) sh *kcc-3* GFP$^+$ and *ttr-43* mScarlet$^+$ reporters showing overlapping expression, except the region anterior to the CEPsh (arrows) and (f′, arrowheads). Expression also observed in the PDEsh, PHsh glia in both sexes, and male ray glia. Scale bars, 10 μM, except for midbody and (f′), where scale bars, 5 μM. (G) *zipt-2.2* GFP$^+$ and *ttr-43* mScarlet$^+$ reporters showing non-overlapping expression. Scale bars, 10 μM, midbody image scale bar, 5 μM.

Please cite this article in press as: Purice et al., Molecular profiling of adult *C. elegans* glia across sexes by single-nuclear RNA-seq, Developmental Cell (2025), https://doi.org/10.1016/j.devcel.2025.05.013

CellPress
OPEN ACCESS

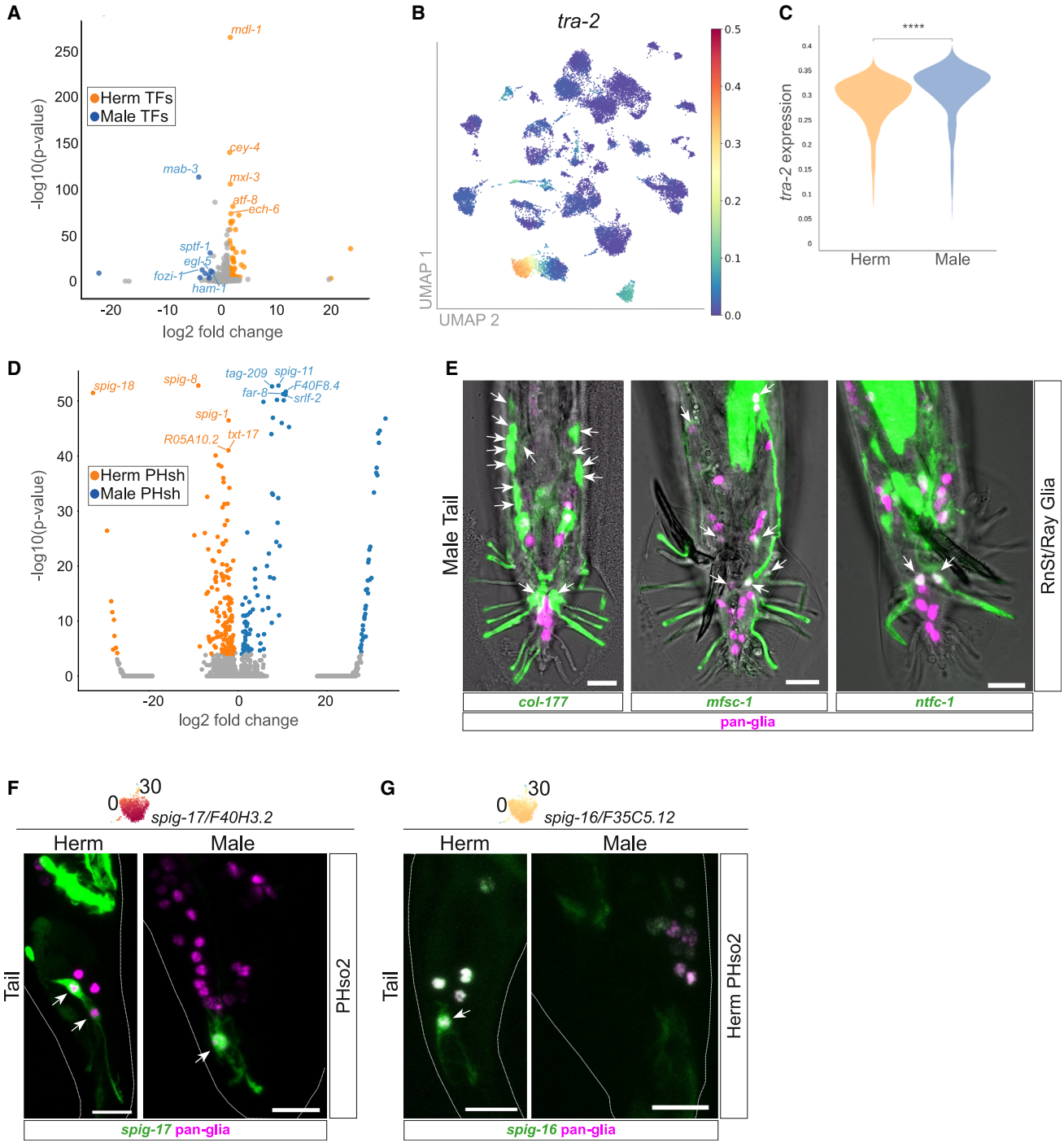

Figure 6. *C. elegans* glia are variably sexually dimorphic

(A) Volcano plot (t test) of sex-specific TFs. Top 5 genes labeled.

(B) UMAP showing imputed expression of *tra-2*.

(C) Differential gene expression of *tra-2* between sexes. ****$p < 1e{-}4$ (t test).

(D) Volcano plot (t test) of PHsh glial gene expression by sex. Top 5 genes labeled.

(E–G) Transcriptional reporter images *in vivo*. (E) GFP reporters for *col-177*, *mfsc-1/T27D12.1*, and *ntfc-1/Y71H10B.1* depicting expression in various combinations of ray glia (arrows). (F) CEG *spig-17/F40H3.2* GFP reporter expression in PHso2 of both sexes. (G) CEG *spig-16/F35C5.12* GFP reporter expression in PHso2 of hermaphrodites but not males. (F and G) MAGIC[148] imputed expression illustrated for all genes. Dotted line, animal outline. All scale bars, 10 μM.

Please cite this article in press as: Purice et al., Molecular profiling of adult *C. elegans* glia across sexes by single-nuclear RNA-seq, Developmental Cell (2025), https://doi.org/10.1016/j.devcel.2025.05.013

anatomy. The PHsh *vap-1*$^{-}$ subcluster in cluster 10 was nearly exclusively comprised of hermaphrodite cells (Figures S2C and S6D), whereas male PHsh glia mapped to cluster 27 (Figures 3A, 3D, and S3D). Thus, the anatomically identical PHsh glia are molecularly sex dimorphic. Differential gene expression and GO analysis of PHsh glia between sexes showed several sex-specific genes (Figure 6D) and divergent GO profiles (Figure S6F). Similarly, two of the four ILsh clusters (clusters 1 and 23) were male specific (Figure 2B), despite no sex dimorphism previously reported for this sense organ. These findings provide molecular insights into sex-specific glia and previously unrecognized molecular sex dimorphism in anatomically identical *C. elegans* glia.

Our validations identified clusters for all male-specific sh/so glia (Figure 2A) (Table S1) but not the R*n*st (nine bilaterally symmetric R*n*st, *n* = ray numbers 1–9). Consistent with the presumed dual sh-so features of R*n*st,[98] reporters for multiple sh (*ttr-43*, *kcc-3*, and *spig-1*) and some so markers (*col-177*), but not others (*zipt-2.2*), expressed in all R*n*st glia (Figures 5E, 6E, and S5J). The only known ray glial gene, *ram-5*[126] expressed in multiple so and sh glia (Figure S6H). Further, reporters for CEGs for different glial clusters expressed differentially in subsets of R*n*st glia *in vivo* (Figures 6E, S2J, and S6G). Although it is possible that lack of an R*n*st cluster/s reflected technical limitation (poor tissue dissociation), these expression patterns lead us to favor the model that, like ray neuron and ray sense organ functions,[98] R*n*st glia are also not equivalent. Rather, they each are molecularly heterogeneous and may have individually clustered with the glia they were most functionally related with.

We next examined the four sex-shared glia with anatomically dimorphic features. The CEPsh/CEPso glia associate with embryonically born CEM neurons only in males.[55,60,72,127,128] However, we found no sex dimorphism for the sex-shared CEPsh/cluster 16 (49.72% male cells) or CEPso/cluster 19 (25% male cells) glia (Figures 2A and S2A). Thus, interaction with a sexually dimorphic neuron does not cause persistent molecular changes in CEPsh/so. Similarly, the AMso of both sexes coalesce into one cluster (Figures 2F and S2G). Finally, PHso2 serves as the male PHso analog to hermaphrodite PHso1,[79,129] and CEGs from the sex-shared AMso/PHso1 cluster also mark male PHso2, suggesting functional molecular convergence. Instead of a male-specific PHso2 cluster, we found the sole hermaphrodite-specific cluster 0/sex-shared cluster 30 to map to PHso2 (Figure 2A). Further, reporters for some CEGs marked PHso2 of both sexes and others only marked hermaphrodite PHso2 (Figures 6F, 6G, S6I, and S6J). We inferred that the hermaphrodite PHso2 is molecularly distinct from male PHso2/hermaphrodite PHso1. These results show that adult glial cells exhibit variable sex dimorphism without following anatomical or sex-determination patterns.

Glia lack the canonical DCV release protein UNC-31/CAPS

Our glial transcriptome included multiple neuropeptide genes (Figures 5C, S7A, and S7B; Table S1). Extending prior reports of predicted glial neuropeptide signaling,[83,84] we confirmed *in vivo* expression of the neuropeptide NLP-16 in glia (Figure S7B). A major mechanism of neuropeptide release is through Ca^{2+}-dependent secretion of dense core vesicle (DCV), mediated by the CAPS protein.[130,131] However, the sole *C. elegans* UNC-31/CAPS was absent in our dataset (Figure 7A). Co-labeling of a P_{unc-31}:GFP transcriptional reporter with the pan-glial $P_{mir-228}$:NLS:RFP confirmed this *in vivo*, consistent with prior reports of UNC-31 expression only in neurons and vulval muscles.[130,131] We did find *unc-31* expression in glia-derived male MCM and PHD neurons (marked by persisting $P_{mir-228}$:NLS:RFP expression) (Figure 7B), indicating that lack of *unc-31* expression is a feature of the glial transcriptional profile. Previous studies have shown glial neuropeptide signaling roles in aging and in response to endoplasmic reticulum (ER) stress.[83,84] However, we found no *unc-31* expression in glia in either aged (day 8) animals or animals subjected to ER stress (Figures S7F, S7H, and S7J). Thus, unlike neurons, glia do not deploy UNC-31 as primary release machinery in either healthy, aged, or ER-stressed adult animals.

This led us to examine other regulators of neuropeptide processing in our datasets. Neuropeptide precursors are first cleaved by proprotein convertases (primarily *egl-3* in neurons but also *kpc-1*, *bli-4*, and *aex-5*).[132,133] Like *unc-31*, *egl-3* was not expressed in any *mir-228*$^{+}$ glia *in vivo* but expressed in *mir-228*$^{+}$ glia-derived male-specific neurons (Figures 7C and 7D). Also, like *unc-31*, *egl-3* expression remained absent from glia of aged or ER-stressed adult animals (Figures S7G, S7I, and S7J).

How do glia process neuropeptides? Two of the remaining three convertases encoded in the *C. elegans* genome, *kpc-1* and *bli-4*, were present in our dataset, and we confirmed glial expression of *bli-4 in vivo* (Figures 7E, 7F, and S7C). Cleaved pro-peptides are edited by carboxypeptidases (mainly *egl-21* in neurons but also *cpd-1* and *cpd-2*), then amidated (by enzymes *pamn-1*, *pghm-1*, and *pgal-1*) and packaged for release.[131,133,134] We found low expression of the carboxypeptidase cpd-1 (Figure S7C) and amidation enzymes (*pamn-1*, *pghm-1*, and *pgal-1*) (Figure S7D) in our glia data. Finally, neuropeptide signals are degraded by different enzymes,[133] multiple of which expressed variably in our dataset (*tpp-2*, *dpf-1*, *dpf-2*, and *acn-1*) (Figure S7E). Together, these results show that although glia express neuropeptides, they process and release these via mechanisms analogous to, but distinct from, neurons.

DISCUSSION

This study reports the complete and validated molecular census of adult neuroectoderm glia of a metazoan, spanning both sexes. By combining snRNA-seq profiling with bespoke computational approaches and *in vivo* validations, we defined pan-glial and glial class signatures, providing molecular markers and mechanistic insights for previously uncharacterized glia. Complementing prior neuronal scRNA-seq,[45,70] this transcriptome establishes *C. elegans* as the first animal with all neural cells (glia and neuron) profiled and annotated.

The molecular profile of glia of an adult nervous system by sex

This molecular map (wormglia.org) provides comprehensive, brain-wide insights into glial biology at the molecular and single-cell levels. All *C. elegans* developmental lineages and glia: neuron contacts are invariant,[58,59] the connectome is mapped in both sexes,[61] and neurons profiled by sex.[45,70] This validated glial transcriptome thus provides unparalleled power to map glial molecular heterogeneity onto functional consequences. Further,

Please cite this article in press as: Purice et al., Molecular profiling of adult *C. elegans* glia across sexes by single-nuclear RNA-seq, Developmental Cell (2025), https://doi.org/10.1016/j.devcel.2025.05.013

CellPress
OPEN ACCESS

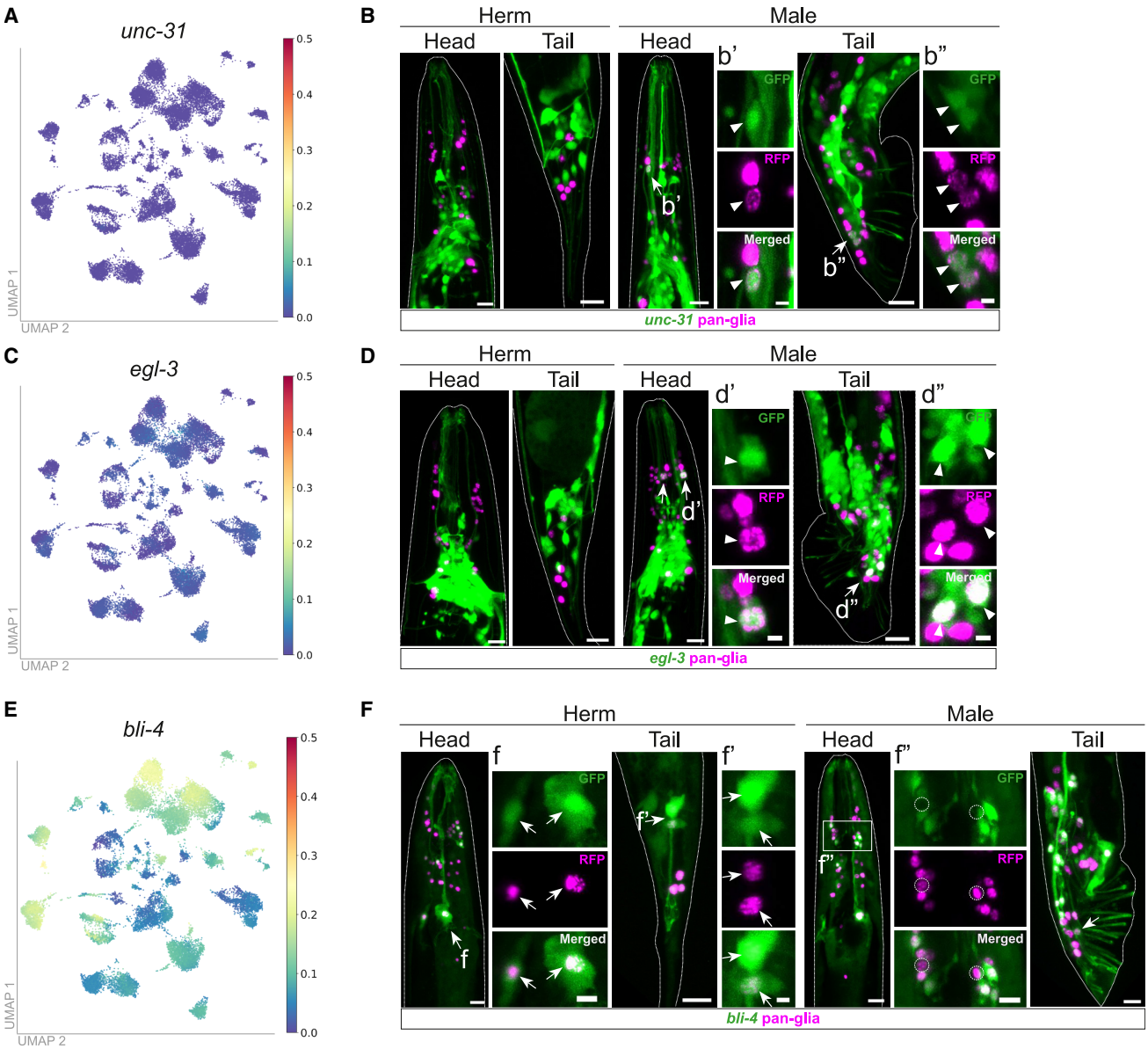

Figure 7. Glia lack canonical neuropeptide processing release mechanisms

(A, C, and E) UMAP showing imputed expression of *unc-31* (A), *egl-3* (C), and *bli-4* (E). MAGIC[148] imputed expression illustrated for all genes.

(B, D, and F) Transcriptional reporter images *in vivo*. Dotted line, animal outline. (B) *unc-31* reporter expression does not overlap with $P_{mir\text{-}228}$:NLS:RFP$^+$ cells of either sex, except male MCM/PHD neurons (arrows). (b′) *unc-31* expression in MCM neuron (b′, arrowhead) but not AMso glia above; (b″) PHD neuron (arrowheads). Scale bars, 10 μM, except (b′) and (b″) scale bars, 2 μM. (D) *egl-3* reporter expression does not overlay with $P_{mir\text{-}228}$:NLS:RFP$^+$ cells of either sex, except male MCM/PHD neurons (arrows). (d′) *egl-3* in the MCM neuron (arrowhead) but not the AMso glia above it; (d″) PHD neurons (arrowheads). Scale bars, 10 μM, except (d′) and (d″) scale bars, 2 μM.(F) *bli-4* reporter expression overlaying with pan-glial $P_{mir\text{-}228}$:NLS:RFP$^+$ cells (arrows). (F–F″) *bli-4* expression in AMsh glia (F); PHsh glia (f′); predicted IL/OLsh glia, but not all RFP$^+$ cells in the head (circles) (f″). No expression is observed in the predicted ILso glia above the box in the male head (f″). Male tail: PHsh glia (arrow) and all ray glia expression. Scale bars, 10 μM, except (f–f″) where scale bars, 5 μM.

our computational signatures can annotate glia across transcriptomic datasets, allowing for rapid and directed inquiry of glia across contexts.[45,85,86,135]

These studies identified four *in vivo*-validated features of glial biology. First, each glial cell in this animal is molecularly distinct, demonstrating extensive molecular heterogeneity across the nervous system. Two, glia group by functional relatedness, not developmental lineage or physical proximity. Three, each glia is variably sex dimorphic, with different mechanisms likely defining this dimorphism in every glial cell. Four, glia release neuropeptides via machinery distinct from that used by neurons.

Computational approaches to dissect glial molecular heterogeneity

Differential gene expression analysis identifies enriched genes in single-cell data but lacks penalties for multi-cluster gene

Please cite this article in press as: Purice et al., Molecular profiling of adult *C. elegans* glia across sexes by single-nuclear RNA-seq, Developmental Cell (2025), https://doi.org/10.1016/j.devcel.2025.05.013

expressions, making it less reliable for differentiating between homotypic cells. PairDEx, a pairwise differential analysis procedure reported and validated in this study, enabled us to define unique CEGs that differentiate between related glia. We anticipate that PairDEx will be a broadly applicable protocol to define any related clusters in single-cell -omics datasets. Further, we employed logistic regression models to identify pan-glial, sh, and so signatures. Several features together ensured the accuracy, robustness, and generalizability of our approach (see STAR Methods). Like PairDEx, this classification model can be broadly applied to derive gene sets that identify user-defined groups of clusters across single-cell datasets (see "data and code availability" section for information/tutorials).

C. elegans neuroectodermal glia are comprised of two distinct classes

We identified a pan-glial signature for neuroectoderm-lineage glia, comprising six genes, that is robust across datasets, as well as signatures for both glial classes. These signatures were based on gene expression alone and were independent of their gene function. That sh and so glia have distinct signatures computationally and *in vivo*, and so glia resemble epithelial cells, indicates that *C. elegans* neuroectodermal glia are comprised of two functionally and molecularly distinct glial types. We posit that these two glial classes are likely specified via distinct developmental programs rather than deriving from a common basal "pro-glial" state.

We also note that although we validated all sex-shared neuroectoderm glia, three sex-shared clusters (17, 18, and 29) remain unmapped and three epithelial clusters (13, 14, and 20) had so glia-like profiles. The relatedness of so glia with epithelial cells suggests shared molecular functions, tracking prior granular studies,[55,69,136] and may explain why developing a marker for all so glia or all glia without labeling epithelial cells is not feasible. Together, we infer that in *C. elegans* some epithelia and other cell types may execute glial-like functions. This mixed fate is reminiscent of mammalian glia-like RPE cells of the retina and radial glia.[137–139] Whether this reflects multifunctional cell types or evolutionary adaptation of the animal having fewer glial cell numbers remains to be determined.

Glial heterogeneity and sexual dimorphism

Glia within each class exhibited molecular heterogeneity in their expression profiles of TFs, transporters, and neuropeptide processing factors. This tantalizingly suggests that each glial cell, rather than glial type, may have a combinatorial identity selector program that builds its functional trait, like neuron fate specification.[140] The molecular markers derived from this molecular map provide valuable tools to examine glial fate specification and functional differences. This study also underscores the importance of examining these features at single-glia resolution.

This glial transcriptome identifies a surprisingly complex molecular map of glia across both space and time. For example, all ILso are anatomically equivalent and generated by symmetric lineages but segregate into three clusters, in accord with their embryonic progenitors likely being non-equivalent.[65] Further, the male R*n*st may be non-equivalent. The implied functional heterogeneity of this awaits inquiry. Finally, we note that none of the embryonic genes expressed by CEPsh glia that are required for nerve ring assembly (*kpc-1*, *chin-1*, *unc-6*, and *mab-20*)[141] appear enriched in adult CEPsh.

Our data found that *C. elegans* glia have varying degrees of molecular sexual dimorphism, independent of their anatomical or dimorphic features. This dimorphism can also vary temporally: some sex-shared glia show dimorphic expression of certain factors during development,[55] whereas others retain expression of sex-determination factors into adulthood (this study). If true evolutionarily, it may explain why studies of glial sexual dimorphism are challenging in other systems.[48,142,143] This transcriptome provides a powerful single-cell resolution platform to interrogate the molecular mechanisms and regulatory processes underlying glial sex dimorphism.

Glial neuropeptide processing

Neuropeptides are a diverse class of signaling molecules.[144] Although glia across mammals and *C. elegans* express neuropeptides, how these are processed remains unclear.[83,145] Our studies on glial neuropeptides and neuropeptide processing machinery demonstrate that glia regulate these processes differently from neurons. How and why different glia do so differently will be an exciting avenue for future study.

Molecular signature of *C. elegans* glia and their similarity to mammalian glia

Most *C. elegans* glial genes enrich in human glia,[69,117,146] highlighting the evolutionary conservation of molecular pathways. Although WebCSEA[115] is limited by scarcity of adult brain datasets, and our dependency on OrthoList2[116] to capture accurate orthologs may introduce additional constraints, the analogies are suggestive, nonetheless. The resemblance of individual *C. elegans* glial cells to various combinations of human glia suggests potential shared functions. This also leads us to speculate that unlike each human glial subtype with dedicated functions, each *C. elegans* glia may combine multiple functional molecular modules in varying ways to account for fewer numbers of available dedicated glia.

Limitations of the study

As with all single-cell transcriptomic studies, ours is also limited by 3′ sequencing bias, potential loss of low-abundance transcripts, and a lack of information on isoform-specific gene expression. We note that lack of a transcript is uninformative unless validated *in vivo* (e.g., *unc-31* and *ptr-10*). Further, CEG transcriptional reporters are extrachromosomal mosaic arrays. Like all such studies in *C. elegans*, these can vary by copy number, fluorescence reporter perdurance, and brightness. For example, CEG *spi-2* expresses brightly in arcade cells and lowly in ILsh glia by GFP, but the ILsh glia are easily identified with mScarlet. Finally, our high-throughput transcriptional reporters may have missed relevant enhancer elements.

RESOURCE AVAILABILITY

Lead contact

Further information and reasonable requests for resources and reagents should be directed to, and fulfilled by the lead contact, Aakanksha Singhvi (asinghvi@fredhutch.org), and co-corresponding author, Manu Setty (msetty@fredhutch.org).

Materials availability

Plasmids and strains generated in this study are available, without restriction, by contacting Aakanksha Singhvi (asinghvi@fredhutch.org).

Data and code availability

- Raw and processed snRNA-seq dataset of males and hermaphrodites are available on the Gene Expression Omnibus (GEO) accession number: GEO: GSE256266 (https://www.ncbi.nlm.nih.gov/geo/query/acc.cgi?acc=GSE256266).
- Jupyter notebooks for reproducing figures in the manuscript are available at https://github.com/singhvilab/glia-atlas-reproducibility. Jupyter notebook tutorials for pairwise differential analysis, classification model, and gene ranking are available at https://github.com/settylab/worm-glia-atlas.[147]
- Mendeley data: PairDEx related to Figures 2 and 3, and Purice et al. pan-glial signature versus Roux et al.[86] at days 1, 5, and 11 related to Figure 4, were deposited on Mendeley (doi: https://doi.org/10.17632/sfnrgj5y4c.1)
- Any additional information required to reanalyze the data reported in this work paper is available from the lead contact upon request.

ACKNOWLEDGMENTS

We thank the Singhvi and Setty labs for discussions and comments on this manuscript, Robert Waterston and Chau Huynh for early discussions on dissociation protocols, and Sam Minot for discussions on the online portal. We thank the Shai Shaham, Erik Jorgensen, Jessica Tanis, Nicholas Lehrbach, Jihong Bai, Linda Buck, Jim Priess, Emily Hatch, and Keith Nehrke laboratories for generously sharing reagents or equipment. This work was funded by a Washington Research Foundation Postdoctoral Fellowship and NIH-T32 in Interdisciplinary Training Grant award (5T32CA080416-25) to M.D.P., NIH-T32 in Biological Mechanisms of Healthy Aging Training Grant award (5T32AG066574-04) to L.J.S., NIH-T32 Cellular and Molecular Biology Training Grant award (T32 GM007270) and NSF-GRFP (1000321739) to V.S., and NIH/NIGMS R35GM147125 to M.S. This work was funded by Simons Foundation/SFARI grant (488574), Esther A. & Joseph Klingenstein Fund and the Simons Foundation Award in Neuroscience (227823), Brain Research Foundation Seed Grant (BRFSG-2023-10), and NIH/NINDS funding (NS114222) to A.S. This work was performed while A.S. was a Glenn Foundation for Medical Research and AFAR Junior Faculty Grant Awardee. A.S. is sincerely thankful to philanthropic donors for their support to her laboratory. Some work was performed in the Cellular Imaging (RRID:SCR_022609), Flow Cytometry (RRID:SCR_022613), and Genomics & Bioinformatics Shared Resources (RRID:SCR_022606) of the Fred Hutch Cancer Center/University of Washington/Seattle Children's Cancer Consortium (P30 CA015704). Some strains were sourced from the CGC, funded by NIH Office of Research Infrastructure Programs (P40 OD010440). This work also relied on information curated at WormBase, including the reference *C. elegans* genome WormBase WS280, funded by NIH U24 HG002223.

AUTHOR CONTRIBUTIONS

M.D.P., A.S., and M.S. conceptualized all aspects of this study. M.D.P. performed all snRNA-seq experiments and validations, with R.S.M., N.-T.T., and L.J.S. assisting on transgenic reporter constructions. V.S. assisted in sorting male animals. M.D.P. and A.S. wrote the manuscript, with E.J.A.Q., C.F., and M.S. writing the computational methods sections, and M.S. helped edit the manuscript. E.J.A.Q. and C.F. performed the computational analyses under primary supervision from M.S. and conceptual inputs from M.D.P. and A.S. F.W. performed preprocessing of fastq data. M.Z. created the wormglia.org portal. M.D.P., A.S., M.S., R.S.M., and E.J.A.Q. analyzed all results.

DECLARATION OF INTERESTS

The authors declare no competing interests.

STAR★METHODS

Detailed methods are provided in the online version of this paper and include the following:

SUPPLEMENTAL INFORMATION

Supplemental information can be found online at https://doi.org/10.1016/j.devcel.2025.05.013.

Received: May 21, 2024
Revised: November 14, 2024
Accepted: May 22, 2025

REFERENCES

1. View of Astrocytes. Cerebrum Dana Forum Brain Sci. 2016, cer-12-16.
2. Herculano-Houzel, S., and Dos Santos, S. (2018). You Do Not Mess with the Glia. Neuroglia *1*, 193–219. https://doi.org/10.3390/neuroglia1010014.
3. Duan, Duo, Zhang, Hu, Yue, Xiaomin, Fan, Yuedan, Xue, Y., Shao, J., Ding, G., Chen, D., Li, S., Cheng, H., et al. (2020). Sensory Glia Detect Repulsive Odorants and Drive Olfactory Adaptation. Neuron *108*, 707–721.e8. https://doi.org/10.1016/j.neuron.2020.08.026.
4. Han, L., Wang, Y., Sangaletti, R., D'Urso, G., Lu, Y., Shaham, S., and Bianchi, L. (2013). Two Novel DEG/ENaC Channel Subunits Expressed in Glia Are Needed for Nose-Touch Sensitivity in Caenorhabditis elegans. J. Neurosci. *33*, 936–949. https://doi.org/10.1523/JNEUROSCI.2749-12.2013.
5. Raiders, S., Black, E.C., Bae, A., MacFarlane, S., Klein, M., Shaham, S., and Singhvi, A. (2021). Glia actively sculpt sensory neurons by controlled phagocytosis to tune animal behavior. eLife *10*, e63532. https://doi.org/10.7554/eLife.63532.
6. Singhvi, A., Liu, B., Friedman, C.J., Fong, J., Lu, Y., Huang, X.-Y., and Shaham, S. (2016). A Glial K/Cl Transporter Controls Neuronal Receptive Ending Shape by Chloride Inhibition of an rGC. Cell *165*, 936–948. https://doi.org/10.1016/j.cell.2016.03.026.

7. Kravchuk, A., and Singhvi, A. (2023). Neuron cilia constrain glial regulators to microdomains around distal neurons. Preprint at bioRxiv. https://doi.org/10.1101/2023.03.18.533255.

8. Choi, D.-J., Lee, Z.-F., Kwon, W., Chen, H.-C., Lozzi, B., Cervantes, A., Rajendran, K., et al. (2023). Induction of astrocytic Slc22a3 regulates sensory processing through histone serotonylation. Science *380*, eade0027. https://doi.org/10.1126/science.ade0027.

9. Abdo, H., Calvo-Enrique, L., Lopez, J.M., Song, J., Zhang, M.-D., Usoskin, D., El Manira, A., Adameyko, I., Hjerling-Leffler, J., and Ernfors, P. (2019). Specialized cutaneous Schwann cells initiate pain sensation. Science *365*, 695–699. https://doi.org/10.1126/science.aax6452.

10. Xin, W., and Chan, J.R. (2020). Myelin plasticity: sculpting circuits in learning and memory. Nat. Rev. Neurosci. *21*, 682–694. https://doi.org/10.1038/s41583-020-00379-8.

11. Chi, S., Cui, Y., Wang, H., Jiang, J., Zhang, T., Sun, S., Zhou, Z., Zhong, Y., and Xiao, B. (2022). Astrocytic Piezo1-mediated mechanotransduction determines adult neurogenesis and cognitive functions. Neuron *110*, 2984–2999.e8. https://doi.org/10.1016/j.neuron.2022.07.010.

12. Parkhurst, C.N., Yang, G., Ninan, I., Savas, J.N., Yates, J.R., Lafaille, J.J., Hempstead, B.L., Littman, D.R., and Gan, W.-B. (2013). Microglia promote learning-dependent synapse formation through brain-derived neurotrophic factor. Cell *155*, 1596–1609. https://doi.org/10.1016/j.cell.2013.11.030.

13. Cornell, J., Salinas, S., Huang, H.-Y., and Zhou, M. (2022). Microglia regulation of synaptic plasticity and learning and memory. Neural Regen. Res. *17*, 705–716. https://doi.org/10.4103/1673-5374.322423.

14. Garofalo, S., Picard, K., Limatola, C., Nadjar, A., Pascual, O., and Tremblay, M.-È. (2020). Role of Glia in the Regulation of Sleep in Health and Disease. Compr. Physiol. *10*, 687–712. https://doi.org/10.1002/cphy.c190022.

15. Gourine, A.V., Kasymov, V., Marina, N., Tang, F., Figueiredo, M.F., Lane, S., Teschemacher, A.G., Spyer, K.M., Deisseroth, K., and Kasparov, S. (2010). Astrocytes Control Breathing Through pH-Dependent Release of ATP. Science *329*, 571–575. https://doi.org/10.1126/science.1190721.

16. Krohn, F., Novello, M., van der Giessen, R.S., De Zeeuw, C.I., Pel, J.J.M., and Bosman, L.W.J. (2023). The integrated brain network that controls respiration. eLife *12*, e83654. https://doi.org/10.7554/eLife.83654.

17. Hardaway, J.A., Sturgeon, S.M., Snarrenberg, C.L., Li, Z., Xu, X.Z.S., Bermingham, D.P., Odiase, P., Spencer, W.C., Miller, D.M., Carvelli, L., et al. (2015). Glial Expression of the Caenorhabditis elegans Gene swip-10 Supports Glutamate Dependent Control of Extrasynaptic Dopamine Signaling. J. Neurosci. *35*, 9409–9423. https://doi.org/10.1523/JNEUROSCI.0800-15.2015.

18. Katz, M., Corson, F., Iwanir, S., Biron, D., and Shaham, S. (2018). Glia Modulate a Neuronal Circuit for Locomotion Suppression during Sleep in C. elegans. Cell Rep. *22*, 2575–2583. https://doi.org/10.1016/j.celrep.2018.02.036.

19. Coll-Tané, M., Gong, N.N., Belfer, S.J., van Renssen, L.V., Kurtz-Nelson, E.C., Szuperak, M., Eidhof, I., van Reijmersdal, B., Terwindt, I., Durkin, J., et al. (2021). The CHD8/CHD7/Kismet family links blood-brain barrier glia and serotonin to ASD-associated sleep defects. Sci. Adv. *7*, eabe2626. https://doi.org/10.1126/sciadv.abe2626.

20. Allen, M., Huang, B.S., Notaras, M.J., Lodhi, A., Barrio-Alonso, E., Lituma, P.J., Wolujewicz, P., Witztum, J., Longo, F., Chen, M., et al. (2022). Astrocytes derived from ASD individuals alter behavior and destabilize neuronal activity through aberrant Ca2+ signaling. Mol. Psychiatry *27*, 2470–2484. https://doi.org/10.1038/s41380-022-01486-x.

21. Jin, X., Simmons, S.K., Guo, A., Shetty, A.S., Ko, M., Nguyen, L., Jokhi, V., Robinson, E., Oyler, P., Curry, N., et al. (2020). In vivo Perturb-Seq reveals neuronal and glial abnormalities associated with autism risk genes. Science *370*, eaaz6063. https://doi.org/10.1126/science.aaz6063.

22. Patel, D.C., Tewari, B.P., Chaunsali, L., and Sontheimer, H. (2019). Neuron-glia interactions in the pathophysiology of epilepsy. Nat. Rev. Neurosci. *20*, 282–297. https://doi.org/10.1038/s41583-019-0126-4.

23. Dietz, A.G., Goldman, S.A., and Nedergaard, M. (2020). Glial cells in schizophrenia: A unified hypothesis. Lancet Psychiatry *7*, 272–281. https://doi.org/10.1016/S2215-0366(19)30302-5.

24. Bennett, M.L., and Viaene, A.N. (2021). What are activated and reactive glia and what is their role in neurodegeneration? Neurobiol. Dis. *148*, 105172. https://doi.org/10.1016/j.nbd.2020.105172.

25. Hartline, D.K. (2011). The evolutionary origins of glia. Glia *59*, 1215–1236. https://doi.org/10.1002/glia.21149.

26. Hanani, M., and Reichenbach, A. (1994). Morphology of horseradish peroxidase (HRP)-injected glial cells in the myenteric plexus of the guinea-pig. Cell Tissue Res. *278*, 153–160. https://doi.org/10.1007/BF00305787.

27. Zhang, Y., and Barres, B.A. (2010). Astrocyte heterogeneity: an underappreciated topic in neurobiology. Curr. Opin. Neurobiol. *20*, 588–594. https://doi.org/10.1016/j.conb.2010.06.005.

28. Boisvert, M.M., Erikson, G.A., Shokhirev, M.N., and Allen, N.J. (2018). The Aging Astrocyte Transcriptome from Multiple Regions of the Mouse Brain. Cell Rep. *22*, 269–285. https://doi.org/10.1016/j.celrep.2017.12.039.

29. Batiuk, M.Y., Martirosyan, A., Wahis, J., de Vin, F., Marneffe, C., Kusserow, C., Koeppen, J., Viana, J.F., Oliveira, J.F., Voet, T., et al. (2020). Identification of region-specific astrocyte subtypes at single cell resolution. Nat. Commun. *11*, 1220. https://doi.org/10.1038/s41467-019-14198-8.

30. Hasel, P., Rose, I.V.L., Sadick, J.S., Kim, R.D., and Liddelow, S.A. (2021). Neuroinflammatory astrocyte subtypes in the mouse brain. Nat. Neurosci. *24*, 1475–1487. https://doi.org/10.1038/s41593-021-00905-6.

31. Lago-Baldaia, I., Cooper, M., Seroka, A., Trivedi, C., Powell, G.T., Wilson, S., Ackerman, S., and Fernandes, V.M. (2022). A *Drosophila* glial cell atlas reveals that transcriptionally defined cell types can be morphologically diverse. PLoS. Biol. *21*, e3002328. https://doi.org/10.1101/2022.08.01.502305.

32. Zeisel, A., Hochgerner, H., Lönnerberg, P., Johnsson, A., Memic, F., van der Zwan, J., Häring, M., Braun, E., Borm, L.E., Manno, G.L., et al. (2018). Molecular Architecture of the Mouse Nervous System. Cell *174*, 999–1014.e22. https://doi.org/10.1016/j.cell.2018.06.021.

33. Zhang, M., Eichhorn, S.W., Zingg, B., Yao, Z., Cotter, K., Zeng, H., Dong, H., and Zhuang, X. (2021). Spatially resolved cell atlas of the mouse primary motor cortex by MERFISH. Nature *598*, 137–143. https://doi.org/10.1038/s41586-021-03705-x.

34. Valihrach, L., Matusova, Z., Zucha, D., Klassen, R., Benesova, S., Abaffy, P., Kubista, M., and Anderova, M. (2022). Recent advances in deciphering oligodendrocyte heterogeneity with single-cell transcriptomics. Front. Cell. Neurosci. *16*, 1025012. https://doi.org/10.3389/fncel.2022.1025012.

35. Masuda, T., Sankowski, R., Staszewski, O., and Prinz, M. (2020). Microglia Heterogeneity in the Single-Cell Era. Cell Rep. *30*, 1271–1281. https://doi.org/10.1016/j.celrep.2020.01.010.

36. Seguella, L., and Gulbransen, B.D. (2021). Enteric glial biology, intercellular signalling and roles in gastrointestinal disease. Nat. Rev. Gastroenterol. Hepatol. *18*, 571–587. https://doi.org/10.1038/s41575-021-00423-7.

37. Tasdemir-Yilmaz, O.E., Druckenbrod, N.R., Olukoya, O.O., Dong, W., Yung, A.R., Bastille, I., Pazyra-Murphy, M.F., Sitko, A.A., Hale, E.B., Vigneau, S., et al. (2021). Diversity of developing peripheral glia revealed by single-cell RNA sequencing. Dev. Cell *56*, 2516–2535.e8. https://doi.org/10.1016/j.devcel.2021.08.005.

38. Kastriti, M.E., and Adameyko, I. (2017). Specification, plasticity and evolutionary origin of peripheral glial cells. Curr. Opin. Neurobiol. *47*, 196–202. https://doi.org/10.1016/j.conb.2017.11.004.

39. Mapps, A.A., Thomsen, M.B., Boehm, E., Zhao, H., Hattar, S., and Kuruvilla, R. (2022). Diversity of satellite glia in sympathetic and sensory ganglia. Cell Rep. *38*, 110328. https://doi.org/10.1016/j.celrep.2022.110328.

40. Hahn, J., Monavarfeshani, A., Qiao, M., Kao, A.H., Kölsch, Y., Kumar, A., Kunze, V.P., Rasys, A.M., Richardson, R., Wekselblatt, J.B., et al. (2023). Evolution of neuronal cell classes and types in the vertebrate retina. Nature *624*, 415–424. https://doi.org/10.1038/s41586-023-06638-9.

41. Zhang, Y., Chen, K., Sloan, S.A., Bennett, M.L., Scholze, A.R., O'Keeffe, S., Phatnani, H.P., Guarnieri, P., Caneda, C., Ruderisch, N., et al. (2014). An RNA-Sequencing Transcriptome and Splicing Database of Glia, Neurons, and Vascular Cells of the Cerebral Cortex. J. Neurosci. *34*, 11929–11947. https://doi.org/10.1523/JNEUROSCI.1860-14.2014.

42. Bennett, M.L., Bennett, F.C., Liddelow, S.A., Ajami, B., Zamanian, J.L., Fernhoff, N.B., Mulinyawe, S.B., Bohlen, C.J., Adil, A., Tucker, A., et al. (2016). New tools for studying microglia in the mouse and human CNS. Proc. Natl. Acad. Sci. USA *113*, E1738–E1746. https://doi.org/10.1073/pnas.1525528113.

43. Clarke, L.E., Liddelow, S.A., Chakraborty, C., Münch, A.E., Heiman, M., and Barres, B.A. (2018). Normal aging induces A1-like astrocyte reactivity. Proc. Natl. Acad. Sci. USA *115*, E1896–E1905. https://doi.org/10.1073/pnas.1800165115.

44. Li, Q., Cheng, Z., Zhou, L., Darmanis, S., Neff, N.F., Okamoto, J., Gulati, G., Bennett, M.L., Sun, L.O., Clarke, L.E., et al. (2019). Developmental Heterogeneity of Microglia and Brain Myeloid Cells Revealed by Deep Single-Cell RNA Sequencing. Neuron *101*, 207–223.e10. https://doi.org/10.1016/j.neuron.2018.12.006.

45. Taylor, S.R., Santpere, G., Weinreb, A., Barrett, A., Reilly, M.B., Xu, C., Varol, E., Oikonomou, P., Glenwinkel, L., McWhirter, R., et al. (2021). Molecular topography of an entire nervous system. Cell *184*, 4329–4347.e23. https://doi.org/10.1016/j.cell.2021.06.023.

46. Davie, K., Janssens, J., Koldere, D., De Waegeneer, M., Pech, U., Kreft, Ł., Aibar, S., Makhzami, S., Christiaens, V., Bravo González-Blas, C., et al. (2018). A Single-Cell Transcriptome Atlas of the Aging Drosophila Brain. Cell *174*, 982–998.e20. https://doi.org/10.1016/j.cell.2018.05.057.

47. Nguon, K., Ladd, B., Baxter, M.G., and Sajdel-Sulkowska, E.M. (2005). Sexual dimorphism in cerebellar structure, function, and response to environmental perturbations. Prog. Brain Res. *148*, 341–351. https://doi.org/10.1016/S0079-6123(04)48027-3.

48. Schwarz, J.M., and Bilbo, S.D. (2012). Sex, glia, and development: Interactions in health and disease. Horm. Behav. *62*, 243–253. https://doi.org/10.1016/j.yhbeh.2012.02.018.

49. Simerly, R.B. (2002). Wired for Reproduction: Organization and Development of Sexually Dimorphic Circuits in the Mammalian Forebrain. Annu. Rev. Neurosci. *25*, 507–536. https://doi.org/10.1146/annurev.neuro.25.112701.142745.

50. Vegeto, E., Villa, A., Della Torre, S., Crippa, V., Rusmini, P., Cristofani, R., Galbiati, M., Maggi, A., and Poletti, A. (2020). The Role of Sex and Sex Hormones in Neurodegenerative Diseases. Endocr. Rev. *41*, 273–319. https://doi.org/10.1210/endrev/bnz005.

51. Garcia-Segura, L.M., Lorenz, B., and DonCarlos, L.L. (2008). The role of glia in the hypothalamus: implications for gonadal steroid feedback and reproductive neuroendocrine output. Reproduction *135*, 419–429. https://doi.org/10.1530/REP-07-0540.

52. Brivio, E., Kos, A., Ulivi, A.F., Karamihalev, S., Ressle, A., Stoffel, R., Hirsch, D., Stelzer, G., Schmidt, M.V., Lopez, J.P., et al. (2023). Sex shapes cell-type-specific transcriptional signatures of stress exposure in the mouse hypothalamus. Cell Rep. *42*, 112874. https://doi.org/10.1016/j.celrep.2023.112874.

53. Chowen, J.A., and Garcia-Segura, L.M. (2021). Role of glial cells in the generation of sex differences in neurodegenerative diseases and brain aging. Mech. Ageing Dev. *196*, 111473. https://doi.org/10.1016/j.mad.2021.111473.

54. Hopkins, B.R., Barmina, O., and Kopp, A. (2023). A single-cell atlas of the sexually dimorphic Drosophila foreleg and its sensory organs during development. PLoS Biol. *21*, e3002148. https://doi.org/10.1371/journal.pbio.3002148.

55. Fung, W., Tan, T.M., Kolotuev, I., and Heiman, M.G. (2023). A sex-specific switch in a single glial cell patterns the apical extracellular matrix. Curr. Biol. *33*, 4174–4186.e7. https://doi.org/10.1016/j.cub.2023.08.046.

56. Acaz-Fonseca, E., Duran, J.C., Carrero, P., Garcia-Segura, L.M., and Arevalo, M.A. (2015). Sex differences in glia reactivity after cortical brain injury. Glia *63*, 1966–1981. https://doi.org/10.1002/glia.22867.

57. Loram, L.C., Sholar, P.W., Taylor, F.R., Wiesler, J.L., Babb, J.A., Strand, K.A., Berkelhammer, D., Day, H.E.W., Maier, S.F., and Watkins, L.R. (2012). Sex and estradiol influence glial pro-inflammatory responses to lipopolysaccharide in rats. Psychoneuroendocrinology *37*, 1688–1699. https://doi.org/10.1016/j.psyneuen.2012.02.018.

58. White, J.G., Southgate, E., Thomson, J.N., and Brenner, S. (1986). The structure of the nervous system of the nematode Caenorhabditis elegans. Philos. Trans. R. Soc. Lond. B Biol. Sci. *314*, 1–340. https://doi.org/10.1098/rstb.1986.0056.

59. Sulston, J.E., and Horvitz, H.R. (1977). Post-embryonic cell lineages of the nematode, Caenorhabditis elegans. Dev. Biol. *56*, 110–156. https://doi.org/10.1016/0012-1606(77)90158-0.

60. Ward, S., Thomson, N., White, J.G., and Brenner, S. (1975). Electron microscopical reconstruction of the anterior sensory anatomy of the nematodecaenorhabditis elegans.?2UU. J. Comp. Neurol. *160*, 313–337. https://doi.org/10.1002/cne.901600305.

61. Cook, S.J., Jarrell, T.A., Brittin, C.A., Wang, Y., Bloniarz, A.E., Yakovlev, M.A., Nguyen, K.C.Q., Tang, L.T.-H., Bayer, E.A., Duerr, J.S., et al. (2019). Whole-animal connectomes of both Caenorhabditis elegans sexes. Nature *571*, 63–71. https://doi.org/10.1038/s41586-019-1352-7.

62. Hall, D.H., and Russell, R.L. (1991). The posterior nervous system of the nematode Caenorhabditis elegans: serial reconstruction of identified neurons and complete pattern of synaptic interactions. J. Neurosci. *11*, 1–22. https://doi.org/10.1523/JNEUROSCI.11-01-00001.1991.

63. Kaletsky, R., Yao, V., Williams, A., Runnels, A.M., Tadych, A., Zhou, S., Troyanskaya, O.G., and Murphy, C.T. (2018). Transcriptome analysis of adult Caenorhabditis elegans cells reveals tissue-specific gene and isoform expression. PLoS Genet. *14*, e1007559. https://doi.org/10.1371/journal.pgen.1007559.

64. Bargmann, C.I. (1998). Neurobiology of the Caenorhabditis elegans genome. Science *282*, 2028–2033. https://doi.org/10.1126/science.282.5396.2028.

65. Packer, J.S., Zhu, Q., Huynh, C., Sivaramakrishnan, P., Preston, E., Dueck, H., Stefanik, D., Tan, K., Trapnell, C., Kim, J., et al. (2019). A lineage-resolved molecular atlas of *C. elegans* embryogenesis at single-cell resolution. Science *365*, eaax1971. https://doi.org/10.1126/science.aax1971.

66. Yemini, E., Lin, A., Nejatbakhsh, A., Varol, E., Sun, R., Mena, G.E., Samuel, A.D.T., Paninski, L., Venkatachalam, V., and Hobert, O. (2021). NeuroPAL: A Multicolor Atlas for Whole-Brain Neuronal Identification in C. elegans. Cell *184*, 272–288.e11. https://doi.org/10.1016/j.cell.2020.12.012.

67. Portman, D.S. (2007). Genetic control of sex differences in C. elegans neurobiology and behavior. Adv. Genet. *59*, 1–37. https://doi.org/10.1016/S0065-2660(07)59001-2.

68. Barr, M.M., García, L.R., and Portman, D.S. (2018). Sexual Dimorphism and Sex Differences in Caenorhabditis elegans Neuronal Development and Behavior. Genetics *208*, 909–935. https://doi.org/10.1534/genetics.117.300294.

69. Singhvi, A., Shaham, S., and Rapti, G. (2024). Glia development and function in the Nematode of Caenorhabditis elegans. Cold Spring Harb. Perspect. Biol. *16*, a041346. https://doi.org/10.1101/cshperspect.a041346.

70. Morillo, K.S., St Ange, J., Weng, Y., Kaletsky, R., and Murphy, C.T. (2024). Single-Nucleus Neuronal Transcriptional Profiling of Male C.

elegans Uncovers Regulators of Sex-Specific and Sex-Shared Behaviors. Preprint at bioRxiv. https://doi.org/10.1101/2024.12.12.628226.

71. Ray, S., and Singhvi, A. (2021). Charging Up the Periphery: Glial Ionic Regulation in Sensory Perception. Front. Cell Dev. Biol. *9*, 687732. https://doi.org/10.3389/fcell.2021.687732.
72. Singhvi, A., and Shaham, S. (2019). Glia-Neuron Interactions in *Caenorhabditis elegans*. Annu. Rev. Neurosci. *42*, 149–168. https://doi.org/10.1146/annurev-neuro-070918-050314.
73. Raiders, S., Han, T., Scott-Hewitt, N., Kucenas, S., Lew, D., Logan, M.A., and Singhvi, A. (2021). Engulfed by Glia: Glial Pruning in Development, Function, and Injury across Species. J. Neurosci. *41*, 823–833. https://doi.org/10.1523/JNEUROSCI.1660-20.2020.
74. Stefanakis, N., Jiang, J., Liang, Y., and Shaham, S. (2024). LET-381/FoxF and its target UNC-30/Pitx2 specify and maintain the molecular identity of C. elegans mesodermal glia that regulate motor behavior. EMBO J. *43*, 956–992. https://doi.org/10.1038/s44318-024-00049-w.
75. Altun, Z.F., and Hall, D.H. (2003). WormAtlas Hermaphrodite Handbook - Nervous System - Neuronal Support Cells. In WormAtlas (Cold Spring Harbor Laboratory Press). https://doi.org/10.3908/wormatlas.1.19.
76. Shaham, S. (2006). Glia-neuron interactions in the nervous system of Caenorhabditis elegans. Curr. Opin. Neurobiol. *16*, 522–528. https://doi.org/10.1016/j.conb.2006.08.001.
77. Lints, R., and Hall, D.H. (2009). Male neuronal support cells, overview. In WormAtlas (Cold Spring Harbor Laboratory Press).
78. Sammut, M., Cook, S.J., Nguyen, K.C.Q., Felton, T., Hall, D.H., Emmons, S.W., Poole, R.J., and Barrios, A. (2015). Glia-derived neurons are required for sex-specific learning in C. elegans. Nature *526*, 385–390. https://doi.org/10.1038/nature15700.
79. Sulston, J.E., Albertson, D.G., and Thomson, J.N. (1980). The Caenorhabditis elegans male: Postembryonic development of nongonadal structures. Dev. Biol. *78*, 542–576. https://doi.org/10.1016/0012-1606(80)90352-8.
80. Molina-García, L., Lloret-Fernández, C., Cook, S.J., Kim, B., Bonnington, R.C., Sammut, M., O'Shea, J.M., Gilbert, S.P., Elliott, D.J., Hall, D.H., et al. (2020). Direct glia-to-neuron transdifferentiation gives rise to a pair of male-specific neurons that ensure nimble male mating. eLife *9*, e48361. https://doi.org/10.7554/eLife.48361.
81. Ryan, D.A., Miller, R.M., Lee, K., Neal, S.J., Fagan, K.A., SenGupta, P., and Portman, D.S. (2014). Sex, age, and hunger regulate behavioral prioritization through dynamic modulation of chemoreceptor expression. Curr. Biol. *24*, 2509–2517. https://doi.org/10.1016/j.cub.2014.09.032.
82. Emmons, S.W. (2018). Neural Circuits of Sexual Behavior in Caenorhabditis elegans. Annu. Rev. Neurosci. *41*, 349–369. https://doi.org/10.1146/annurev-neuro-070815-014056.
83. Frakes, A.E., Metcalf, M.G., Tronnes, S.U., Bar-Ziv, R., Durieux, J., Gildea, H.K., Kandahari, N., Monshietehadi, S., and Dillin, A. (2020). Four glial cells regulate ER stress resistance and longevity via neuropeptide signaling in *C. elegans*. Science *367*, 436–440. https://doi.org/10.1126/science.aaz6896.
84. Yin, J.-A., Gao, G., Liu, X.-J., Hao, Z.-Q., Li, K., Kang, X.-L., Li, H., Shan, Y.-H., Hu, W.-L., Li, H.-P., et al. (2017). Genetic variation in glia–neuron signalling modulates ageing rate. Nature *551*, 198–203. https://doi.org/10.1038/nature24463.
85. Cao, J., Packer, J.S., Ramani, V., Cusanovich, D.A., Huynh, C., Daza, R., Qiu, X., Lee, C., Furlan, S.N., Steemers, F.J., et al. (2017). Comprehensive single-cell transcriptional profiling of a multicellular organism. Science *357*, 661–667. https://doi.org/10.1126/science.aam8940.
86. Roux, A.E., Yuan, H., Podshivalova, K., Hendrickson, D., Kerr, R., Kenyon, C., and Kelley, D. (2023). Individual cell types in C. elegans age differently and activate distinct cell-protective responses. Cell Rep. *42*, 112902. https://doi.org/10.1016/j.celrep.2023.112902.
87. Ghaddar, A., Armingol, E., Huynh, C., Gevirtzman, L., Lewis, N.E., Waterston, R., and O'Rourke, E.J. (2023). Whole-body gene expression atlas of an adult metazoan. Sci. Adv. *9*, eadg0506. https://doi.org/10.1126/sciadv.adg0506.
88. Weng, Y., Zhou, S., Morillo, K., Kaletsky, R., Lin, S., and Murphy, C.T. (2024). The neuron-specific IIS/FOXO transcriptome in aged animals reveals regulatory mechanisms of cognitive aging. eLife *13*, RP95621. https://doi.org/10.7554/eLife.95621.
89. Hart, A.C. (2006). Behavior. WormBook. https://doi.org/10.1895/wormbook.1.87.1.
90. Fung, W., Wexler, L., and Heiman, M.G. (2020). Cell-type-specific promoters for *C. elegans* glia. J. Neurogenet. *34*, 335–346. https://doi.org/10.1080/01677063.2020.1781851.
91. Wallace, S.W., Singhvi, A., Liang, Y., Lu, Y., and Shaham, S. (2016). PROS-1/Prospero Is a Major Regulator of the Glia-Specific Secretome Controlling Sensory-Neuron Shape and Function in C. elegans. Cell Rep. *15*, 550–562. https://doi.org/10.1016/j.celrep.2016.03.051.
92. Chasnov, J.R., and Chow, K.L. (2002). Why Are There Males in the Hermaphroditic Species *Caenorhabditis elegans*? Genetics *160*, 983–994. https://doi.org/10.1093/genetics/160.3.983.
93. Bacaj, T., Tevlin, M., Lu, Y., and Shaham, S. (2008). Glia Are Essential for Sensory Organ Function in *C. elegans*. Science *322*, 744–747. https://doi.org/10.1126/science.1163074.
94. Bianchi, L. (2020). C. elegans Glia Are Bona Fide Odorant Receptor Cells. Neuron *108*, 588–589. https://doi.org/10.1016/j.neuron.2020.10.026.
95. Perens, E.A., and Shaham, S. (2005). C. elegans daf-6 encodes a patched-related protein required for lumen formation. Dev. Cell *8*, 893–906. https://doi.org/10.1016/j.devcel.2005.03.009.
96. Yoshimura, S., Murray, J.I., Lu, Y., Waterston, R.H., and Shaham, S. (2008). mls-2 and vab-3 Control glia development, hlh-17/Olig expression and glia-dependent neurite extension in C. elegans. Development *135*, 2263–2275. https://doi.org/10.1242/dev.019547.
97. Peden, E.M., and Barr, M.M. (2005). The KLP-6 kinesin is required for male mating behaviors and polycystin localization in Caenorhabditis elegans. Curr. Biol. *15*, 394–404. https://doi.org/10.1016/j.cub.2004.12.073.
98. Lints, R., and Hall, D.H. (2005). WormAtlas Male Handbook - Neuronal Support Cells - Rays. In WormAtlas (Cold Spring Harbor Laboratory Press). https://doi.org/10.3908/wormatlas.2.10.
99. LeBoeuf, B., Correa, P., Jee, C., and García, L.R. (2014). Caenorhabditis elegans male sensory-motor neurons and dopaminergic support cells couple ejaculation and post-ejaculatory behaviors. eLife *3*, e02938. https://doi.org/10.7554/eLife.02938.
100. Altun, Z.F., and Hall, D.H. (2009). Epithelial system, interfacial cells. In WormAtlas (Cold Spring Harbor Laboratory Press).
101. Hao, L., Johnsen, R., Lauter, G., Baillie, D., and Bürglin, T.R. (2006). Comprehensive analysis of gene expression patterns of hedgehog-related genes. BMC Genomics *7*, 280. https://doi.org/10.1186/1471-2164-7-280.
102. Pierce, M.L., Weston, M.D., Fritzsch, B., Gabel, H.W., Ruvkun, G., and Soukup, G.A. (2008). MicroRNA-183 family conservation and ciliated neurosensory organ expression. Evol. Dev. *10*, 106–113. https://doi.org/10.1111/j.1525-142X.2007.00217.x.
103. Fuxman Bass, J.I., Pons, C., Kozlowski, L., Reece-Hoyes, J.S., Shrestha, S., Holdorf, A.D., Mori, A., Myers, C.L., and Walhout, A.J. (2016). A gene-centered C. elegans protein-DNA interaction network provides a framework for functional predictions. Mol. Syst. Biol. *12*, 884. https://doi.org/10.15252/msb.20167131.
104. Labouesse, M., Sookhareea, S., and Horvitz, H.R. (1994). The Caenorhabditis elegans gene lin-26 is required to specify the fates of hypodermal cells and encodes a presumptive zinc-finger transcription factor. Development *120*, 2359–2368. https://doi.org/10.1242/dev.120.9.2359.
105. Labouesse, M., Hartwieg, E., and Horvitz, H.R. (1996). The Caenorhabditis elegans LIN-26 protein is required to specify and/or

maintain all non-neuronal ectodermal cell fates. Development *122*, 2579–2588. https://doi.org/10.1242/dev.122.9.2579.

106. Chisholm, A.D., and Hodgkin, J. (1989). The mab-9 gene controls the fate of B, the major male-specific blast cell in the tail region of Caenorhabditis elegans. Genes Dev. *3*, 1413–1423. https://doi.org/10.1101/gad.3.9.1413.

107. Khakh, B.S., and Sofroniew, M.V. (2015). Diversity of astrocyte functions and phenotypes in neural circuits. Nat. Neurosci. *18*, 942–952. https://doi.org/10.1038/nn.4043.

108. Song, S., Luo, L., Sun, B., and Sun, D. (2020). Roles of glial ion transporters in brain diseases. Glia *68*, 472–494. https://doi.org/10.1002/glia.23699.

109. Fernandez-Abascal, J., Johnson, C.K., Graziano, B., Wang, L., Encalada, N., and Bianchi, L. (2022). A glial ClC Cl− channel mediates nose touch responses in C. elegans. Neuron *110*, 470–485.e7. https://doi.org/10.1016/j.neuron.2021.11.010.

110. Wang, L., Graziano, B., Encalada, N., Fernandez-Abascal, J., Kaplan, D. H., and Bianchi, L. (2022). Glial regulators of ions and solutes required for specific chemosensory functions in Caenorhabditis elegans. iScience *25*, 105684. https://doi.org/10.1016/j.isci.2022.105684.

111. Albertini, R., and Bianchi, R. (2010). Aquaporins and Glia. Curr. Neuropharmacol. *8*, 84–91. https://doi.org/10.2174/157015910791233178.

112. Nagelhus, E.A., Mathiisen, T.M., and Ottersen, O.P. (2004). Aquaporin-4 in the central nervous system: Cellular and subcellular distribution and coexpression with KIR4.1. Neuroscience *129*, 905–913. https://doi.org/10.1016/j.neuroscience.2004.08.053.

113. Wojtovich, A.P., DiStefano, P., Sherman, T., Brookes, P.S., and Nehrke, K. (2012). Mitochondrial ATP-sensitive potassium channel activity and hypoxic preconditioning are independent of an inwardly rectifying potassium channel subunit in Caenorhabditis elegans. FEBS Lett. *586*, 428–434. https://doi.org/10.1016/j.febslet.2012.01.021.

114. Allen, N.J., and Lyons, D.A. (2018). Glia as Architects of Central Nervous System Formation and Function. Science *362*, 181–185. https://doi.org/10.1126/science.aat0473.

115. Dai, Y., Hu, R., Liu, A., Cho, K.S., Manuel, A.M., Li, X., Dong, X., Jia, P., and Zhao, Z. (2022). WebCSEA: web-based cell-type-specific enrichment analysis of genes. Nucleic Acids Res. *50*, W782–W790. https://doi.org/10.1093/nar/gkac392.

116. Kim, W., Underwood, R.S., Greenwald, I., and Shaye, D.D. (2018). OrthoList 2: A New Comparative Genomic Analysis of Human and Caenorhabditis elegans Genes. Genetics *210*, 445–461. https://doi.org/10.1534/genetics.118.301307.

117. Purice, M.D., Severs, L.J., and Singhvi, A. (2024). Glia in Invertebrate Models: Insights from Caenorhabditis elegans. Adv. Neurobiol. *39*, 19–49. https://doi.org/10.1007/978-3-031-64839-7_2.

118. Tanis, J.E., Bellemer, A., Moresco, J.J., Forbush, B., and Koelle, M.R. (2009). The Potassium Chloride Cotransporter KCC-2 Coordinates Development of Inhibitory Neurotransmission and Synapse Structure in Caenorhabditis elegans. J. Neurosci. *29*, 9943–9954. https://doi.org/10.1523/JNEUROSCI.1989-09.2009.

119. Chung, W.-S., Clarke, L.E., Wang, G.X., Stafford, B.K., Sher, A., Chakraborty, C., Joung, J., Foo, L.C., Thompson, A., Chen, C., et al. (2013). Astrocytes mediate synapse elimination through MEGF10 and MERTK pathways. Nature *504*, 394–400. https://doi.org/10.1038/nature12776.

120. Le Rouzic, P., Ivanov, T.R., Stanley, P.J., Baudoin, F.M.-H., Chan, F., Pinteaux, E., Brown, P.D., and Luckman, S.M. (2006). KCC3 and KCC4 expression in rat adult forebrain. Brain Res. *1110*, 39–45. https://doi.org/10.1016/j.brainres.2006.06.055.

121. Yoshida, A., Nakano, S., Suzuki, T., Ihara, K., Higashiyama, T., and Mori, I. (2016). A glial K(+) /Cl(-) cotransporter modifies temperature-evoked dynamics in Caenorhabditis elegans sensory neurons. Genes Brain Behav. *15*, 429–440. https://doi.org/10.1111/gbb.12260.

122. Angeles-Albores, D., N Lee, R.Y., Chan, J., and Sternberg, P.W. (2016). Tissue enrichment analysis for C. elegans genomics. BMC Bioinformatics *17*, 366. https://doi.org/10.1186/s12859-016-1229-9.

123. Angeles-Albores, D., Lee, R.Y.N., Chan, J., and Sternberg, P.W. (2018). Two new functions in the WormBase Enrichment Suite. MicroPubl. Biol. *2018*. https://doi.org/10.17912/W25Q2N.

124. Haag, E.S. (2005). The evolution of nematode sex determination: C. elegans as a reference point for comparative biology. WormBook, 1–14. https://doi.org/10.1895/wormbook.1.120.1.

125. Yi, W., Ross, J.M., and Zarkower, D. (2000). Mab-3 is a direct tra-1 target gene regulating diverse aspects of C. elegans male sexual development and behavior. Development *127*, 4469–4480. https://doi.org/10.1242/dev.127.20.4469.

126. Yu, R.Y.L., Nguyen, C.Q., Hall, D.H., and Chow, K.L. (2000). Expression of ram-5 in the structural cell is required for sensory ray morphogenesis in Caenorhabditis elegans male tail. EMBO J. *19*, 3542–3555. https://doi.org/10.1093/emboj/19.14.3542.

127. Chasnov, J.R., So, W.K., Chan, C.M., and Chow, K.L. (2007). The species, sex, and stage specificity of a Caenorhabditis sex pheromone. Proc. Natl. Acad. Sci. USA *104*, 6730–6735. https://doi.org/10.1073/pnas.0608050104.

128. Srinivasan, J., Kaplan, F., Ajredini, R., Zachariah, C., Alborn, H.T., Teal, P. E.A., Malik, R.U., Edison, A.S., Sternberg, P.W., and Schroeder, F.C. (2008). A blend of small molecules regulates both mating and development in Caenorhabditis elegans. Nature *454*, 1115–1118. https://doi.org/10.1038/nature07168.

129. Hall, D.H. (1977). The posterior nervous system of the nematode Caenorhabditis elegans. J Neurosci. *11*, 1–22.

130. Ailion, M., Inoue, T., Weaver, C.I., Holdcraft, R.W., and Thomas, J.H. (1999). Neurosecretory control of aging in *Caenorhabditis elegans*. Proc. Natl. Acad. Sci. USA *96*, 7394–7397. https://doi.org/10.1073/pnas.96.13.7394.

131. Speese, S., Petrie, M., Schuske, K., Ailion, M., Ann, K., Iwasaki, K., Jorgensen, E.M., and Martin, T.F.J. (2007). UNC-31 (CAPS) Is Required for Dense-Core Vesicle But Not Synaptic Vesicle Exocytosis in Caenorhabditis elegans. J. Neurosci. *27*, 6150–6162. https://doi.org/10.1523/JNEUROSCI.1466-07.2007.

132. Kass, J., Jacob, T.C., Kim, P., and Kaplan, J.M. (2001). The EGL-3 Proprotein Convertase Regulates Mechanosensory Responses of *Caenorhabditis elegans*. J. Neurosci. *21*, 9265–9272. https://doi.org/10.1523/JNEUROSCI.21-23-09265.2001.

133. Hobert, O. (2013). The neuronal genome of Caenorhabditis elegans. WormBook, 1–106. https://doi.org/10.1895/wormbook.1.161.1.

134. Van Bael, S., Watteyne, J., Boonen, K., De Haes, W., Menschaert, G., Ringstad, N., Horvitz, H.R., Schoofs, L., Husson, S.J., and Temmerman, L. (2018). Mass spectrometric evidence for neuropeptide-amidating enzymes in Caenorhabditis elegans. J. Biol. Chem. *293*, 6052–6063. https://doi.org/10.1074/jbc.RA117.000731.

135. Ange, J.S., Weng, Y., Stevenson, M.E., Kaletsky, R., Moore, R.S., Zhou, S., and Murphy, C.T. (2024). Adult Single-nucleus Neuronal Transcriptomes of Insulin Signaling Mutants Reveal Regulators of Behavior and Learning. Cell Genom. *4*, 100720. https://doi.org/10.1101/2024.02.07.579364.

136. Serra, N.D., Darwin, C.B., and Sundaram, M.V. (2023). C. elegans Hedgehog-related proteins are tissue- and substructure-specific components of the cuticle and pre-cuticle. Genetics *227*, iyae081. https://doi.org/10.1101/2023.12.26.573316.

137. Kriegstein, A., and Alvarez-Buylla, A. (2009). The Glial Nature of Embryonic and Adult Neural Stem Cells. Annu. Rev. Neurosci. *32*, 149–184. https://doi.org/10.1146/annurev.neuro.051508.135600.

138. Campbell, K., and Götz, M. (2002). Radial glia: multi-purpose cells for vertebrate brain development. Trends Neurosci. *25*, 235–238. https://doi.org/10.1016/s0166-2236(02)02156-2.

139. Strauss, O. (2005). The retinal pigment epithelium in visual function. Physiol. Rev. *85*, 845–881. https://doi.org/10.1152/physrev.00021.2004.

140. Hobert, O. (2010). Neurogenesis in the nematode Caenorhabditis elegans. WormBook, 1–24. https://doi.org/10.1895/wormbook.1.12.2.

141. Rapti, G., Li, C., Shan, A., Lu, Y., and Shaham, S. (2017). Glia initiate brain assembly through noncanonical Chimaerin-Furin axon guidance in C. elegans. Nat. Neurosci. *20*, 1350–1360. https://doi.org/10.1038/nn.4630.

142. Han, J., Fan, Y., Zhou, K., Blomgren, K., and Harris, R.A. (2021). Uncovering sex differences of rodent microglia. J. Neuroinflammation *18*, 74. https://doi.org/10.1186/s12974-021-02124-z.

143. Rurak, G.M., Woodside, B., Aguilar-Valles, A., and Salmaso, N. (2021). Astroglial cells as neuroendocrine targets in forebrain development: Implications for sex differences in psychiatric disease. Front. Neuroendocrinol. *60*, 100897. https://doi.org/10.1016/j.yfrne.2020.100897.

144. Burbach, J.P.H. (2011). What Are Neuropeptides? In Neuropeptides Methods in Molecular Biology, A. Merighi, ed. (Humana Press), pp. 1–36. https://doi.org/10.1007/978-1-61779-310-3_1.

145. Ubink, R., Calza, L., and Hökfelt, T. (2003). 'Neuro'-peptides in glia: Focus on NPY and galanin. Trends Neurosci. *26*, 604–609. https://doi.org/10.1016/j.tins.2003.09.003.

146. Purice, M.D., Lago-Baldaia, I., Fernandes, V.M., and Singhvi, A. (2025). Molecular profiling of invertebrate glia. Glia *73*, 632–656. https://doi.org/10.1002/glia.24623.

147. Quitevis, E., and Setty, M. (2025). settylab/worm-glia-atlas: v1.0.0. Zenodo. https://doi.org/10.5281/zenodo.15080360.

148. van Dijk, D., Sharma, R., Nainys, J., Yim, K., Kathail, P., Carr, A.J., Burdziak, C., Moon, K.R., Chaffer, C.L., Pattabiraman, D., et al. (2018). Recovering Gene Interactions from Single-Cell Data Using Data Diffusion. Cell *174*, 716–729.e27. https://doi.org/10.1016/j.cell.2018.05.061.

149. Yanagi, K.S., and Lehrbach, N. (2024). Streamlined single shot safe harbor transgene integration in C. elegans using unc-119 rescue. MicroPubl. Biol. *2024*. https://doi.org/10.17912/micropub.biology.001230.

150. Schindelin, J., Arganda-Carreras, I., Frise, E., Kaynig, V., Longair, M., Pietzsch, T., Preibisch, S., Rueden, C., Saalfeld, S., Schmid, B., et al. (2012). Fiji: an open-source platform for biological-image analysis. Nat. Methods *9*, 676–682. https://doi.org/10.1038/nmeth.2019.

151. Davis, M.W., and Jorgensen, E.M. (2022). ApE, A Plasmid Editor: A Freely Available DNA Manipulation and Visualization Program. Front. Bioinform. *2*, 818619. https://doi.org/10.3389/fbinf.2022.818619.

152. Wolf, F.A., Angerer, P., and Theis, F.J. (2018). SCANPY: large-scale single-cell gene expression data analysis. Genome Biol. *19*, 15. https://doi.org/10.1186/s13059-017-1382-0.

153. Pedregosa, F., Varoquaux, G., Gramfort, A., Michel, V., Thirion, B., Grisel, O., Blondel, M., Prettenhofer, P., Weiss, R., Dubourg, V., et al. (2011). Scikit-learn: Machine Learning in Python. J. Mach. Learn. Res. *12*, 2825–2830.

154. Virtanen, P., Gommers, R., Oliphant, T.E., Haberland, M., Reddy, T., Cournapeau, D., Burovski, E., Peterson, P., Weckesser, W., Bright, J., et al. (2020). SciPy 1.0: fundamental algorithms for scientific computing in Python. Nat. Methods *17*, 261–272. https://doi.org/10.1038/s41592-019-0686-2.

155. Setty, M., Kiseliovas, V., Levine, J., Gayoso, A., Mazutis, L., and Pe'er, D. (2019). Characterization of cell fate probabilities in single-cell data with Palantir. Nat. Biotechnol. *37*, 451–460. https://doi.org/10.1038/s41587-019-0068-4.

156. Korsunsky, I., Millard, N., Fan, J., Slowikowski, K., Zhang, F., Wei, K., Baglaenko, Y., Brenner, M., Loh, P.R., and Raychaudhuri, S. (2019). Fast, sensitive and accurate integration of single-cell data with Harmony. Nat. Methods *16*, 1289–1296. https://doi.org/10.1038/s41592-019-0619-0.

157. Brenner, S. (1974). The genetics of Caenorhabditis elegans. Genetics *77*, 71–94. https://doi.org/10.1093/genetics/77.1.71.

158. Stiernagle, T. (2006). Maintenance of C. elegans. WormBook, 1–11. https://doi.org/10.1895/wormbook.1.101.1.

159. Mello, C.C., Kramer, J.M., Stinchcomb, D., and Ambros, V. (1991). Efficient gene transfer in C.elegans: extrachromosomal maintenance and integration of transforming sequences. EMBO J. *10*, 3959–3970. https://doi.org/10.1002/j.1460-2075.1991.tb04966.x.

160. Abraham, M.C., Lu, Y., and Shaham, S. (2007). A morphologically conserved nonapoptotic program promotes linker cell death in Caenorhabditis elegans. Dev. Cell *12*, 73–86. https://doi.org/10.1016/j.devcel.2006.11.012.

161. Miyabayashi, T., Palfreyman, M.T., Sluder, A.E., Slack, F., and SenGupta, P. (1999). Expression and function of members of a divergent nuclear receptor family in Caenorhabditis elegans. Dev. Biol. *215*, 314–331. https://doi.org/10.1006/dbio.1999.9470.

162. Malaiwong, N., Porta-de-la-Riva, M., and Krieg, M. (2023). FLInt: single shot safe harbor transgene integration via Fluorescent Landmark Interference. G3 (Bethesda) *13*, jkad041. https://doi.org/10.1093/g3journal/jkad041.

163. Lesch, B.J., Gehrke, A.R., Bulyk, M.L., and Bargmann, C.I. (2009). Transcriptional regulation and stabilization of left–right neuronal identity in C. elegans. Genes Dev. *23*, 345–358. https://doi.org/10.1101/gad.1763509.

164. McInnes, L., Healy, J., Saul, N., and Großberger, L. (2018). UMAP: Uniform Manifold Approximation and Projection. J. Open Source Softw. *3*, 861. https://doi.org/10.21105/joss.00861.

165. Traag, V.A., Waltman, L., and van Eck, N.J. (2019). From Louvain to Leiden: guaranteeing well-connected communities. Sci. Rep. *9*, 5233. https://doi.org/10.1038/s41598-019-41695-z.

166. Davis, P., Zarowiecki, M., Arnaboldi, V., Becerra, A., Cain, S., Chan, J., Chen, W.J., Cho, J., da Veiga Beltrame, E., Diamantakis, S., et al. (2022). WormBase in 2022—data, processes, and tools for analyzing Caenorhabditis elegans. Genetics *220*, iyac003. https://doi.org/10.1093/genetics/iyac003.

167. Han, X., Zhou, Z., Fei, L., Sun, H., Wang, R., Chen, Y., Chen, H., Wang, J., Tang, H., Ge, W., et al. (2020). Construction of a human cell landscape at single-cell level. Nature *581*, 303–309. https://doi.org/10.1038/s41586-020-2157-4.

168. Lake, B.B., Chen, S., Sos, B.C., Fan, J., Kaeser, G.E., Yung, Y.C., Duong, T.E., Gao, D., Chun, J., Kharchenko, P.V., et al. (2018). Integrative single-cell analysis of transcriptional and epigenetic states in the human adult brain. Nat. Biotechnol. *36*, 70–80. https://doi.org/10.1038/nbt.4038.

169. Voigt, A.P., Mulfaul, K., Mullin, N.K., Flamme-Wiese, M.J., Giacalone, J.C., Stone, E.M., Tucker, B.A., Scheetz, T.E., and Mullins, R.F. (2019). Single-cell transcriptomics of the human retinal pigment epithelium and choroid in health and macular degeneration. Proc. Natl. Acad. Sci. USA *116*, 24100–24107. https://doi.org/10.1073/pnas.1914143116.

Please cite this article in press as: Purice et al., Molecular profiling of adult *C. elegans* glia across sexes by single-nuclear RNA-seq, Developmental Cell (2025), https://doi.org/10.1016/j.devcel.2025.05.013

CellPress
OPEN ACCESS

STAR★METHODS

KEY RESOURCES TABLE

REAGENT or RESOURCE	SOURCE	IDENTIFIER
Bacterial and virus strains		
E. coli OP50	Caenorhabditis Genetics Center	OP50
E. coli DH5α competent cells	Fisher Scientific	Cat#18-265-017
E. coli NEB 5-alpha competent	NEB	Cat#C2987
Chemicals, peptides, and recombinant proteins		
Sodium azide	Sigma-Aldrich	Cat#S-2002
Taq DNA Polymerase	Takara	Cat#R001B
ExTaq DNA polymerase	Takara	Cat#RR01AM
Phosphate-Buffered Saline (10X)	ThermoFisher	Cat#AM9625
Leibovitz's L-15 Medium, no phenol red	ThermoFisher	Cat#21083027
Protector RNase Inhibitor	Millipore Sigma	Cat#3335399001
Fetal Bovine Serum, certified, heat inactivated	Invitrogen	Cat#10082-139
Pronase, Protease from *Streptomyces griseus*	Sigma-Aldrich	Cat#P6911
TRIzol LS	Ambion	Cat#10296010
5Prime-Heavy Phase Lock Gel	VWR	Cat#10847-802
BamHI	NEB	Cat#R3136L
SphI	NEB	Cat#R3182L
AgeI	NEB	Cat#R3552S
Alt-R S.p. Cas9 Nuclease V3	IDT	Cat#1081058
Alt-R CRISPR-Cas9 tracrRNA	IDT	Cat#1072532
Alt-R CRISPR-Cas9 crRNA (tdTom target GGAGTTCAAGACCATCTACA)[149]	IDT	Custom guide
Tunicamycin	EMD Millipore	Cat#654380
DMSO	Sigma-Aldrich	Cat#472301
Critical commercial assays		
Gibson Assembly Cloning Kit	NEB	Cat#E5510S
PureLink Genomic DNA Mini Kit	ThermoFisher	Cat#K182001
QIAquick Gel Extraction Kit	Qiagen	Cat# 28704
QIAquick PCR Purification Kit	Qiagen	Cat#28104
QIAprep Spin Miniprep Kit	Qiagen	Cat#27106
Monarch Mini Prep Kit	NEB	Cat#T1110L
RNeasy Mini Elute Cleanup Kit	Qiagen	Cat#74204
QuantiTect Rev. Transcription Kit	Qiagen	Cat#205311
TaqMan Fast Advanced Master Mix	Fisher Scientific	Cat#4444557
Chromium Next GEM Single Cell 3' Kit v3.1	10x Genomics	Cat#1000269
unc-119 TaqMan assay	ThermoFisher	Cat#Ce02452615_g1
spig-9/F53F4.13 TaqMan assay	ThermoFisher	Cat#Ce02484052_g1
kcc-3 TaqMan assay	ThermoFisher	Cat#Ce02434964_g1
ptr-10 TaqMan assay	ThermoFisher	Cat# Ce02418075_g1
Deposited data		
Raw and processed snRNA-seq dataset of male and hermaphrodites	This paper	GEO: GSE256266
Jupyter notebook tutorials for pairwise differential analysis, classification model and gene ranking	This paper	https://github.com/settylab/worm-glia-atlas[147]

(*Continued on next page*)

Please cite this article in press as: Purice et al., Molecular profiling of adult *C. elegans* glia across sexes by single-nuclear RNA-seq, Developmental Cell (2025), https://doi.org/10.1016/j.devcel.2025.05.013

Continued

REAGENT or RESOURCE	SOURCE	IDENTIFIER
Mendeley Data: PairDEx and comparison to Roux et al.	This paper	https://doi.org/10.17632/sfnrgj5y4c.1
Experimental models: Organisms/strains		
C. elegans: Strain N2	Caenorhabditis Genetics Center	WormBase: N2; WormBase: WBStrain00000001
nsIs708 [$P_{mir-228}$:NLS:RFP + $P_{unc-122}$:RFP]	Sean Wallace/ Shaham lab, The Rockefeller University	OS11514
him-5(e1490) V	Caenorhabditis Genetics Center	CB4088; Wormbase: WBStrain00004536
him-5(e1490) V; nsIs708 [$P_{mir-228}$: NLS:RFP + $P_{unc-122}$:RFP]	This study	ASJ857
rnyEx043 [*pKT54* (P_{irk-3}:GFP); *pCL1 (pha-1+)*]	Wojtovich et al.[113], Nehrke Lab, University of Rochester Medical Center	KWN83
oxEx608 [*lin-15(+), pSS1.7, unc-31* promoter PCR fragment]	Wojtovich et al.,[113] Speese et al.[131], Jorgensen Lab, University of Utah	EG3410
nicSi3 II; unc-119(ed3) III	Yanagi and Lehrbach[149], Lehrbach Lab, FHCC	NJL3730
nicSi2 I; unc-119(ed3) III	Yanagi and Lehrbach[149], Lehrbach Lab, FHCC	NJL3729
sIs10739 [*rCesC51E3.7a*:GFP + P_{Ceh361}]; *dpy-5(e907) I*	Caenorhabditis Genetics Center[131]	BC12649; Wormbase: WBStrain00002237
dpy-5(e907) I; *sEx11763* [*rCesK04F10.4*: GFP + P_{Ceh361}]	Caenorhabditis Genetics Center	BC11763; Wormbase: WBStrain00001874
dnaEx231 [P_{srlf-2}:GFP + $P_{unc-122}$:GFP]; *him-5 V; nsIs708* [$P_{mir-228}$:NLS:RFP + $P_{unc-122}$:RFP]	This study	ASJ760
dnaEx395 [P_{nxnr-1}:GFP + $P_{unc-122}$:GFP]; *him-5(e1490) V; nsIs708* [$P_{mir-228}$: NLS:RFP + $P_{unc-122}$:RFP]	This study	ASJ890
dnaEx331 [P_{ntfc-1}:GFP + $P_{unc-122}$:GFP]; *him-5 V; nsIs708* [$P_{mir-228}$: NLS:RFP + $P_{unc-122}$:RFP]	This study	ASJ895
dnaEx246 [$P_{spig-14}$:GFP + $P_{unc-122}$:GFP]; *him-5 V; nsIs708* [$P_{mir-228}$: NLS:RFP + $P_{unc-122}$:RFP]	This study	ASJ767
dnaEx604 [P_{cat-2}:NLS:RFP + $P_{spig-14}$: GFP + $P_{unc-122}$:GFP]; *him-5(e1490) V*	This study	ASJ1308
dnaEx373 [P_{spig-8}:GFP + $P_{unc-122}$:GFP]; *him-5(e1490) V; nsIs708* [$P_{mir-228}$: NLS:RFP + $P_{unc-122}$:RFP]	This study	ASJ946
dnaEx508 [P_{spi-2}:GFP + $P_{unc-122}$:GFP]; *nsIs708* [$P_{mir-228}$:NLS:RFP + $P_{unc-122}$:RFP]; *him-5 V*	This study	ASJ1209
dnaEx616 [P_{klp-6}:GFP + P_{spi-2}: mScarlet + $P_{unc-122}$:RFP]; *him-5 V*	This study	ASJ1351
dnaEx632 [$P_{col-177}$:GFP + P_{spi-2}: mScarlet + $P_{unc-122}$:RFP]	This study	ASJ1406
rnyEx043 [pKT54 (P_{irk-3}:GFP); pCL1 (pha-1+)]; pha-1(e2123ts) III; nsIs708 [$P_{mir-228}$: NLS:RFP + $P_{unc-122}$:RFP]; *him-5(e1490) V*	This study	ASJ1307
dnaEx451 [$P_{zipt-2.2}$:GFP + $P_{unc-122}$:GFP]; *him-5(e1490) V; nsIs708* [$P_{mir-228}$: NLS:RFP + $P_{unc-122}$:RFP]	This study	ASJ1020

(*Continued on next page*)

Please cite this article in press as: Purice et al., Molecular profiling of adult *C. elegans* glia across sexes by single-nuclear RNA-seq, Developmental Cell (2025), https://doi.org/10.1016/j.devcel.2025.05.013

CellPress
OPEN ACCESS

Continued

REAGENT or RESOURCE	SOURCE	IDENTIFIER
dnaEx586 [P_{kcc-3}:GFP + P_{ttr-43}: NLS:RFP]; him-5(e1490) V	This study	ASJ1259
dnaIs638 [unc-119(+) + $P_{zipt-2.2}$:GFP] I; dnaIs31 [unc-119(+) + P_{ttr-43}:mScarlet] II; unc-119(ed3) III; him-5(e1490) V	This study	ASJ1439
dnaEx377 [$P_{col-177}$:GFP + $P_{unc-122}$:GFP]; him-5(e1490) V; nsIs708 [$P_{mir-228}$:NLS: RFP + $P_{unc-122}$:RFP]	This study	ASJ966
dnaEx30 5[P_{mfsc-1}:GFP + $P_{unc-122}$:GFP]; him-5(e1490) V; nsIs708 [$P_{mir-228}$: NLS:RFP + $P_{unc-122}$:RFP]	This study	ASJ779
dnaEx304 [$P_{spig-17}$:GFP + $P_{unc-122}$:GFP]; him-5(e1490) V; nsIs708 [$P_{mir-228}$: NLS:RFP + $P_{unc-122}$:RFP]	This study	ASJ1022
dnaEx307 [$P_{spig-16}$:GFP + $P_{unc-122}$:GFP]; him-5(e1490) V; nsIs708 [$P_{mir-228}$: NLS:RFP + $P_{unc-122}$:RFP]	This study	ASJ781
oxEx608 [lin-15(+), pSS1.7, unc-31 promoter PCR fragment]; him-5(e1490) V; nsIs708 [$P_{mir-228}$:NLS:RFP + $P_{unc-122}$:RFP]	This study	ASJ1055
sIs10739 [rCesC51E3.7a:GFP + P_{Ceh361}]; dpy-5(e907) I; him-5(e1490) V; nsIs708 [$P_{mir-228}$:NLS:RFP + $P_{unc-122}$:RFP]	This study	ASJ1000
dpy-5(e907) I; sEx11763 [rCesK04F10.4: GFP + P_{Ceh361}]; him-5(e1490) V; nsIs70 8[$P_{mir-228}$:NLS:RFP + $P_{unc-122}$:RFP]	This study	ASJ1363
dnaIs638 [unc-119(+) + $P_{zipt-2.2}$:GFP] I; dnaIs31 [unc-119(+) + P_{ttr-43}:mScarlet] II; unc-119(ed3) III; him-5(e1490) V	This study	ASJ1439
See Table S4 for complete list of strains		N/A
Oligonucleotides		
See Table S4 for a list of all oligonucleotides		N/A
Recombinant DNA		
See Table S4 for a list of all plasmids		N/A
Software and algorithms		
Fiji (2.16.0)	Schindelin et al.[150]	https://imagej.net/software/fiji/; RRID:SCR_003070
ApE	Davis and Jorgensen[151]	https://jorgensen.biology.utah.edu/wayned/ape/; RRID:SCR_014266
Adobe Creative Suite	N/A	https://adobe.com; RRID:SCR_014199
GraphPad Prism (9.5.1)	N/A	https://www.graphpad.com/; RRID:SCR_002798
R (4.1.1)	N/A	https://www.r-project.org/; RRID:SCR_001905
Cell Ranger (v5.0.1)	10X Genomics	https://support.10xgenomics.com/single-cell-gene-expression/software/downloads/latest
Python (v3.8.10)	Python	N/A
Python package scanpy (v1.9.1)	SCANPY: large-scale single-cell gene expression data analysis[152]	https://scanpy.readthedocs.io/en/stable/installation.html
Python package scikit-learn (v0.24.2)	Scikit-learn: Machine Learning in Python[153]	https://scikit-learn.org/stable/install.html

(*Continued on next page*)

Please cite this article in press as: Purice et al., Molecular profiling of adult *C. elegans* glia across sexes by single-nuclear RNA-seq, Developmental Cell (2025), https://doi.org/10.1016/j.devcel.2025.05.013

Continued

REAGENT or RESOURCE	SOURCE	IDENTIFIER
Python package scipy (v1.7.0)	SciPy 1.0: fundamental algorithms for scientific computing in Python[154]	https://scipy.org/install/
Python package palantir (v1.0.0)	Characterization of cell fate probabilities in single-cell data with Palantir[155]	https://github.com/dpeerlab/Palantir https://scipy.org/install/
Python package harmonypy (v0.0.5)	Fast, sensitive and accurate integration of single-cell data with Harmony[156]	https://harmony-py.readthedocs.io/en/stable/user/install.html
Other		
Confocal Laser Scanning	Zeiss	LSM780
COPAS Biosort System	UNION BIOMETRICA	N/A
Cell strainer (50 μm)	pluriStrainer	Cat#43-50050-03
Cell strainer (40 μm)	pluriStrainer	Cat#43-50030-40
Cell strainer (30 μm)	pluriStrainer	Cat#43-50030-50
Mendeley Data: PairDEx and comparison to Roux et al.	This study	https://doi.org/10.17632/sfnrgj5y4c.1
Glial Atlas Website	This study	https://wormglia.org

EXPERIMENTAL MODEL AND STUDY PARTICIPANT DETAILS

Husbandry conditions of experimental animals

C. elegans were cultured and maintained at 20°C. Animals were grown on NGM-agar plates supplemented with cholesterol and seeded with *E. coli* OP50 strain as food source, per standard practice.[157,158]

METHOD DETAILS

Transgenesis methods

Transgenic reporters were generated using standard techniques[159] with injections of 100 ng/μL DNA (5-50 ng/μL per plasmid). All transgenic arrays were generated with 30 ng/μl P_{mig-24}:Venus or 10-20 ng/μL $P_{unc-122}$:GFP as co-injection markers[160,161] and 1-4 transgenes evaluated per genotype. Integrated reporters were created using FLInt (**F**luorescent **L**andmark **Int**erference)[162] landing pad strains.[149] All strains are listed in Table S4. For all reporter analyses, animals were picked as L4, and expression analyzed a day later as day 1 adult animals. Unless otherwise noted, all male data was acquired in *him-5 (e1490)* mutant background.

Preparation of adults for dissociation

Worms were grown on 10 cm, standard 1% NGM agar plates seeded with *E.coli* strain OP50. To obtain synchronized day 1 adult worms, embryos were first obtained by hypochlorite treatment (1N NaOH + 4% NaOCl freshly made) of gravid adult hermaphrodites. The embryos were plated and hatched overnight (16-20 hours) on unseeded NGM agar plates and L1 arrested worms were allowed to recover on 10 cm OP50-seeded plates at 20°C for 64-68 hours. For each hermaphrodite sample, about 50,000 day 1 adult worms were washed off plates with M9 into 50 ml conical tubes that were fitted with a 50μm pluriStrainer® filter to separate day 1 adults from embryos or hatched L1s. Filtered day 1 adult hermaphrodite population were spot verified by eye for age, transferred to 15 ml conical tubes and washed 3x with M9 with centrifugation at 1200 rcf for 1 min. For each male sample, about 150,000 day 1 adult worms of mixed sexes were washed off plates with M9 into 50 ml conical tubes fitted with stacked 50μm, 40 μm, and 30μm pluriStrainer® filters to separate adult males from hermaphrodites. The stacked filtration was repeated 1x. Worms from the 30μm filter were a mix of 80-90% males and some young day 1 adult hermaphrodites. To further enrich for a male only population, this fraction was sorted using a Union BioMetrica COPAS worm sorter and gated to select animals by size and lack of P_{mig-24}: mVenus staining. This recovered 50,000 males. After sorting, 5x10 μl aliquots of worms were visualized under a light microscope and confirmed to contain 100% males. We also recovered ~50,000 *him-5* hermaphrodites from the worm sorter. All worms were washed again 3x with M9 with centrifugation at 1200 rcf for 1 min, before proceeding to dissociation.

Dissociation

Single nuclei suspensions were obtained as described[63] with modifications to further dissociate the cell membranes. For the hermaphrodite samples, worms were split into 1.6 ml clear tubes with M9, containing 250 μl pellets. A tabletop mini centrifuge was used to pellet worms during all dissociation steps. After removing the M9 solution, worms were quickly washed once in 500 μl lysis buffer (200mM DTT, 0.25% SDS, 20mM HEPES pH 8.0, 3% sucrose), and lysed with 750 μl lysis buffer for 5 min for hermaphrodites and 3 minutes for males (longer lysis time caused the males to rupture during the downstream M9 washing steps). Cuticle disruption was monitored by examining 1 μl of sample under a microscope. Lysis was noted as complete when worms had a slightly blunt head

Please cite this article in press as: Purice et al., Molecular profiling of adult *C. elegans* glia across sexes by single-nuclear RNA-seq, Developmental Cell (2025), https://doi.org/10.1016/j.devcel.2025.05.013

but were not ruptured. Reaction was stopped by adding 500 μl M9 and 6x quick washes in M9. Lysed worms were then dissociated by adding 500 μl freshly made 20 mg/ml Pronase mix (resuspended in water) to the worm pellet for 15-20 minutes (adjusted based on variable Pronase activity/lot). Males were dissociated in 15 mg/ml Pronase. During Pronase incubation, worms were dissociated by pipetting vigorously with a P1000 pipette set to 400 μl every 45 seconds, rotating between samples for 10 minutes, followed by trituration with a P200 pipette set to 200 μl for 5-10 minutes. Worms were quickly spun down between trituration so that the worm pellet size could be monitored. Between pipetting, 2 μl of worms were examined on a dissecting scope to assess level of dissociation. Dissociation was continued until large fragments were gone and the pellet of worms was less than 20μl after centrifugation. With this protocol, most cell membranes were digested away. To stop the digestion, 750 μL of ice-cold 1xPBS/10%FBS was added to the tube. Dissociated nuclei were transferred to a 1 ml syringe using a 27-gauge needle. The needle was replaced by a 5 μM syringe filter that was pre-wetted with ice cold 1xPBS. The nuclei were gently passed through the syringe filter directly into the FACS collection tube on ice. Protector RNase Inhibitor was added to the following solutions: Pronase, PBS-FBS, and PBS-L15-FBS to get final concentration of 2U/μl inhibitor.

Cell sorting and single nuclear RNA-sequencing

Nuclei were sorted with a Sony MA900 cell sorter fitted with a 100 μm nozzle running at a speed of 10-12k events/second using the PE (R-Phycoerythrin) filter set channel FL2 (585/30). For hermaphrodite samples, age matched N2 worms were used as negative control to set FACS gates. For male samples, *him-5* males were used as negative controls. In either case, negative controls were taken through identical dissociation protocols. All nuclei samples were sorted into 1:1 1xPBS:L15 + 30%FBS 2U/μl Protector RNAse inhibitor, transferred to a low-bind 2 ml tube and centrifuged 9600g for 5 min at 4°C. Once an RFP^+ pellet was confirmed under a fluorescent dissection scope, the nuclei were gently resuspended in 1xPBS/10%FBS buffer to an approximate final concentration of 1000 nuclei/μL, which was then verified by hemocytometer counting. Each sample approximated 10,000 cells and was then processed on the 10X Chromium platform using 10X NextGem v3.1 chemistry. cDNA was amplified for 12 cycles and the index PCR was cycled 12 times. Final libraries were brought to 10 nM concentration and processed on an Illumina HiSeq2500 sequencer. Male and hermaphrodite samples were prepared and sequenced on different days, for a total of 2 biological replicates for either sex.

RT-qPCR

About 200,000 RFP^+ nuclei were sorted directly into Trizol LS and stored at −80°C until RNA extraction. "Whole animal" controls consisted of dissociated nuclei of N2 worms stored on ice during FACS to mimic the same amount of time the RFP^+ samples were being sorted; and 100 μl of this nuclei suspension was added to Trizol LS after FACS was complete. After thawing, samples were incubated at 65°C for 5 min with vortexing every 1 minute. One fifth volume of chloroform was added to each sample and mixed in a 5Prime-Heavy Phase Lock Gel, and samples were then centrifuged (12,000g, 15 min). The upper aqueous phase was removed, and RNA was isolated using Qiagen RNeasy MinElute Cleanup Kit. RNA was quantified using the Qubit fluorometer. DNase digestion and RNA reverse transcription was performed using Qiagen QuantiTect Reverse Transcription Kit. The resulting cDNA was diluted 1:5, and 2μl was used for each RT-qPCR reaction. Real time assays were performed using TaqMan gene expression assays (ThermoFisher) and TaqMan Fast Advanced Master Mix on a QuantStudio™ 5 system (ThermoFisher). Gene *pmp-3* (TaqMan assay Ce02485188_m1) was used as the control housekeeping gene. The following TaqMan assays were also utilized: *unc-119* (TaqMan assay Ce02452615_g1), *spig-9/F53F4.13* (TaqMan assay Ce02484052_g1), *kcc-3* (TaqMan assay Ce02434964_g1), *ptr-10* (Taqman assay Ce02418075_g1).

Transcriptional reporter plasmids

For each CEG transcriptional reporter, the promoter sequence was determined as the sequence upstream of the ATG start codon and up to either 3kb upstream or to the nearest upstream gene, whichever came first. This was PCR-amplified from genomic DNA with SphI and BamHI enzymes in the promoter sequence and the amplicon was ligated into pSM:GFP.[163] Some plasmids were generated by restriction cloning into pSM:GFP vector, and most via Gibson assembly. Briefly, the PCR-amplicon also contained the AgeI enzyme site in the promoter sequence. Gibson assembly was performed by mixing fragments of the different DNAs at a 2:1 or 3:1 ratio (insert:vector) and a 2X Gibson Assembly Master Mix. The bacterial transformation was done using either Invitrogen Subcloning Efficiency™ DH5α Competent Cells or NEB 5-alpha Competent *E. coli* (High Efficiency). All plasmid sequences (Table S4) were verified by standard Sanger sequencing or Oxford Nanopore Technologies whole plasmid sequencing (plasmidsaurus).

Microscopy, Image Processing, and Analysis

Day 1 animals were immobilized with 40mM sodium azide. Images were collected on a Zeiss 780 LSM NLO with a 40x/1.3NA Plan Neofluar oil-immersion. Image processing was done in FIJI ImageJ and Adobe Photoshop. Outlines of head and tail regions were based on reference transmitted light images acquired simultaneously and overlayed in FIJI and Adobe InDesign. For each genotype analyzed, 1-4 transgenes were examined (Table S4). From the 10-20 animals evaluated for each transgene and sex, on average, 2-5 animals displaying clear expressions in the correct orientation were imaged for documentation. All images in figures shown as Z-stack projections.

Please cite this article in press as: Purice et al., Molecular profiling of adult *C. elegans* glia across sexes by single-nuclear RNA-seq, Developmental Cell (2025), https://doi.org/10.1016/j.devcel.2025.05.013

Aging and tunicamycin stress

For the aging experiments, L4 staged animals were picked onto fresh NGM plates seeded with OP50 and maintained at 20°C. The adults were transferred daily to new plates to avoid overcrowding, and this process continued until the animals reached 8 days of age, at which point they were imaged. For inducing stress in young animals experiments, endoplasmic reticulum (ER) stress was induced using previously described protocols[83] with UPR^{ER} reporter animals (P_{hsp-4}::GFP) as positive control to monitor stress induction (Figure S7J). Briefly, animals were age-synchronized by bleaching and grown to the L4 stage at 20°C on OP50. At the L4 stage, the animals were washed off the plates using M9 buffer, washed once more with M9, and resuspended in M9 containing either 25 ng/μL tunicamycin (EMD Millipore, 654380) or DMSO (Sigma, 472301) as a control. The animals were incubated at 20°C on a rotating platform for 3 hours. After incubation, the animals were washed twice with M9, replated onto fresh NGM plates seeded with OP50, and allowed to recover overnight at 20°C. The following morning, the animals were imaged.

Single-cell data analysis

10X Cell Ranger (v5.0.1) was used to generate the count matrices for each sample. The 3' untranslated regions (UTRs) in the reference transcriptome (WormBase WS280) were previously reported to be too short for reliable gene assignment.[45,65] Therefore, following the previously published approaches for prior genome releases, we extended 3' UTRs for the WS280 genome.[45,65] Specifically, for genes not overlapping with a downstream gene, 3' UTRs were extended by 50, 100, 150, 200, 250, 300, 400 and 500bp. If the extended sequence collided with a downstream gene, it was trimmed back to the base next to the gene. The unmodified and eight modified GTF files were each used to build a reference genome. Protein-coding genes and non-coding RNA genes (lincRNAs, ncRNAs and antisense RNAs) were included for gene expression count determination. Cell Ranger was used to generate a count matrix for each sample relative to each reference and the optimal 3' UTR extension was defined as follows: 20 reads were considered as a significant gain by an extension interval. For each gene, the cumulative sums from 3' (the longest extension) to 5' was calculated after subtracting 20 from read increment in each extension interval. The optimal extension for a given sample was set to the point which had the smallest cumulative sum of less than 0. If cumulative sums were all greater than zero, the optimal extension was set to 500bp. The final extension of a gene was set to the point supported by most samples and by at least two samples. Cell-containing droplets by 10X Cell Ranger were used for downstream analysis (16687 cells in hermaphrodites and 14723 cells in males replicates respectively, for a total of 31410 cells measured across 28045 genes). Housekeeping genes were excluded from all downstream analyses (Table S1). The four samples were concatenated resulting in a final count matrix of 31410 cells and 12376 genes. For hermaphrodites, this reflected 1114 UMIs/cells and 458 genes/cell detected; for males 1350UMIs/cell and 525 genes/cell; which globally averaged to 1224 UMIs/cell and 491 genes/cell detected, and ~90k-100k mean reads per cell, which accounts for ~92-94% of genome. Thus, recovery from our single-nuclear RNA-seq approximated that of reported single-cell RNA-seq studies.[65,86]

Data processing

Data processing was performed using the scanpy package[152] with default parameters unless specified. Raw counts were normalized by dividing the counts by total counts per cell. The normalized data was multiplied by the median of total counts across cells to avoid numerical issues and log-transformed with a pseudo count of 1. Feature selection was then performed to select the top 2500 most highly variable genes (using **scanpy.pp.highly_variable_genes**), which was used as input for principal component (PC) analysis with 50 components. PCs were used as input for generating UMAPs[164] (with **min_dist=0.2**) and clustering with Leiden,[165] resulting in 51 clusters. MAGIC[148] imputation was used to visualize gene expression on UMAPs.

Annotation of glial, neuronal, and anatomical compartments

We utilized a multi-pronged approach to annotate each of the 51 clusters as belonging to one of glial, neuronal, and non-neural compartments. First, we identified differentially expressed genes for each cluster using **scanpy.tl.rank_gene_groups** by comparing gene expression in each cluster to all other cells (adjusted **p-value < 1e-3**, **logFC > 1.5**). We then performed a literature survey to identify cell types where possible (Table S1).

Next, we utilized the CeNGEN[45] dataset to identify neuronal, and other non-glial clusters. Count matrices and annotations were downloaded from the NCBI Gene Expression Omnibus (GEO) at https://www.ncbi.nlm.nih.gov/geo/query/acc.cgi?acc=GSE136049. Data was processed as described in the "data processing" section. Differential expression was performed to identify sets of genes that define each cell type (adjusted **p-value < 1e-3**, **logFC > 1.5**) in the CenGEN data (Table S1). Each set of genes for a given cell type in the CeNGEN data were then used to derive gene signature scores for each cell in our dataset: We first z-scored the expression of each gene across all cells and a signature score was computed for each cell by averaging the z-scores expression across the gene set. Gene signature scores were then used to associate compartments to our clusters based on the enrichment of a particular CenGEN cell type signature. As a complement and to corroborate our findings, the same analysis was done with the Roux dataset[86] where the same enrichment analysis was performed using the D1 hermaphrodite cells to derive signatures. Using this approach, we identified clusters that were consistently highly enriched for anatomical or neuronal signatures in either CeNGEN and Roux data by visual inspection (Figure 1F; Table S1). The remainder of the clusters were annotated as putative glial cells. These clusters were also enriched for glial signatures from either dataset (Figure 1F; Table S1).

Please cite this article in press as: Purice et al., Molecular profiling of adult *C. elegans* glia across sexes by single-nuclear RNA-seq, Developmental Cell (2025), https://doi.org/10.1016/j.devcel.2025.05.013

Batch effect correction between all hermaphrodite and male cells

We excluded mitochondrial genes prior to batch correction (Table S1). We then identified highly variable genes separately amongst the hermaphrodite and male cells (2500 genes for each sex) and used the union of these highly variable genes for downstream analysis (3355 genes) as input to PCA (50 components). Harmony[156] was used to perform batch effect correction and the corrected PCs were used as input for UMAP and Leiden clustering (Figure S4A). We identified 43 clusters following batch-correction (Figure S4A). Cell type compartments were transferred by computing the fractions of glia, neuronal and anatomical cells within each cluster and assigning labels to each cluster based on the highest proportion of cells that make up a particular cluster. Batch corrected data was used for visualizations and for identification of pan-glial marker genes.

Glial compartment batch correction

Normalized count matrix was subset to contain only the annotated glial clusters. Batch correction was performed as described above after reselecting highly variable genes using only the glial cells (3626 genes). Leiden clustering led to identification of 32 clusters (Figure 2A). We note that batch-correction may mask biological variance between sexes, hence this conservative data processing will, if at all, under-report inherent sexual dimorphism.

PairDEx for computational annotation of glial types

We observed that standard differential expression analysis that compares cells of one cluster to all other cells was insufficient to identify genes that are uniquely expressed in each cluster. Therefore, we devised PairDEx to identify genes that are likely expressed specifically in each cluster, which we term CEGs: cluster enriched genes. PairDEx performs pairwise differential expression analysis procedurewhere each cluster is compared to every other cluster leading to higher degree of specificity for CEGs. Thus, CEGs served as input for our *in-vivo* experiments to annotate glial cell types.

Given a cluster that needs to be annotated, we first performed differential expression analysis using **scanpy.tl.rank_gene_groups** to compare cells of the cluster with cells of every other cluster separately. We then enumerated the number of comparisons in which a gene was significantly higher (adjusted **p-value < 1e-25, logFC > 1.5** - stringent filtering criteria was used to ensure specificity). Genes were ranked based on their frequency of significant differential expression and visualized using heatmaps (e.g: Figure 2C). Candidates for in vivo validation were selected based on the frequency of differential expression and their mean expression in the cluster. Clusters were annotated as a particular glial cell type based on in vivo anatomical locations and previously characterized marker genes (Table S2).

Additionally, these results were used to create a table of top markers (Table S2). In brief the top 10 markers in terms of number of significant comparisons were identified for each cluster. If a cluster had more than 10 marker genes which were significant in all 31 comparisons, all were used. Additional information such as the percent of the cells in the cluster expressing the gene, and other cell types identified as expressing the gene were recorded.

Sex-specific and sex-shared glial types

We nominated a cluster as sex-specific or shared based on the fraction of male and hermaphrodite cells in the cluster. A cluster was assigned as hermaphrodite-specific if it comprised of >90% hermaphrodite cells, as male-specific if it comprised of >90% male cells, and as a shared cluster otherwise (Figure S2A). The thresholds were chosen such that the quantification should reflect the true biology of sex-specific glia. We expected one or two hermaphrodite specific glial clusters to account for hermaphrodite specific glia.

Sexually dimorphic PHsh glia analysis

We compared the *vap-1*$^{-}$ (hermaphrodite enriched) cells from Cluster 10-AMsh/PHsh with the cells of the male Cluster 27-PHsh. Differential expression between the hermaphrodite and male PHsh glial cells was performed with **scanpy.tl.rank_gene_groups** function (**method = "wilcoxon"**). Genes that met the following criteria were considered significant and highlighted on the volcano plot: adjusted **p-value** < 1e-4, absolute logFC > 1.5, and expression in greater than 10% of cells in either group.

Sheath and Socket glia annotations

Sheath and socket glia annotations were determined using hierarchical clustering. Mean of batch corrected principal components for each cluster were used to compute the pairwise cosine similarities between each pair of clusters within the glia only dataset. The pairwise similarity matrix was hierarchically clustered using the **scipy.cluster.hierarchy** function (**linkage='average'** and **metric='euclidean'**). This resulted in two distinct clades which were annotated as sheath and socket based on annotation of glial cell types (Figure 5A).

Determination of pan-glial markers

A supervised classification approach was used to identify a core set of markers that could accurately distinguish between glia and non-glial cells based on gene expression. Specifically, we trained a logistic regression model to distinguish between glial cells and non-glial cells (Neurons/Non-Neural/Coelomocyte cells) using gene expression as features and devised a feature ranking scheme to identify a small set of markers that span all glial cells.

Please cite this article in press as: Purice et al., Molecular profiling of adult *C. elegans* glia across sexes by single-nuclear RNA-seq, Developmental Cell (2025), https://doi.org/10.1016/j.devcel.2025.05.013

Gene selection

The following criteria were used for selection of genes as features: (i) Genes that are highly variable in either hermaphrodite or male glial and non-glial cells and (ii) Genes detected in at least of 40% of cells in at least one cluster. MAGIC imputed gene expression[148] following batch correction was used as features for training the classifier.

Cell selection

Hermaphrodite cells were used for training to test for generalization. Cells that were part of the in vivo validated glia types were used as the glial class for training. Cells from neuronal, non-neuronal and coelomocyte clusters were used as the negative class. Glial-like cells that were identified in our dataset were excluded (Clusters 13, 14, 17, 18, 20, 29). The classification model was trained using hermaphrodite cells and the male cells were used for inference and validation of the selected genes (Figure S4A).

Logistic regression

Formally, the gene expression matrix can be represented as $X \in \mathbb{R}^{n_{cell} \times m_{gene}}$, where n_{cell} is the total number of cells (both glia and non-glia) and m_{gene} is the number of genes. Each cell i was associated with a label such that $y_i = 1$ is cell i is a glial cell and that $y_i = -1$ is cell i is a non-glial cell. Cells were randomly split into training (70%), validation (20%) and test (10%). The sampling was performed separately for each cluster to ensure representation of each cluster across all the splits.

A logistic regression model was trained using **sklearn.linear_model.LogisticRegression**[153] with L1-lasso regularization penalty. L1 regularization effectively eliminates genes that are not informative in predicting class labels and retains genes that are most informative for distinguishing glial and non-glial cells. The model is defined as follows:

$$P_{Glia}(x_i, w) = \frac{1}{1+e^{-(x_i w + w_0)}}$$

$$P_{Non-Glia}(x_i, w) = 1 - P_{Glia}(x_i) = \frac{e^{-(x_i w + w_0)}}{1+e^{-(x_i w + w_0)}}$$

Where:

- x_i is the gene expression vector of length m_{genes} for cell i
- $w \in \mathbb{R}^{m_{genes} \times 1}$ represents the parameters of the logistic regression model and represents the importance of each gene in distinguishing glial and non-glial cells. Genes with positive weights are more informative for glial cells whereas genes with negative weights are more informative for non-glial cells.
- w_0 is the intercept term.
- $P_{Glia}(x_i, w)$ is the probability of cell i belonging to the glial class.
- $P_{Non-Glia}(x_i, w)$ is the probability of cell i belonging to the non-glial class.
- By definition, $P_{Glia}(x_i, w) + P_{Non-Glia}(x_i, w) = 1$

Given label y for each cell, the parameters were estimated using L1-lasso regularization penalty:

$$\min_w J(y, P_{class}(x), c), \forall_c \in C$$

Where $J(y, P_{class}(x), c)$ is the log-loss cost function with L1 penalty defined as follows

$$\min_w J(y, P_{class}(x), c) = \sum_{i=1}^{n} [y_i \log(P_{Glia}(x_i)) - (1 - y_i) \log(P_{Non-Glia}(x_i))] + \frac{1}{c} \sum_{i=1}^{m_{genes}} ||w_i||_1$$

$c$is the inverse of regularization parameter that controls the degree of regularization. We trained the model using a set of inverse regularization parameter **c={0.001, 0.005, 0.01, 0.05, 0.1, 0.5, 1.0, 5.0}** and chose the parameter with highest classification accuracy in the validation dataset. We then retrained the model with this parameter using all hermaphrodite cells for downstream analysis.

Gene ranking and selection

We developed an iterative feature ranking procedure to identify the most informative features that can confidently predict all glial cells and thus represent a core set of pan-glial markers. The ranking procedure ensures that the selected markers are informative across the heterogenous glial types.

We first ranked individual genes by their ability to distinguish glial from non-glial cells based on their inferred logistic regression weights. Briefly, if w is the set of inferred weights, the ability of a gene g to predict glial class is given by $P_{Glia}(x_i, w^{(g)})$ where $w^{(g)} : w \; \exists w_i = 0, \forall_{i \neq g}$ i.e., we zero-ed out all the weights of all genes except for gene g and thus estimated the probability of predicting the glial class using only gene g for cell i.

The probabilities for a gene were summarized across all glial cells to derive a score for the gene as follows:

$$GlialScore(g) = \frac{1}{n_{Glia}} \sum_{i \in I}^{n_{Glia}} P_{Glia}(x_i, w^{(g)})$$

Where x_i is a glial cell.

Please cite this article in press as: Purice et al., Molecular profiling of adult *C. elegans* glia across sexes by single-nuclear RNA-seq, Developmental Cell (2025), https://doi.org/10.1016/j.devcel.2025.05.013

This process was repeated for all genes used in the model and the gene with the highest score was the selected as the first glial marker.

$$\underset{g \in G}{\text{argmax}}[GlialScore(g)] = \underset{g \in G}{\text{argmax}}\left[\frac{1}{n_{Glia}}\sum_{i \in I}^{n_{Glia}} P_{Glia}\left(x_i, w^{(g)}\right)\right]$$

Additional markers were selected in an iterative manner. Let S be the current set of glial markers initialized with the gene with the highest *GlialScore*. Using only this set of genes, we computed the average probability for each glial cluster in the data and identified a glial cluster, k with the lowest probability.

$$ClusterScore(c, S) = \frac{1}{n_{cell}}\sum_{i \in c}^{n_{cell}} P_{Glia}\left(x_i, w^{(S)}\right)$$

$$k = \underset{c \in K}{\text{argmin}}[ClusterScore(c, S)\ ]$$

where $w^{(S)} : w\ \exists w_i = 0, \forall_{i \notin S_g}$ i.e., weights of all gene not in the marker set S are set to 0, K is the set of glial clusters, i is a cell in cluster c.

The next gene chosen as a glial marker thus should be informative for cluster k and was chosen as follows:

$$g_{add} = \underset{g \in G}{\text{argmax}}[ClusterScore(k, S')\ ]\ |\ S' = S \cup \{g\}$$

The marker set was then updated as $S' = S \cup \{g_{add}\}$

Pan-glial signature

We defined the pan-glial signature as the minimal set of genes that could distinguish all glial clusters from non-glial clusters with >95% accuracy. Starting with the top 10 genes (Figure S4E), we determined the predictive power of all possible subsets of these genes (individual genes, two-gene combinations, three-gene combinations through the full set of 10 genes) and identified the smallest subset that could serve as the pan-glial signature.

To test the predictive power of a given subset in distinguishing glial cells from non-glial cells, we modified the gene ranking procedure to derive a score for groups of genes rather than ranking of individual genes. Specifically, we determined the glial probability estimates using only the subset of genes under consideration. If w is the set of inferred weights from logistic regression, the ability of a set of genes z_{genes} to predict glial class is given by $P_{Glia}(x_i, w^{(z_{genes})})$ where $w^{(z_{genes})} : w\ \exists w_i = 0, \forall_{i \notin z\_genes}$ i.e., we zero out all the weights of all genes except for genes in the set z_{genes} and thus estimate the probability of predicting the glial class using only the set z_{genes} for cell i. We then compute a *CombinationClusterScore* for cluster $c$as follows:

$$CombinationClusterScore\left(c, z_{genes}\right) = \frac{1}{n_{Cells\ in\ Cluster\ c}}\sum_{i \in I}^{n_{Cells\ in\ Cluster\ c}} P_{Glia}\left(x_i, w^{(z_{genes})}\right)$$

The subset z_{genes} with the fewest genes with *CombinationClusterScore* > 0.95 for all clusters was chosen as the pan-glial signature shown in Figure 4A.

Robustness checks

We applied the model trained on hermaphrodite cells to the male cells and achieved near perfect classification accuracy (Figure S4B, right). This demonstrates the generalization of our pan-glial signature the male cells are comprised of a number of male-specific glial clusters that were not part of the training procedure.

We further tested the robustness of our pan glia signature by utilizing the Roux dataset.[86] We combined our data with Roux data by performing batch correction using Harmony using genes that were highly variable in either dataset (5246 genes). Leiden clustering led to identification of 111 clusters. Clusters were annotated as Glia if 80% of the cells from the Purice data found in the cluster were of one of the previously annotated glial types and were annotated as non-Glial otherwise. The model was trained to distinguish glia from our dataset (Purice et al.) from non-glia from the Roux et al. dataset.[86]

Identification of sheath and socket markers

Markers for sheath and socket glia were determined using the same classification and gene ranking procedure defined in pan-glial marker analyses section. Without loss of generalization, socket cells were used as a positive class and sheath cells were used as the negative class. Like the pan-glial marker analysis, we used genes that were highly variable in either hermaphrodite or male cells. Only the subset of these genes that were detected in at least 45% of cells in at least one cluster were used as features for classification. In vivo validated glia types were used, and glial-like cells were excluded (Figure S5A). Male cells were used for training since there are higher number of male-specific glial types.

Please cite this article in press as: Purice et al., Molecular profiling of adult *C. elegans* glia across sexes by single-nuclear RNA-seq, Developmental Cell (2025), https://doi.org/10.1016/j.devcel.2025.05.013

In contrast to identification of pan-glial markers, gene ranking analysis was performed separately for sheath and socket glia. We selected 7 genes for socket and sheath respectively with the final gene set containing 14 genes (Figure 5C). The selected genes consistently showed robust performance in distinguishing and classifying the sheath and socket clusters and generalizes across both male and hermaphrodite sheath and socket glia.

To identify sheath and socket glial signatures, we employed the same framework applied for identification of the pan-glial signature to identify minimal sets of genes that distinguish sheath and socket clusters from each other. This identified a 2 gene signature for sheath and a 3 gene signature for socket glia (Figure S5D).

Cell counting

Heads, midbody (posterior deirid/PDE sense organ) and tails of hermaphrodites expressing $P_{mir\text{-}228}$:NLS:RFP pan-glial reporter were imaged using settings that allowed for capturing dim nuclei. For nuclei counting, the head was segmented into three zones, using the mid-point of the first and second pharyngeal bulbs as borders between zones. If a nuclei was on the border, it was counted in the zone with higher overlap. Sheath glia were counted using $P_{ttr\text{-}43}$:mScarlet and $P_{mir\text{-}228}$:GFP as reporter transgenes. Socket glia were counted using $P_{zipt\text{-}2.2}$:GFP and $P_{mir\text{-}228}$:NLS:RFP as reporter transgenes. Cell counting of $P_{ttr\text{-}43}$:mScarlet^{+}and $P_{mir\text{-}228}$:GFP^{+} cells in hermaphrodite images consistently yielded 22-23 sheath cells, instead of the expected 24 (Figure S5E), with one or a combination of the AMsh, ADEsh, and PDEsh glia missing. We verified that this was simply a limitation of imaging/animal orientation. 4-5 animals were counted for each reporter using the multi point tool in FIJI. Graphs were created in GraphPad PRISM.

Gene Ontology (GO) analysis

Genes were filtered by log fold change of 1.5 and *p* value cut off 1e-3. GO term analysis was performed by using the ''Enrichment Analysis'' Tool on *wormbase.org*.[166] Default q value threshold: 0.1 was selected. Graph colors were edited in Adobe Illustrator.

Comparison to human glia

To compare molecular profiles of *C. elegans* and human glia, we first defined a *C. elegans* glia-enriched gene set using differential gene expression analysis for glial vs non-glial clusters, single cell type (AMsh, CEPsh, ADEsh) versus remaining clusters and sheath glia versus socket glia, and vice versa (Table S3). Genes were filtered by mlogfc of 1.5 and p value cut off 1e-3. We then used OrthoList2[116] to translate this glia-enriched list to its conserved human orthologs with the default ''Fields searched'' options clicked (WormBase ID, Common Name, Locus ID, Ensembl ID, HGNC Symbol), minimum one number of programs, and no partial matches allowed (Table S3). This was then used to uncover the cell type signature using WebCSEA (Web-based Cell type Specific Enrichment Analysis of Genes)[115] which aggregates single-cell transcriptomic data including some adult brain tissues. A p-value of 0.05 was selected under the interactive p-value heat map and the following datasets were used for enrichment analysis: AdultCerebellum, Lake_2017_FrontalCortex, Lake_2017_VisualCortex, Voigt_2019_retina_1.[167–169] Only the values for oligodendrocytes, astrocytes, microglia, OPCs, pericytes, macrophages, RPE, and Schwann cells were selected and recreated in Adobe Illustrator. Mammalian orthologues of *C. elegans* genes that were enriched under each glial cell type and tissue are in Table S3.

Comparison between *him-5* and N2 hermaphrodite glial cells

Data for *him-5* and N2 hermaphrodites were combined and batch effect corrected using Harmony as described above. Variable genes were selected using the N2 hermaphrodite data (2500 genes). Leiden clustering led to identification of 29 clusters. Clusters were annotated using the cell type labels generated for this publication from the N2 hermaphrodite data. Only two clusters were not found to overlap with any of the wildtype data, one appeared to be of a neuronal signature, while the other overlapped with male ILsh glia when integrated with the *him-5* negative male data. This could be due to the presence of some males in the *him-5* hermaphrodite samples. These clusters and all other clusters associated with non-glial populations were excluded, the data was re-clustered, and UMAP was rerun.

Hierarchical Clustering

Whole Data

Hierarchical clustering of the whole data was performed using **scanpy.tl.dendrogram** function using default parameters.

Glial Clusters

To identify the transcriptomic similarities amongst our glial clusters, we constructed a matrix containing the mean expression of the highly variable genes for each of our 32 clusters and used **sklearn.pairwise (metric='cosine')** cosine similarity to create a pairwise distance matrix which was subsequently clustered using the same clustering function **scipy.cluster.hierarchy (linkage='average' and metric='euclidean')**.

QUANTIFICATION AND STATISTICAL ANALYSIS

All quantification and all statistical analyses details are included in the relevant Figure Legends and sections of method details.

Developmental Cell, Volume *60*

Supplemental information

Molecular profiling of adult *C. elegans* glia across sexes by single-nuclear RNA-seq

Maria D. Purice, Elgene J.A. Quitevis, R. Sean Manning, Liza J. Severs, Nina-Tuyen Tran, Violet Sorrentino, Connor Finkbeiner, Feinan Wu, Michael Zager, Manu Setty, and Aakanksha Singhvi

Figure S1

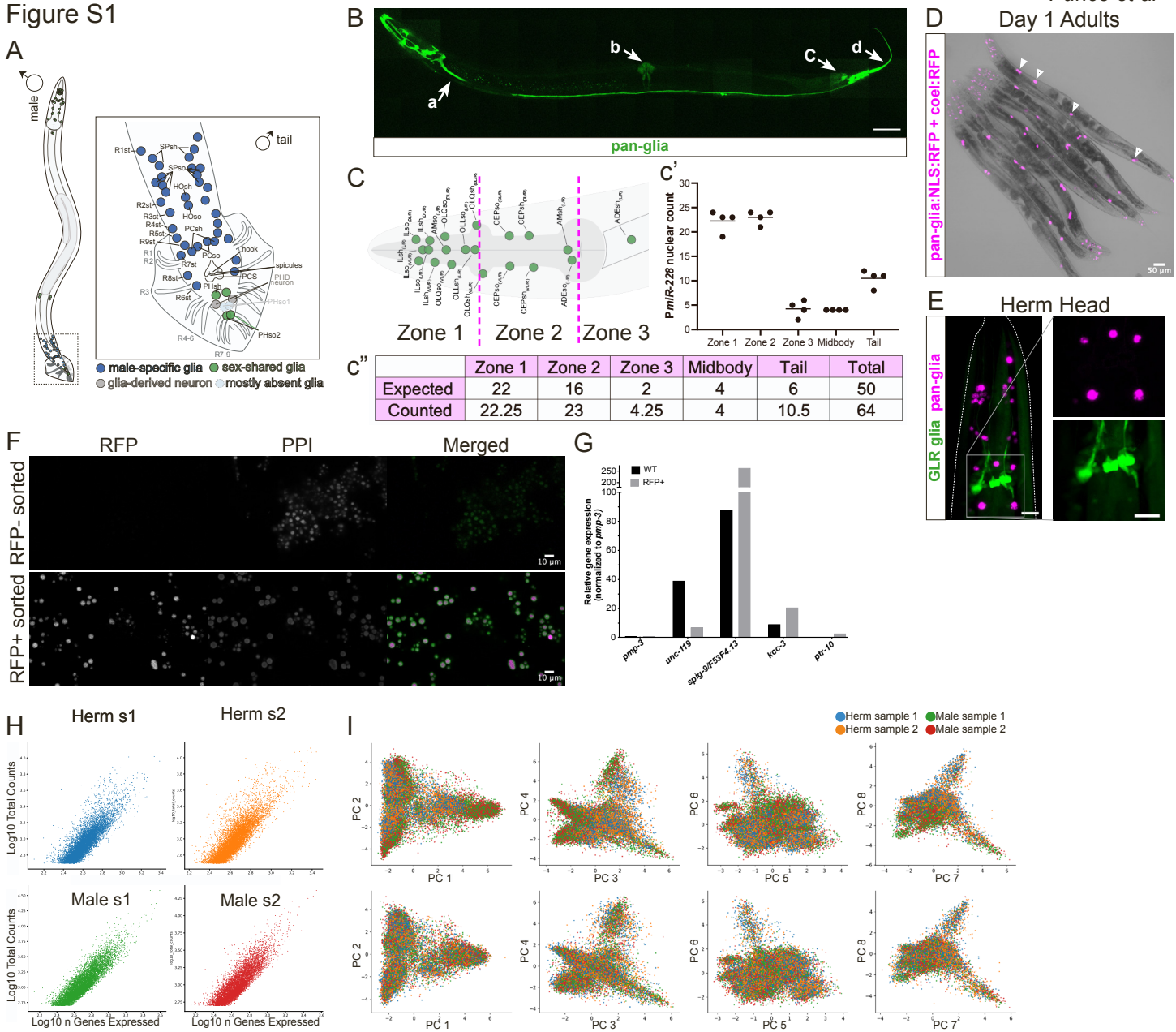

	Zone 1	Zone 2	Zone 3	Midbody	Tail	Total
Expected	22	16	2	4	6	50
Counted	22.25	23	4.25	4	10.5	64

Figure S1(related to Figure 1 and STAR Methods): **Characterization of adult *C. elegans* glia using pan-glial transcriptional reporter and validations.** (**A**) Schematic of adult male glial nuclei, ventral view in zoomed in panel, showing nuclei of sex shared (green), male-specific (blue), and PHso1 glia (light blue), and PH neurons (light gray). (**B**) Z-stack projection and stitched tiles of adult hermaphrodite expressing $P_{mir-228}$:GFP. Arrows denote non-glial expression in (**a**) excretory canal, (**b**) vulva, (**c**) rectum, and (**d**) posterior epithelia. Scale bar = 50mM. (**C**) Cell counts of $P_{mir-228}$:NLS:RFP$^+$ nuclei across three zones in the head of the animal (**C**), midbody, and tail. Actual (**c'**, **c''**) and expected glial (**c''**) cell counts across four animals. (**D**) Z-stack projection of adult hermaphrodites expressing $P_{mir-228}$:NLS:RFP and co-injection marker $P_{unc-122}$:RFP (arrowheads). Scale bar = 50mM. (**E**) Z-stack projection of adult hermaphrodite head showing that GFP$^+$ GLR glia do not colocalize with $P_{mir-228}$:NLS:RFP. Scale bars = 10mM. (**F**) Single one-micron images of RFP$^-$ and RFP$^+$ sorted nuclei after FACS stained with DNA dye propidium iodide (PPI). Scale bars = 10mM. (**G**) Quantitative real-time PCR of selected neuronal (*unc-119*) and glial (*F53F4.13/spig-9, kcc-3, ptr-10*) genes in RFP$^+$ sorted nuclei and dissociated WT animals. (**H**) Scatter plots showing the relationship between the number of molecules and the number of genes per cell for each sample. (**I**) PCA colored by sample prior to batch correction (top) and after harmony correction by sample (bottom). Scatterplots of the first eight principal components (PCs) illustrating th distribution of single cells from four different samples. (**J**): UMAP of 51 non-batch corrected clusters where each dot color represents a sample group.

Figure S2

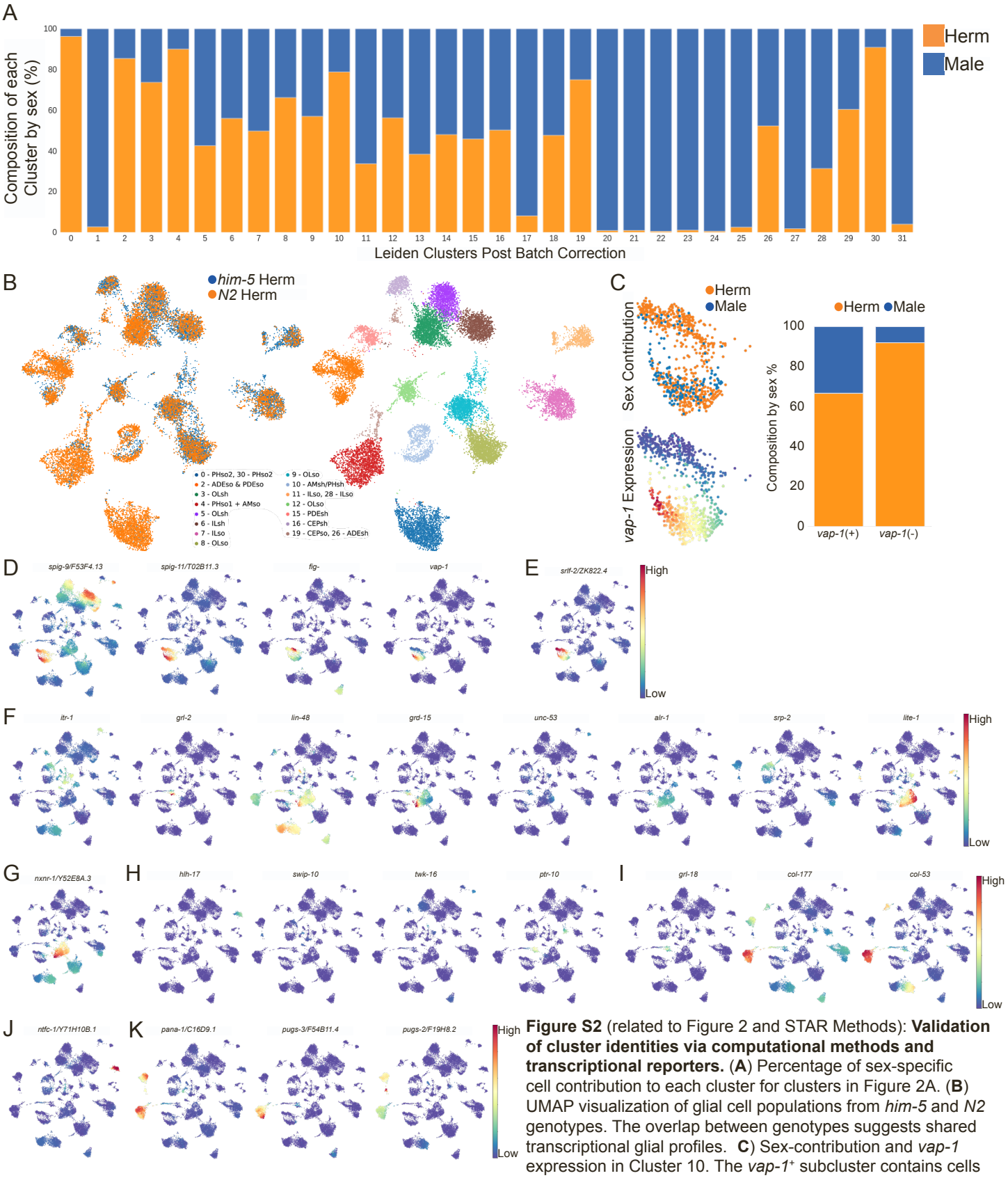

Figure S2 (related to Figure 2 and STAR Methods): **Validation of cluster identities via computational methods and transcriptional reporters.** (**A**) Percentage of sex-specific cell contribution to each cluster for clusters in Figure 2A. (**B**) UMAP visualization of glial cell populations from *him-5* and *N2* genotypes. The overlap between genotypes suggests shared transcriptional glial profiles. **C**) Sex-contribution and *vap-1* expression in Cluster 10. The *vap-1*$^{+}$ subcluster contains cells from both sexes while the *vap-1*$^{-}$ subcluster is primarily composed of hermaphrodite cells. (**D**) UMAP colored by MAGIC imputed expression of AMsh/PHsh genes in Figure 2D. (**E**) Same as **D** for AMsh/PHsh gene *srlf-2/ZK822.4*. (**F**) Same as **D** for *itr-1*, *grl-2, lin-48, grd-15, unc-53, alr-1, srp-2,* and *lite-1*. Expression was not detected for *abt-4* and *grl-6* in our dataset. (**G**) Expression of novel AMso/PHso1 marker gene *nxnr-1/Y52E8A.3*. (**H**) Same as **D** for *hlh-17*, *swip-10*, *twk-16,* and *ptr-10*. (**I**) Same as **D** for *grl-18, col-177,* and *col-53.* Expression was not detected for *delm-1* and *delm-2* in our dataset. (**J**) Expression of novel CEPsh marker gene *ntfc-1/Y71H10B.1.* (**K**) Same as **D** for *pana-1/C16D9.1, pugs-3/F54B11.4*, and *pugs-2/F19H8.2.*

Figure S3

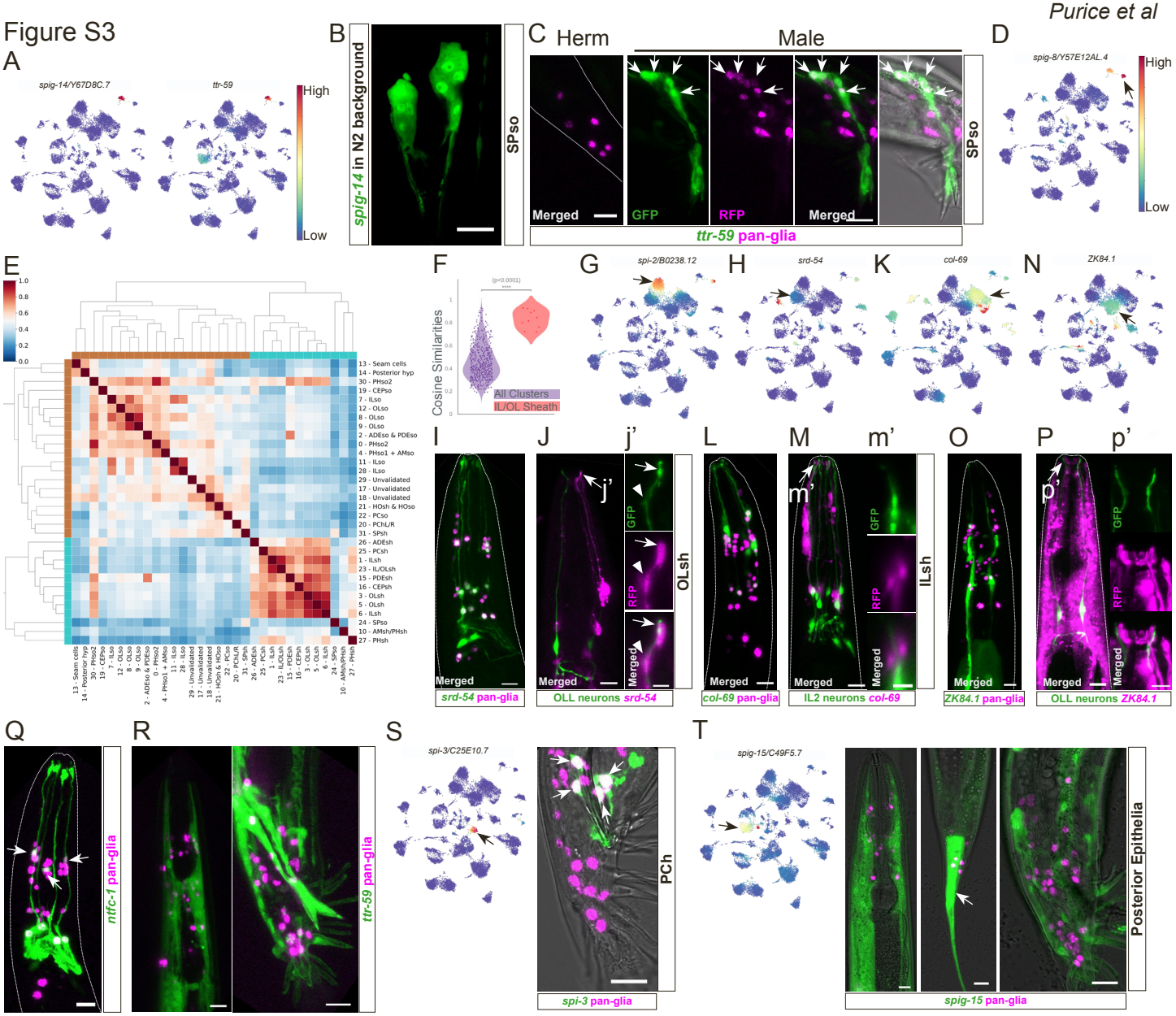

Figure S3 (related to Figure 3 and STAR Methods): **Computational and experimental annotation of glial cell types**. (**A**) UMAP colored by MAGIC imputed expression of *spig-14/Y67D8C.7* and *ttr-59*. (**B**) Expression of *spig-14/Y67D8C.7* in N2 males. (**C**) Transcriptional reporter for *ttr-59* depicting no expression in hermaphrodite tails. Expression in the male SPso (arrows). (**D**) Same as (**A**), for *spig-8/Y57E12AL.4*. Arrow shows high expression in Cluster 27/PHsh. (**E**) Heatmap showing the cosine similarity between each pair of clusters. Average batch-corrected principal components were used for computing similarities. (**F**) Distributions of cosine similarities of all clusters and the predicted ILsh/OLsh clusters show that the IL/OLsh clusters have a higher degree of similarity (**p-value** < 1e-4, Mann-Whitney U test). (**G**) Same as (**A**) for *spi-2/B0238.12*. (**H**) Same as (**A**) for *srd-54*. (**I**) Transcriptional reporter for *srd-54* depicting varied GFP$^+$ expression that overlaps with RFP. Scale bar = 10 mM (**J**). mScarlet transcriptional reporter for *srd-54* and GFP transcriptional reporter for OLL neurons. Zoom in (**j'**) shows single GFP$^+$ OLL dendritic tip in close contact with mScarlet$^+$ OLsh glia (arrowhead, arrow). Scale bar = 10 mM and 2 mM in (**j'**) zoom in. (**K**) Same as (**A**) for *col-69*. (**L**) Transcriptional reporter for *col-69*. Scale bar = 10 mM (**M**). mScarlet transcriptional reporter for *col-69* and GFP transcriptional reporter for IL2 neurons. Zoom in (**m'**) shows single GFP$^+$ IL2 dendritic tip in close contact with mScarlet$^+$ ILsh glia. Scale bar = 10 mM and 1 mM in (**m'**) zoom in. (**N**) Same as (**A**) for *ZK84.1* (**O**) Transcriptional reporter for *ZK84.1*. Scale bar = 10 mM. (**P**). mScarlet transcriptional reporter for *ZK84.1* and GFP transcriptional reporter for OLL neurons. Zoom in (**p'**) shows single GFP$^+$ OLL dendritic tips that do not overlap with mScarlet$^+$ glia – suggesting they are ILsh glia. Scale bar = 10 mM and 5 mM in (**p'**) zoom-in. (**Q**) CEPsh GFP transcriptional reporter *ntfc-1/Y71H10B.1* depicting expression in a second subset of cell near the first pharyngeal bulb (arrows). (**R**) SPso GFP transcriptional reporter *ttr-59* depicting expression in head and tail epithelia. (**S**) Same as (**A**) for *spi-3/C25E10.7*. Right: Transcriptional reporter *spi-3/C25E10.7* expression in two bilateral cells in the postcloaca region, suggesting they are the hypodermal PCh cells. (**T**) Same as (**A**) for *spig-15/C49F5.7*. Right: Transcriptional reporter *spig-15/C49F5.7* expression in the head of hermaphrodites and tails of both sexes, suggesting this gene has strong expression in the posterior epithelia. (**U**) Same as (**A**) for *grd-10*, suggesting this is the seam cells cluster, which the $P_{mir-228}$ promoter also expresses in. Panels **Q-T** scale bars = 10mM.

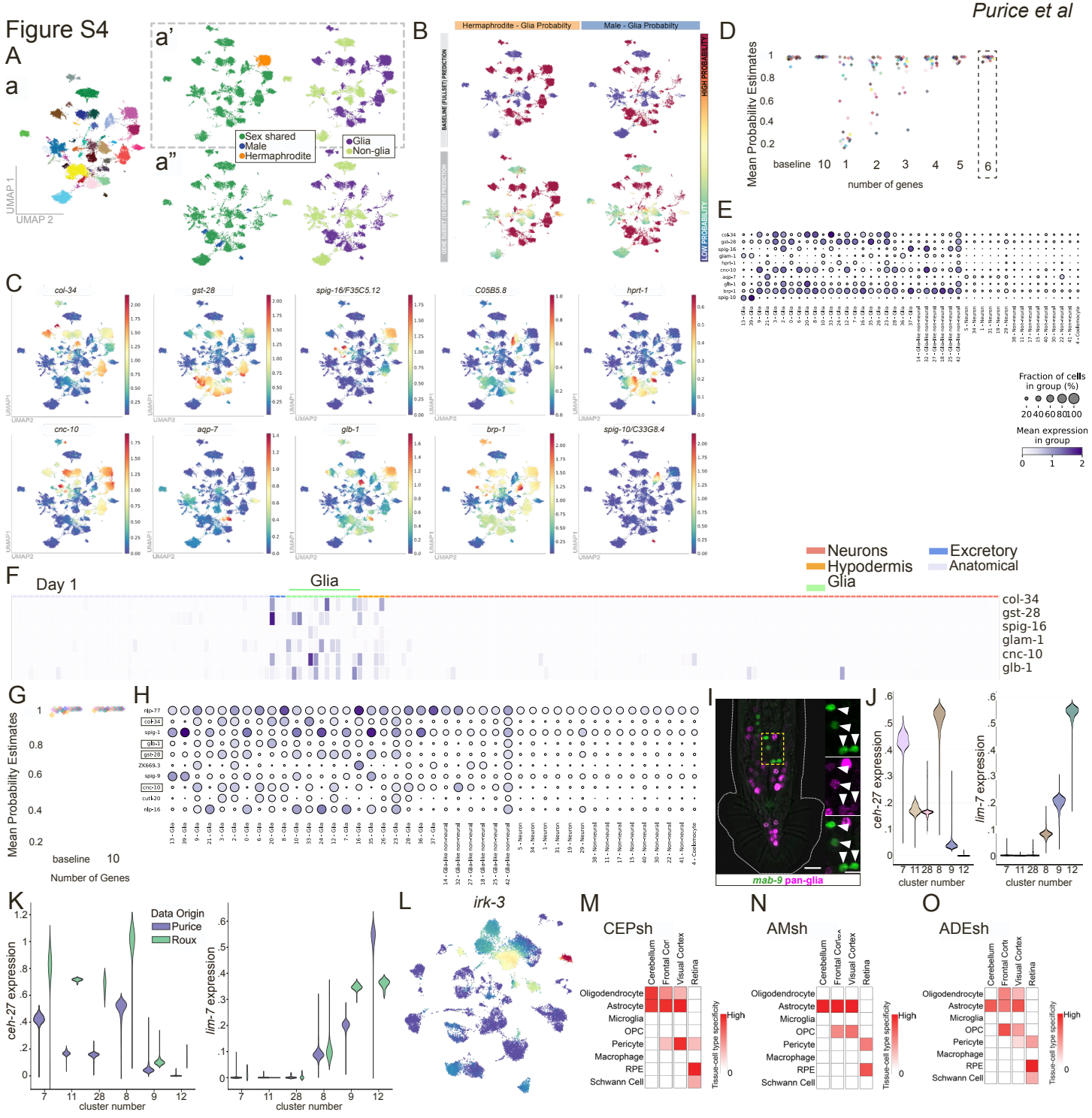

Figure S4 (related to Figure 4 and STAR Methods): **Molecular characteristics of *C. elegans* glia.** (**A**) Glial vs non-glial clusters after batch-correction. (**a**) UMAP showing all in vivo validated clusters and identified neuron, non-neural, and coelomocyte clusters. **a'**) UMAP showing the subset of hermaphrodite cells labeled by sex (left) and tissue type (right). (**a"**) Same as (**a'**), for male cells. (**B**) Left: UMAPs colored by glial probability estimates from the logistic regression model trained using hermaphrodite cells: Using the full set of genes (top) and the identified subset of 10 genes (bottom) using the feature ranking procedure. Right: Same for male cells. **C**) MAGIC imputed expression of the selected top 10 genes on the batch-corrected UMAP. (**D**) Strip plot showing the predictive confidence of gene combinations compared to the full set of genes in distinguishing glia from non-glia. Each dot is the mean glial probability estimate for a glial cluster colored by colors in panel (**A**). (**E**) Dot plot showing the expression of the top 10 ranked genes. Display as per Figure 4A-C. (**F**) Pan-glial gene expression pattern in Day 1 Roux et al., 2023. Expression for genes *col-34, gst-28, spig-16/F35C5.12, C0585.8, cnc-10,* and *glb-1* shown. (**G**) Same as (**D**) in distinguishing Purice et al., glia (this study) from Roux et al., 2023 non-glia. (**H**) Same as (**E**) to distinguish between Purice et al., glia and Roux et al., 2023 non-glia with >99% confidence. Boxes = overlapping genes. **I**) *mab-9* expression in a subset of *mir-228*$^{+}$ glia in male tail. Scale bar = 10 mM, inset = 5 mM (**J**) MAGIC imputed gene expression of *ceh-27* and *lim-7* across the ILso/OLso clusters. (**K**) MAGIC imputed gene expression of *ceh-27* and *lim-7* across the ILso/OLso clusters in Purice et al and Roux et al., 2023 datasets. (**L**) UMAP colored by MAGIC imputed expression of *irk-3*. (**M**) Enrichment of *C. elegans* differentially expressed AMsh genes in different human glia and glia-like cells using WebCSEA. (**N**) Same as (**M**) for CEPsh. (**O**) Same as (**M**) for ADEsh. **M**-**O**: Uncorrected p value < 0.05. Heatmap color is proportional to the tissue-cell type specificity of inquiry gene list

Figure S5

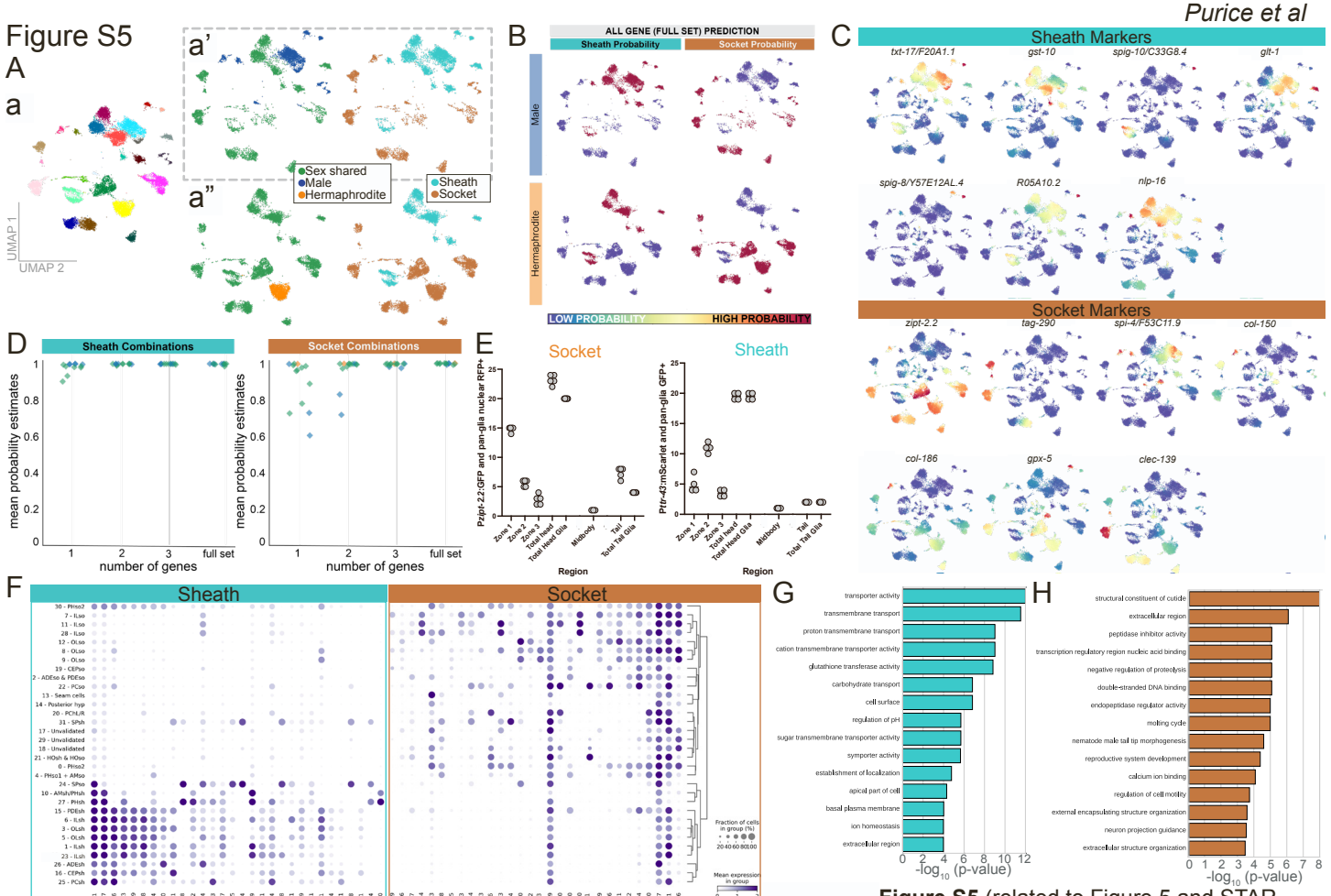

Figure S5 (related to Figure 5 and STAR Methods): **Identification of glial class signatures.** (**A**) Sheath vs socket clusters (**a**) UMAP of sheath and socket clusters (same as in Fig 2A). (**a'**) UMAP of hermaphrodite cells labeled by sex (left) and tissue type (right). (**a"**) Same as (**a'**), for male cells. (**B**) Top: Sheath and socket probabilities using logistic regression model trained using male cells. Bottom: Same as top for hermaphrodite cells. (**C**) UMAP colored by MAGIC imputed expression of the top 7 sheath and socket genes. (**D**) Strip plot demonstrating the predictive confidence of gene combinations compared to all genes, and minimal set of genes. Each dot is the mean sheath or socket probability estimate for the corresponding sheath or socket cluster and colored by colors in panel (**A**). (**E**) Cell counts of socket ($P_{mir-228}$:NLS:RFP$^+$ and $P_{zipt-2.2}$:GFP$^+$) and sheath ($P_{mir-228}$:GFP$^+$ and P_{ttr-43}:mScarlet$^+$) nuclei across the head, midbody, and tail. (**F**) Dot plot of mean gene expression for sheath-vs-socket binary classifier model using L2 penalty. Top 30 sheath and socket genes shown. (**G**) GO term analysis on sheath clusters compared to socket clusters. (**H**) GO term analysis on socket clusters compared to sheath clusters. (**I**) $P_{zipt-2.2}$:GFP$^+$ transcriptional reporter shown in Figure 5E with increased GFP brightness. In the head, faint expression is observed in head epithelia (arrowhead) and excretory gland cell (asterisk). In the male tail, expression is observed in the putative PCso (arrows) and HOso (wide arrow). In the hermaphrodite tail, expression is observed in glia (arrows) and epithelial cells (arrowheads) that co-localize with pan-glia nuclear RFP. (**J**) Three putative sheath GFP transcriptional reporters for *spig-1, ttr-43,* and *kcc-3.* Expression consistently absent from AMso and PHso1/2 (arrowheads). (**K**) Hierarchical clustering of non-batch corrected clusters. (**L**) Enrichment of *C. elegans* differentially expressed sheath and socket genes in different human glia and glia-like cells using WebCSEA. Uncorrected p value < 0.05. Heatmap color is proportional to the tissue-cell type specificity of inquiry gene list. Scale bars = 10 mM.

Figure S6

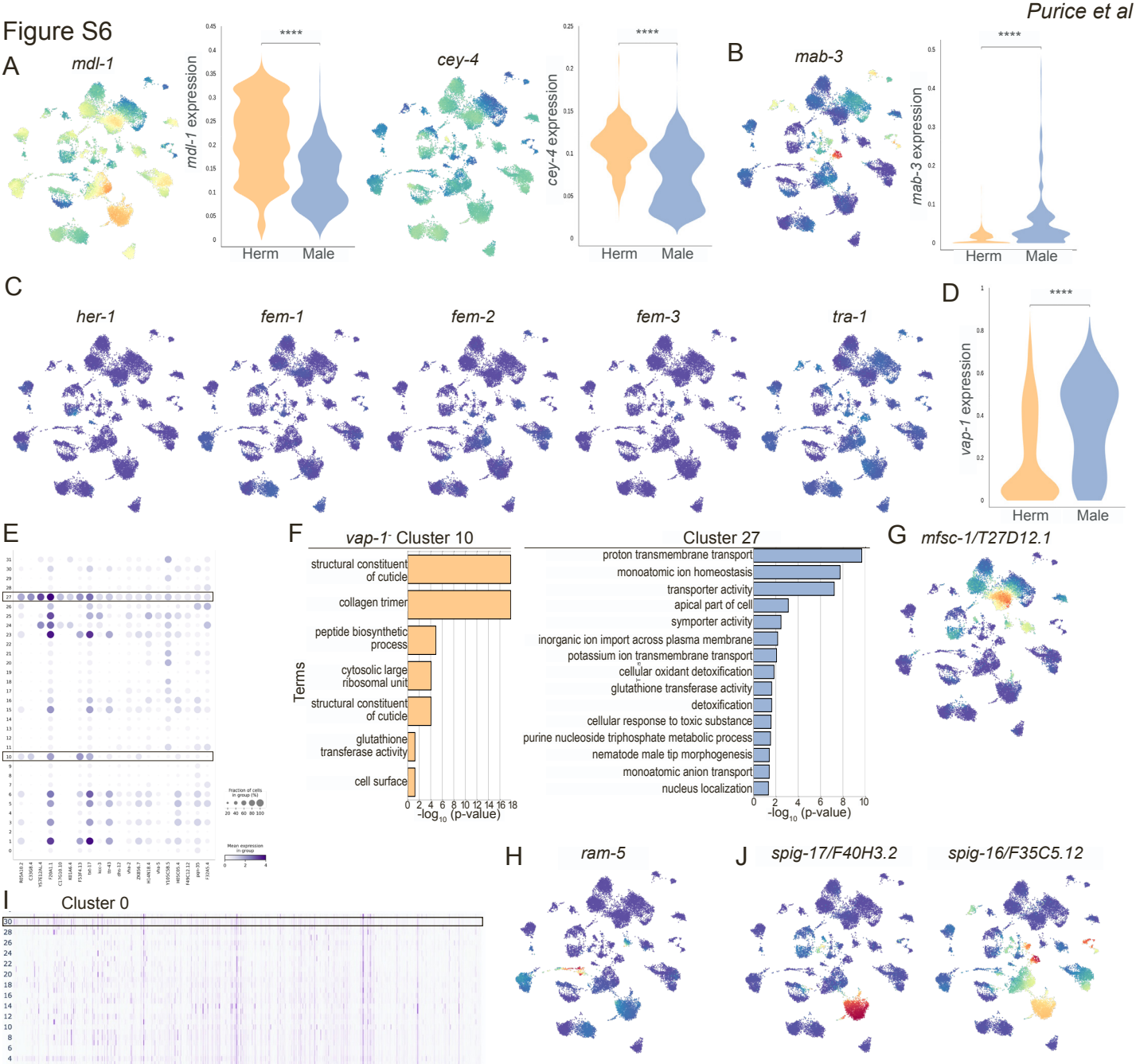

Figure S6 (related to Figure 6 and STAR Methods): ***C. elegans* glia are variably sex-dimorphic.** (**A**) UMAP colored by MAGIC imputed expression of *mdl-1* and *cey-4*. Next to each UMAP, differential gene expression of *mdl-1* and *cey-4* between sexes. **** P < 1e-4 (t-test). (**B**) UMAP colored by MAGIC imputed expression of *mab-3*. Differential gene expression of *mab-3* between sexes. **** P < 1e-4 (t-test). (**C**) UMAP colored by MAGIC imputed expression of *her-1*, *fem-1, fem-2, fem-3, and tra-1*. (**D**) Differential gene expression of *vap-1* between sexes. **** P < 1e-4 (t-test). (**E**) Dot plot displaying the expression patterns of Cluster 27 CEGs. Displayed as per Figure 4A-C. Clusters 10 and 27 outlines depict that Cluster 27 (male PHsh) contains distinct gene expression from Cluster 10 (AMsh/PHsh). (**F**) GO term analysis on putative hermaphrodite specific PHsh glia *vap-1*- cells in Cluster 10) compared to PHsh glial genes from Cluster 27. (**G**) UMAP colored by MAGIC imputed expression of *mfsc-1*/*T27D12.1.* (**H**) UMAP colored by MAGIC imputed expression of *ram-5.* (**I**) Pairwise comparison of Cluster 0 and 30 with these clusters outlined on each heatmap. For Cluster 0, every 12th gene shown. (**J**) UMAP colored by MAGIC imputed expression of *spig-17*/*F40H3.2* and *spig-16/F35C5.12*.

Purice et al

Figure S7

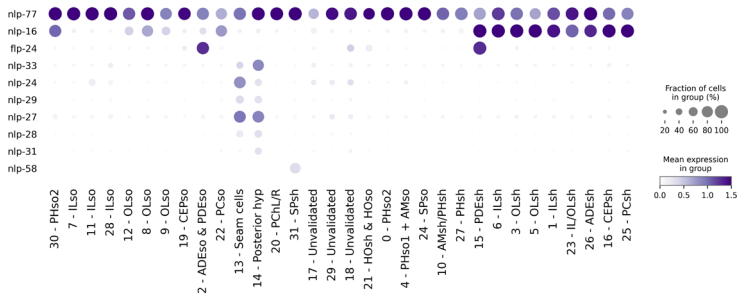

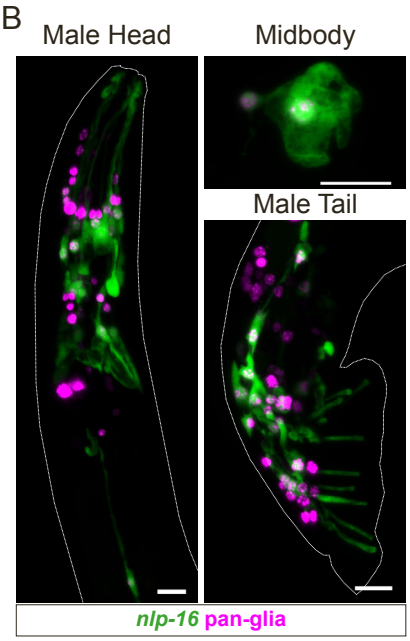

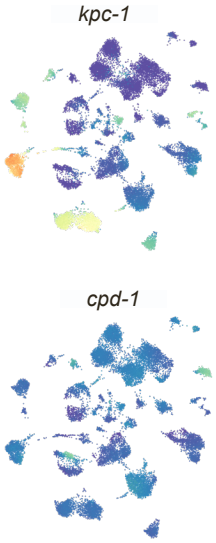

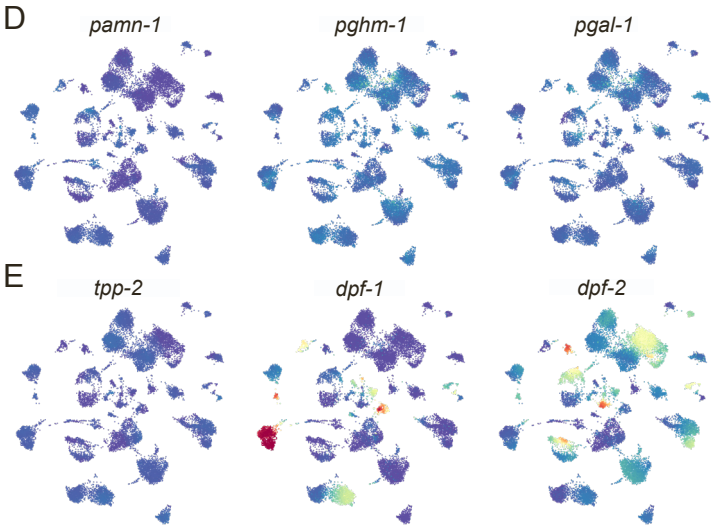

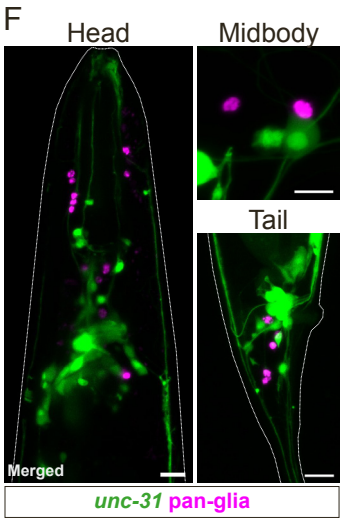

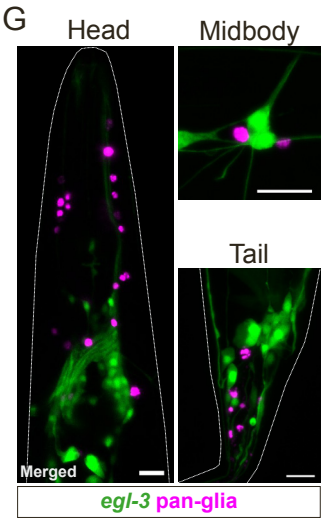

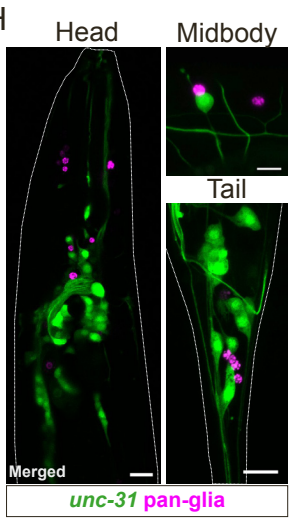

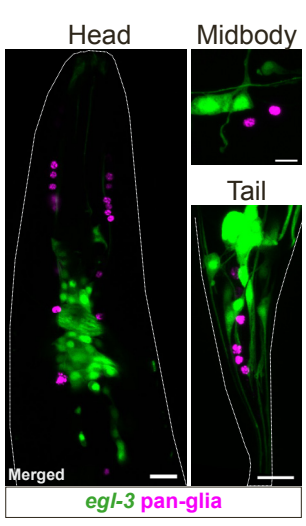

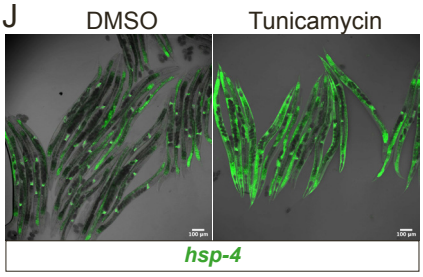

Figure S7 (related to Figure 7 and STAR Methods): **Glia lack canonical neuropeptide processing and DCV release mechanisms.** (**A**) Dot plot of mean neuropeptide gene expression, displayed as per Figure 4A-C. (**B**) Z-stack projections of adult male head, midbody, and tail showing *nlp-16* transcriptional reporter expression. (**C-E**) UMAPs shown like Figure 7A for: (**C**) *kpc-1* and *cpd-1*; (**D**) amidation enzymes (*pamn-1, pghm-1, pgal-1*); (**E**) degradation enzymes (*tpp-2, dpf-1, dpf-2, acn-1*). (**F-G**) Z-stack projections of adult male head, midbody, and tail showing transcriptional reporter expression in aged D8 animals for (**F**) *unc-31* and (**G**) *egl-3*. (**H-I**) Z-stack projections of tunicamycin-stressed D1 adult head, midbody, and tail showing transcriptional reporter expression of (**H**) *unc-31* and (**I**) *egl-3*. (**J**) Related to (**H-I**). *hsp-4* transcriptional reporter expression animals under DMSO and tunicamycin conditions. Scale bars = 10 mM except midbody panels scale bars = 5 mM, and **J** scale bars = 100 mM.